CARLETON UNIVERSITY

# Piezoelectric Sensor and Respiration Simulator System for Sleep Monitoring

by

Dilshad (Dilly) Mohamed

A Thesis submitted to the Faculty of Graduate Studies and Research in partial fulfillment of the requirements for the degree of Masters of Applied Science in Biomedical Engineering.

Ottawa- Carleton Institute for Biomedical Engineering

Department of Systems and Computer Engineering

Carleton University

Ottawa, Ontario, Canada

August 27, 2008

*Your file Votre référence*
*ISBN: 978-0-494-44053-7*
*Our file Notre référence*
*ISBN: 978-0-494-44053-7*

# Abstract

Apnea and hypopnea are sleep disorders whereby there is complete or partial cessation of breathing during sleep. Airflow monitoring is an effective way to diagnose such sleep disorders. The objective of this thesis is to investigate the feasibility of a piezoelectric unimorph bending sensor to detect and quantify airflow during breathing. Both the piezoelectric and pyroelectric responses of the sensor that produce output voltages due to airflow pressure and/or temperature variations have been investigated.

A mathematical model for the sensor output with respect to the airflow speed has been developed for the presented measurement configuration using piezoelectric theory and Bernoulli's law. In addition, sensor design parameters are theoretically investigated to find a suitable material for the sensor substrate and an adequate thickness ratio of the piezoelectric/substrate layers. A respiration simulator system has been developed in order to study the sensor response under different airflow conditions such as cycle, volume and temperature. The simulator is capable of isolating the pressure and temperature responses of the sensor so that these responses could be studied independently.

Experimental results with the simulator showed that the sensor output voltage due to piezoelectric effect was dependent on the square of the airflow speed, which agreed with the mathematical model developed, under the experimental conditions employed. A calibration curve was obtained experimentally, which enables to measure airflow variations quantitatively using the output voltage measured. The sensor output signals due to changes in air temperature could be used to qualitatively monitor presence or absence of airflow.

# Acknowledgements

I am deeply grateful to my supervisor, Dr. Yuu Ono for his dedication, guidance, support, patience and invaluable contribution throughout my graduate studies at Carleton. Dr. Ono has been very generous with his time and knowledge and was always available to assist me and provide guidance, for which he has my deepest gratitude. I would also like to thank Dr. C.-K. Jen and Dr. M. Kobayashi at Industrial Materials Institute of National Research Council Canada for providing piezoelectric membrane transducers for this thesis work. I would also like to thank NSERC for financial support of research assistantship.

Lastly, I would like to especially thank my family for their continued support and encouragement. I am deeply indebted to my mother who instilled in me the importance of education. Her determination and strength have been a constant source of inspiration throughout my life. To my Father, who through his example taught me to be the voice for the voiceless and to standup for what is right. To my Sisters, for their special friendships, and to my Partner for his quiet strength, love and support, I will always cherish you all.

# Table of Contents

## LIST OF TABLES

## LIST OF FIGURES

# Chapter 1
# Introduction

## 1.1 Overview

Sleep Apnea is usually a chronic condition that is very common, and if left untreated can be potentially life threatening leading, to constant fatigue, impairment, depression, hypertension and other cardiovascular diseases resulting from constant interruption in breathing which significantly lowers the oxygen levels in the blood [1].

Apnea is defined as a cessation of airflow at the nose and mouth lasting at least ten seconds in duration. Shorter respiratory pauses of less than ten seconds are ignored and do not represent an apneic episode. Measurements leading to diagnosis of sleep apnea are quite clearly understood in literature and a standard baseline is used in the diagnosis. Hypopnea, on the other hand, is less precisely defined and more difficult to measure and quantify [1], [2].

Due to the lack of standardized definition, hypopnea is usually missed or undiagnosed even though it is as serious a condition as apnea for patients suffering from these sleep disorders. Although there is consensus that hypopnea occurs where there is a reduction in airflow during sleep, opinions vary widely with regards to the best way to measure the reduction in airflow as well as how much reduction in the airflow would correspond to the condition of hypopnea [2].

A polysomnogram (PSG) is considered to be the gold standard in the diagnosis and evaluation of sleep disorders and is usually conducted in a sleep clinic requiring patients to sleep at the clinic for the night. Polysomnography is conducted by simultaneous recording of multiple sleep parameters, including electroencephalogram, respiratory parameters, chest excursion, limb movements, and the electrocardiogram [3], [4], [5], and [6]. By its very nature, polysomnography is an expensive resource requiring trained personnel, sophisticated equipment, and an entire night or more of recording and thus not surprisingly, it is a scarce resource. Most sleep centers typically have long waiting lists for patients with possible sleep apnea to have a polysomnogram performed so that a diagnosis can be ascertained and a treatment plan made available for the patients.

To help mitigate some of the above challenges, an inexpensive home device that can be used as an initial diagnostic tool to determine which patients may or may not have sleep apnea is very attractive and can enable health care providers to allocate the limited polysomnography resources for patients who would benefit the most from the investigation. The intent of the home apnea diagnostic device is not to replace polysomnography, but rather to complement and enable efficient allocation of the polysomnography resources.

Many of the current home based devices that can be used to determine occurrence of apnea are based on thermistors and/or thermocouples. These sensors utilize the thermal measurements to estimate airflow. The temperature around the sensor placed in the path of the airflow changes due to exhalation and inhalation. However, these devices have a

slow response time and the relationship between sensor temperature and true air flow is not straightforward.

Temperature and airflow are related by a non linear differential equation as the output signal from these devices is directly related to the temperature of the sensing element and indirectly related to the air flow. Temperature readings are also affected by the environmental conditions introducing variables that are difficult to control. Airflow reductions are highly underestimated with these devices. This behavior is undesirable especially for the detection of hypopnea, which requires a quantitative measurement of reduction in airflow [7]. Chapter 2 of this dissertation will cover these devices in more detail. A company- Dymedix Cooperation (Shoreview, MN, USA) has developed a piezoelectric polymer based airflow sensor that uses pyroelectric effect of the polyvinylidene fluoride (PVDF) to measure temperature variations. These devices appear to produce signals that more accurately estimate changes in airflow and have a faster response time than the traditional thermocouple based devices, however the sensor requires to be connected into the polysomnograph rather than being available as a standalone home based device [8], [9].

Recently, piezoelectric ceramic membrane sensors have been developed at Industrial Materials Institute (IMI), National Research Council (NRC) Canada [9], [10], [11], and [12]. These sensors consist of a metal foil, a piezoelectric ceramic film and a top electrode. Detailed sensor configuration will be provided in Chapter 2 of this dissertation. It is interesting to note that while these sensors have been applied for various industrial applications for non destructive testing of products and materials such as thickness measurements, defect inspection and real-time process monitoring for

various kinds of polymer injection molding processes in automobile and aerospace, these sensors could be also be used for medical and biomedical applications [9],[12]. The flexible nature of these sensors as well as the low cost of production provides a possibility and potential to develop a low cost home device using these membrane sensors.

# 1.2 Problem of Interest

One of the benefits of using the piezoelectric membrane sensor to quantify airflow is the flexible nature of the sensor that is attributed to the porosity in the piezoelectric film and the thin metallic membrane structure [9]. The relative low cost of the sensor also makes it suitable for home based diagnostic device.

There are two problems of interests in this dissertation: The first one is to determine if the piezoelectric membrane sensor can be employed to accurately measure airflow using piezoelectric response, and therefore be a viable technology that can be used to detect apnea and especially hypopnea in a home setting. This dissertation also demonstrates the use of pyroelectric effects for qualitative measure of airflow. The dissertation will also investigate how to use piezoelectric effects and/or pyroelectric effects for quantification of airflow. For such purpose, an airflow simulator which can simulate breathing conditions such as airflow rate and air temperature was developed as part of this thesis.

The second problem of interest in this dissertation is to investigate the design and configuration of the sensor. In this case the design of the sensor refers to the ratio of the

substrate material and the piezoelectric material as well as the substrate material to be used. This was accomplished by calculating the electromechanical coupling factor of several combinations of commonly used substrates and piezoelectric material with respect to the thickness ratios of substrate to piezoelectric materials.

# 1.3 Objectives

The overall objective of the work presented in this thesis was to evaluate the feasibility of using the flexible membrane sensor to accurately measure airflow using the piezoelectric and pyroelectric response of the sensor. A parallel objective was also to determine if the experimental results of airflow measurements correlate with the underlying mathematical models.

The second objective of this work was also to come up with design guidelines for the sensor. The guidelines in this case include the thickness ratio of substrate over the piezoelectric material to provide the maximum output as well as guidelines for the effective substrate selection. The second objective of this dissertation was accomplished using theoretical work that is currently available in the literature.

The work of thesis can be classified into five main stages. Each stage has a specific set of goals and objectives. However, most of these stages were often interrelated and some stages were revisited and refined as progress was made during the course of this work.

The first stage of this thesis was to conduct background literature research. The objective of the background research was to understand the current challenges in the

diagnosis of sleep apnea and hypopnea. The research included both the current challenges with the gold standard diagnostic tool, the polysomnogram as well as the existing home diagnostic devices currently available in the market. A better understanding of the existing challenges provided for an opportunity to focus on more specific aspects of these issues for the purposes of this thesis.

The second stage was the research of measurement principle and relevant mathematical models that can be used to correlate the sensor output signals with the air flow speed quantitatively. Using the principles of unimorph bending sensors using piezoelectric materials as well as the constitutive equations derived from other works for the behavior of unimorph structures under stress, a mathematical model describing the relationship between the output voltage from the piezoelectric material and the applied force was ascertained. The second mathematical correlation that was ascertained was using the Bernoulli theorem. The Bernoulli theorem provided a relationship between the pressure and the airflow speed. These two theories were used to develop measurement principle and its mathematical model. Also relationship between the ratio of thickness of the substrate to the piezoelectric material and the electromechanical coupling factor was also used to provide design guidelines for the unimorph bending sensor theoretically.

The third stage was the development of the respiration simulator system as well as the development of the unimorph piezoelectric bending sensor to be used specifically for the work carried out for this dissertation, for the verification of measurement principle and mathematical model developed in the second stage. The airflow simulator was necessary to model breathing under different conditions by varying the air volume and breathing cycle. The simulator also enabled the application of pressure effects on the

sensor independently of the temperature effects and hence allowing the study of these effects in isolation. A piston pump was used to generate respiration airflow. The output signal resulting from the sensor was measured using a voltage probe and data were acquired using a data acquisition package. In parallel to the sensor signal acquisition, airflow rate was also measured using a commercial spirometer simultaneously for comparison purpose.

The fourth stage was the experimental work. The objective of this stage was twofold; one was to ensure that the airflow simulator and the data acquisition tools and systems would enable the quality of data collection necessary. This stage of the work needed to be revisited a few times to ensure the suitability of experimental set up, the airflow simulator and the data acquisition system. The second objective of this stage was to implement the methodology necessary for data acquisition to ensure reproducibility, control and correlation of the experimental work.

The final stage of this work was data analysis. The objective of this stage was to verify the correlation between the experimental data and the mathematical models and to analyze the feasibility of using the piezoelectric membrane sensor as a device for airflow measurement.

# 1.4 Outline of the Dissertation

Following this introduction, Chapter 2 provides background on sleep apnea and the necessity of a home based apnea monitoring device. The gold standard currently used in diagnosis of apnea is described and the motivation for a cost effective home based

device to complement the polysomnogram is ascertained. Technologies currently used in commercially available home based apnea monitoring devices are discussed as well as the challenges associated with these devices for the quantification of hypopnea are discussed. This chapter also provides the background on the piezoelectric membrane sensor as well as the basics of piezoelectricity. This chapter also discusses the motivation for proposing this technology for airflow measurement for the purposes of detecting apnea and hypopnea.

Chapter 3 provides the measurement principle and mathematical models that will be used to compare the experimental results to the theoretical models. Theories from literature regarding piezoelectric unimorph will be used for the design guidelines of the sensor configuration.

Chapter 4 will develop the respiration simulator system and the piezoelectric unimorph sensor that was used for the experimental work for this dissertation. The motivation for the development of the simulator is also addressed.

Chapter 5 presents the experimental results and discussion. Experiments were carried out in two stages. The first stage of the experiment only applied the pressure effects to the sensor to quantify piezoelectric effects only. The second stage of the experiment added the temperature effects to the piezoelectric material resulting in the pyroelectric effect. Experiments of the actual breathing were also carried out using a spirometer to understand the baseline of expected airflow volumes and speeds. Results from the experiments are presented and analyzed to discuss how the experimental data correlate to the mathematical models.

Chapter 6 will provide the summary and conclusion as well as contributions made by this dissertation and some suggestions for possible future work.

Appendix A provides the data used for the calculation of electromechanical coupling coefficient. Appendix B includes tables of data collected, additional graphs that were not included in chapter 5 as well as any additional data used as part of this thesis but not included in chapter 5 of this dissertation.

# Chapter 2
# Background

## 2.1 Overview

This chapter presents background information on sleep apnea and current gold standard for diagnosis of apnea- the polysomnogram. This chapter also discusses current technologies used in home based devices for sleep monitoring and the associated challenges. Finally a brief background on piezoelectricity and the piezoelectric membrane sensor is also provided.

## 2.2 Sleep Apnea

While sleep Apnea is a common condition, a large number of patients remain undiagnosed due to the lack of awareness by the patient and because the diagnosis of sleep apnea requires sophisticated equipment and trained health care professionals.

According to the National Institute of Health, obstructive sleep apnea affects more than twelve million American adults and incurs an estimated annual cost of 3.4 billion dollars. One of the risk factors of obstructive sleep apnea is increased BMI (body mass index), and as incidences of obesity continue to increase around the world, we could expect the number of people suffering from obstructive sleep apnea to rise significantly in the future.

There are three types of apnea: obstructive sleep apnea, central apnea and mixed apnea. Obstructive sleep apnea, which is by far the most common type of sleep apnea, is caused by the absence of respiratory airflow past the nose, in spite of clear respiratory efforts. This is caused by the obstruction of upper airway, including the nose and the throat and is sometimes also referred to as upper airway apnea [1].

Central apnea is less common and is defined by complete cessation of airflow past nasal accompanied by cessation of respiratory effort. Central Apnea is associated with failure in the respiratory center of the brain [1].

Mixed apnea has attributes of both the upper airway apnea and the Central apnea. Mixed apnea is defined by cessation of airflow and an absence of respiratory effort early in the apneic episode, followed by resumption of unsuccessful respiratory effort in the latter part of the episode [1].

Hypopnea is also a form of sleep disorder but in this case, the patient does not experience total absence of respiratory airflow, but rather a significant reduction in airflow past the nasal. Needless to say, lack of standard definition for hypopnea has been causing a significant confusion in its diagnosis and hence treatment. In 1999, a task force of the American Academy of Sleep Medicine made recommendations for the definition of apnea and hypopnea for clinical research. A follow-up report by the Clinical Practice Review Committee of the American Academy of Sleep Medicine published guidelines for scoring hypopnea in adults. For the purposes of this study, the following guidelines will be used [2], [3]:

Apnea is defined as cessation of airflow for more than 10 seconds with a reduction in airflow of 80–100% from the baseline. Baseline airflow is the average

amplitude of stable breathing in the two minutes prior to an apneic event. Hypopnea is defined as a 30% or more decrease (compared with baseline) in airflow [3].

## 2.3 Polysomnogram

A polysomnogram (PSG) is a primary tool used for diagnosis of sleep disorders and is considered the current gold standard. A polysomnogram is a painless diagnostic tool and is usually conducted in a sleep lab with patients requiring to overnight in the lab. PSG involves recording of multiple physiological signals during sleep including electroencephalogram (EEG), electro-oculogram (EOG), electromyogram (EMG), respiratory flow, oxygen saturation (SaO2), and electrocardiogram (ECG). The PSG record is reviewed by a sleep technologist for identification of a variety of events, including sleep stages, movement, abnormal respiratory and cardiac episodes, and arousals. The scored PSG record and a sleep study report are then submitted to a polysomnographer for interpretation and clinical correlation. [10]

Electroencephalogram (EEG) is the brain electrical activity, and is recorded through surface electrodes placed on the skull. The electrodes are placed in accordance with an internationally accepted method [3]. These electrical signals pass from the electrodes and through amplifiers, where high frequency interference is filtered out before being recorded [3] [10].

Eye movements, Electro-oculography (EOG), are recorded from electrodes placed near the outer corner of each eye. Eye movements help establish the presence of REM sleep, (Rapid Eye Movement) which is helpful in defining sleep onset [3].

In routine polysomnography, Electromyogram (EMG) is recorded from chin muscles and anterior tibialis muscles. Chin-muscle EMG is recorded mainly to distinguish REM sleep from non-REM (NREM) sleep. Reduction of muscle tone is one of the requirements for diagnosing REM sleep. Periodic Limb Movements of sleep are diagnosed from limb EMG channels. Sometimes inter costal EMG is used to determine respiratory effort [3].

Several methods can be used to measure respiratory effort during a PSG test, including esophageal pressure monitoring, airflow monitoring by pneumotachometer, airflow monitoring by thermistor and thermocouple, nasal pressure monitoring, and inter costal EMG monitoring. Currently there is no consensus as to which method of monitoring respiratory effort is the best method for the test [3]. The following sections will discuss in more detail each of these methods used for respiratory monitoring.

Parameters from all these different recordings are put together to generate a score. The key scoring categories include main sleep stages, respiratory events, leg movements, and arousals. Many other parameters, such as oximetry, ECG, snoring, and effect of posture are also evaluated and reviewed by a polysomnographer [3] [13].

Figure 2.1 provides an illustration of sensor placements on a patient undergoing a polysomnogram [14].

Figure 2.1: Sensor placements for polysomnogram. [Reproduced from "Principles and Practice of Sleep Medicine"] [14].

### 2.3.1 Nasal Pressure Airflow Monitoring

Nasal cannula pressure systems measure airflow directly and quantitatively with a pressure transducer that detects changes in nasal pressure resulting from inhalation and exhalation. A nasal prong device is connected to a pressure transducer to monitor respiratory events in patients with sleep apnea or hypopnea. The voltage corresponding to the differential pressure is output for data acquisition either to PSG or other recording device. To properly record nasal pressure airflow, decisions regarding amplification of the airflow signal needs to be made as well as whether an AC or DC input of the PSG will be used for data recording. Flow limitations appear as a flattening or plateau on the inspiratory waveform and are best viewed with a low frequency filter of 0.01 Hz or less [15], [16].

The signal from an airflow pressure transducer looks sinusoidal during normal breathing, but appears differently during sleep-disordered breathing. When the top of the inspiratory waveform looks flat, this is an indication of flow reduction [15].

During airflow reduction, the inhalation airflow can be almost constant for two or more seconds. The output of the nasal pressure airflow transducer in such cases will be nearly a constant voltage. If AC input is being used for data recording, the polysomnogram or other recording device should not be set to suppress near constant signals. Therefore the recording device must have the capability of a low frequency cutoff of 0.05Hz or less. The most optimum setting is 0.01Hz, which would provide for respiratory waveforms that are identical to DC signal [15], [16].

The preferred method of recording nasal pressure airflow signals is to use a DC input. In this case one need not concern with low frequency filter settings. Respiratory signals can be sampled at about 10-50 samples per second as higher sampling rates generally do not provide any additional useful information [16].

For an AC input, recommended filter setting is between 0.01-0.03Hz for low frequency filter and 70Hz or higher for high frequency filter, with a sampling rate of 140-200Hz. The sensitivity for the DC input varies from patient to patient and between different polysomnogram, the high frequency filter is set at 5 Hz or higher with a sampling frequency of 10 Hz or higher.

In general the input pressure range of most nasal cannula pressure transducer is in the +/- 20 cm $H_20$ range, with a maximum output voltage of +/- 5V. Studies comparing respiratory events detected by nasal prong devices connected to pressure transducers with

those detected by thermistors indicate that an increased number of respiratory events are detected with a nasal prong than with the thermistor [17].

### 2.3.2 Esophageal Pressure Airflow Monitoring

Esophageal pressure monitoring during polysomnography is the gold standard for detection of increasing upper airway resistance that leads to decrease in airflow and sleep interruption. Esophageal pressure is measured by introducing a thin esophageal balloon or liquid-filled catheters connected to a pressure transducer. The catheter is introduced through the nose into the esophagus to monitor changes in intra thoracic pressures occurring during inspiration and expiration [18] [19]. Esophageal balloons are inflated with air or liquid; liquid-filled catheters are filled with water or saline. Despite it being a reference standard, esophageal pressure monitoring is not widely used, in part because of concern that the procedure may disturb sleep and may cause additional discomfort to the patient due to its invasive nature [18].

When using the pressure transducer for esophageal pressure measurement with a polysomnogram, if a low frequency filter of 0.01 Hz or lower is available the transducer can be used with an AC input into the PSG, however, if the low frequency filter available is only 0.1 Hz then a DC connection should be used. High frequency filter should be set to 30 Hz or higher to avoid electrical and other interference. A minimum sampling rate of 20 or higher would be required to get all the relevant data [15], [16].

Maximum output voltage of a pressure transducer when used for esophageal pressure measurement is in the range of +/- 5V, with an input pressure range of +/- 50cm $H_20$ [16].

### 2.3.3 Pneumotachometer Airflow Monitoring

The use of the pneumotachometer for airflow monitoring during a PSG exam is often limited due to patient discomfort that is results from a tightly fitting facemask that is connected to a pneumotachometer. This often makes it unsuitable for clinical respiratory studies during sleep [20]. One type of pneumotachometer is a differential pressure pneumotachometer in which an air-resistive element located in the air flow path creates a pressure drop which is proportional to the air flow rate during breathing. A pressure transducer converts the differential pressure across the resistive element into an electrical signal indicative of air flow rate. The flow rate signal can be integrated to provide an indication of breath or flow volume [21], [22].

For airflow measurement during sleep, a low pass filter of frequency of 10 Hz is suitable and would eliminate high frequency components due to disruptions caused by movement. A sampling rate of 100 samples/second or higher would be sufficient to provide all the necessary data. The flow range of pneumotachometer used for adults is between 0-800L/min, with an output voltage of 0-10V [18].

### 2.3.4 Thermistor and Thermocouple Airflow Monitoring

Thermistors and thermocouples measure airflow by measuring the temperature changes associated with the patient's breathing, causing an increase and decrease of the voltage being produced by these devices. These changes in voltage are recorded by the polysomnograph (PSG). A disadvantage of thermocouples and thermistors is its slow response to changes in temperature, which can be more than one second in some instances. The slow response time of thermistors and thermocouples is the reason that waveforms produced by these technologies are a smoothened average of the actual changes in airflow temperature that occur as the patient inhales and exhales [16]. Therefore subtle sleep-disordered breathing, such as the flow limitations associated with respiratory effort-related arousals may not be detected by thermistors or thermocouples. The slow response time of these devices is due to the material used to construct the thermocouple and thermistors. The insulating material covering the thermocouple and thermistor must change temperature in order to generate a voltage change. It is the mass of the material that impacts the time to respond to the temperature change [16], [23].

The low frequency filter of 0.1 to 0.3 Hz is required and a high frequency filter of 5 Hz to 15Hz. Studies comparing respiratory events detected by nasal prong devices connected to pressure transducers with those detected by thermistors indicate that an increased number of respiratory events are detected with a nasal prong than with the thermistor [16], [17].

### 2.3.5 Airflow monitoring with Piezoelectric Respiratory Belt

A Piezoelectric belt monitors airflow by measuring changes in thoracic or abdominal circumference during breathing. The transducer most commonly contains a piezoelectric sensor placed between two elastic strips. Stretching of the elastic places a strain on the piezo sensor, this generates a voltage. The device is placed around the body at the level of maximum respiratory expansion. The quality and interpretability of the respiratory signal is affected if the belt slips out of their original position during sleep due to movement or otherwise. Since the belts are generally not calibrated, the displayed data are more qualitative than quantitative.

The respiratory belt can be directly connected into the AC input of the polysomnogram. The low frequency filter should be set to 0.1 Hz and the high frequency filter should be set between 5Hz to 15Hz.

## 2.4 Current Home Diagnostic Technologies for Apnea

Due to lack of resources required to conduct polysomnogram, there is quite often a long waiting list for patients requiring the tests, thereby exposing patients to undue risks and continued discomfort. Home based diagnostic devices for apnea are intended to complement the current gold standard. Home diagnostic devices provide the possibility of assisting practitioners to allocate the scarce PSG resources in a more efficient manner. Results from home based diagnostic devices could be used to categorize patients who

require PSG test right away and those who are most likely able to wait and therefore using PSG resources more efficiently [25].

Thermistors or thermocouples attached onto nasal aperture and/or mouth detect airflow indirectly and semi quantitatively by sensing the temperature change during breathing. The flow signal provided by these sensors is not a direct measure of the actual flow, but rather the sensors sense the temperature difference between the cooler inspiration and warmer expiration. The change in temperature of the sensor is associated with a change of breathing conditions. A thermistor measures this as a change in resistance and a thermocouple measures as a change in electromotive force. This behavior poses a major problem when detecting hypopnea, since the definition of hypopnea events is made in terms of quantitative reduction in airflow [3], [7]. Both thermistors and thermocouples have a slow response time to changes in temperature due to the thermal mass of the devices themselves. The material surrounding these devices has to undergo a change in temperature in order to produce a voltage change. The output from these devices is an averaged output of change in breathing temperature and often subtle changes in breathing temperatures can be missed [16], [23].

Studies into the accuracy of thermistor/thermocouple based devices have shown that flow reductions were quite under estimated using these devices. A 50% reduction in flow only resulted in 18% reduction in the signal of the thermistor. These devices are satisfactory for the detection of apnea, but are not as accurate for detection of hypopnea which is often underestimated [7].

Newer types of thermal sensor using polyvinylidene fluoride (PVDF) film have been developed with a faster response time than those of traditional thermal devices.

Sensors based on this technology appear to produce signals that more accurately estimate changes in airflow. The signal from the PVDF sensor is proportional to the difference in temperature between the two sides of the film [8] [26].

Berry *et al* [8] conducted a study to compare the ability of a PVDF thermal sensor and a pneumotachograph to detect respiratory events in patients with obstructive sleep apnea. PVDF sensors used in the study were disposable airflow sensors from Dymedix Corporation. Their experimental results indicate that PVDF sensors respond linearly and nearly instantaneously to changes in temperature. A 50% reduction in pneumotachograph airflow resulted in only 18% reduction in thermistor airflow signal while there was a linear relationship between the airflow detected by the PVDF sensor and those detected by the pneumotachograph. However, relationship between senor output and flow rate was only discussed experimentally but not discussed theoretically.

# 2.5 Piezoelectricity

## 2.5.1 Basics of Piezoelectricity and Piezoelectric Materials

The word *piezo* comes from the Greek word *piezen* meaning *to press*. The piezoelectric effect is generation of electric charge by a crystalline material upon subjecting it to stress. Natural crystals such as quartz exhibit piezoelectric effects, however, piezoelectric effects can also be found in artificially polarized man-made ceramics and some polymers such as PVDF. The electrical charges developed by the

piezoelectric materials decay with a time constant that is determined by the dielectric constant and the internal resistance of the material. Many piezoelectric materials also exhibit pyroelectric effect, which is generation of an electric charge in response to heat flow [26], [27].

The ability of piezoelectric materials to convert mechanical energy into electrical energy in response to a mechanical stress has enabled these materials to find a wide range of applications in the area of sensors. Piezoelectric materials are dynamic materials that develop an electrical charge that is proportional to a change in mechanical stress.

Man made piezoelectric materials are made by placing a crystalline material which has randomly oriented dipoles (figure 2.2a), in a strong DC electric field at a temperature slightly below the Curie temperature, above which the material looses its characteristics. The strong electric field enables the alignment of the dipoles along the field lines (figure 2.2b). The material is cooled while maintaining the electric field across the thickness of the material. The electric field is removed and the poling process is complete. As long as the poled material is maintained below the Curie temperature, its polarization remains permanent (figure 2.2c) [28].

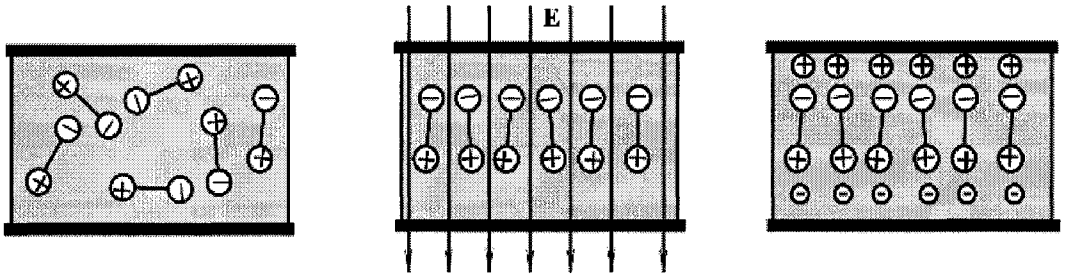


(a) (b) (c)

Figure 2.2: Poling process to align dipoles in the crystal to achieve piezoelectricity. [Reproduced from "Piezoelectric transducers for vibration control and damping"], [28].

The poled piezoelectric material becomes electrically discharged and is electrically neutral as long as it remains under steady-state conditions. When stress is applied, the neutral state is disturbed and the piezoelectric material develops an electric charge. Mechanical compression or tension on the element changes the dipole moment associated with the element and this creates a voltage, as shown in figure 2.3. If the stress is maintained for a while, the charges again will be neutralized by the internal leakage. The piezoelectric sensors is therefore responsive only to changing stress rather than to a steady level of stress.

Compression along the direction of polarization generates voltage of the same polarity as the poling voltage (figure 2.3b). While tension along the direction of polarization, generates a voltage with polarity opposite as the poling voltage (figure 2.3c) [28].

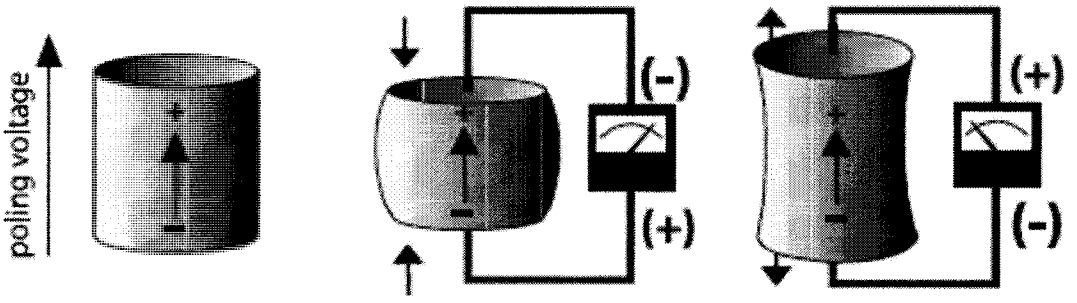


(a) Neutral (b) Compressed (c) Stretched

Figure 2.3: Voltage output due to stress on piezoelectric material. [Reproduced from "Piezoelectric transducers for vibration control and damping"], [28].

When operating in this mode, the device is being used as a sensor. The piezoelectric substance converts the mechanical energy of stress into electrical energy. The material in this case is a charge generator as shown Figure 2.4a. However, the charge generator model is uncommon in circuit analysis and therefore is converted into a voltage source model (Figure 2.4b) using Thevenin/Norton equivalent circuits [29].

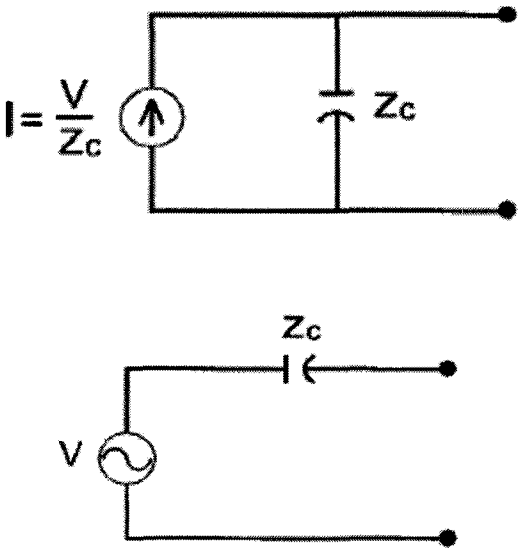


(a) (b)

Figure 2.4: Circuit representation of piezoelectric material. Reproduced from "C.H. Park, "On the circuit model of piezo ceramics" [29].

There have been a number of studies that have used electrical equivalent model to study the dynamic mechanical characteristics of the piezoelectric materials and have shown fair accuracy in various conditions of mechanical stress [30]. The relationship between applied stress and the resulting response is dependent upon the properties of

piezoelectric material, the size and shape of the material used and the direction of electrical and mechanical excitation.

Piezoelectric coefficients relate the electrical and mechanical quantities of the material. There are two subscripts associated with these coefficients, the first referring to the electrical axis, and the second referring to the mechanical axis. The most commonly used piezoelectric coefficients are $d_{ij}$ and $g_{ij}$ denoting charge and voltage respectively, where i (=1, 2, 3) and j (=1, 2, 3) denote the three dimensional orthogonal set of axes used analogous to x, y, z respectively. Since the thickness of the piezoelectric sensor used for our experiments is quite small compared to its length and width, and the electrodes are constructed on the top and bottom surfaces of piezoelectric material, the electrical axis is "i=3", as the charge or voltage is always transferred through the thickness of the film. The mechanical axis (j) can be 1, 2, or 3 denoting length, width or thickness direction, respectively, as illustrated in Figure 2.5. For low frequency applications, the piezo material is quite often used in the mechanical 1 (length) axis due to the direction of applied stress [26], [29], [31].

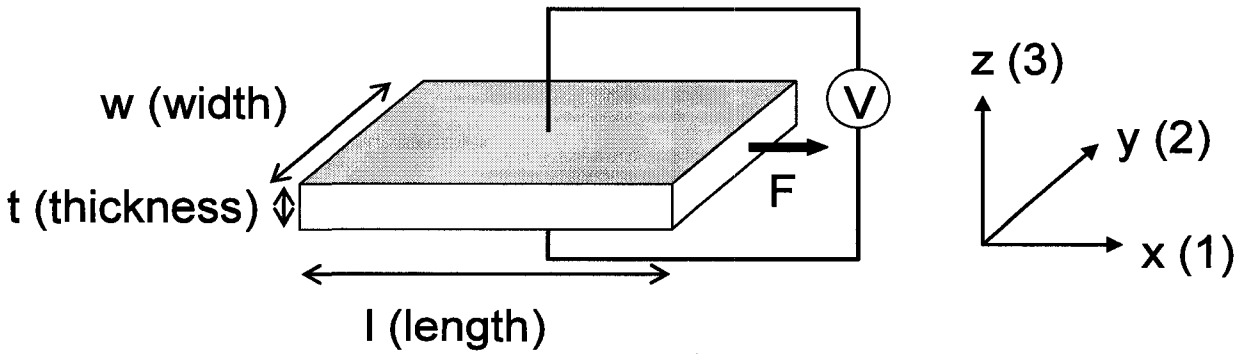


Figure 2.5: Coordinate and dimension of piezoelectric plate

The piezoelectric coefficient $d_{ij}$ can also be interpreted as the ratio of short circuit charge per unit area flowing between connected electrodes perpendicular to direction i to

the stress applied in the direction j. Once a force F is applied to the sensor in the length direction (j = 1), it generates the stress:

$$\sigma = \frac{F}{tw} \qquad (2\text{-}1)$$

$$Y = \sigma / \varepsilon \qquad (2\text{-}2)$$

$$\varepsilon = \Delta l / l \qquad (2\text{-}3)$$

where $F$ is the applied force, $Y$ is the Young's modulus, $\sigma$ is stress and $\varepsilon$ is strain, $l$ is the length, t is the thickness and $w$ is the width. The correlation between strain and the resulting voltage is given by the following relationship: [31].

$$\frac{\Delta l}{l} = \frac{d_{31}}{t} V \qquad (2\text{-}4)$$

where $\Delta l$ is change in film length in meters, $l$ is original film length in meters, $d_{31}$ is piezoelectric coefficient for length change in meters per volt, *and* $V$ is voltage across the thickness $t$. Using equations from (2-1) to (2-4), V is given in equation (2-5).

$$V = \frac{F}{d_{31} Y w} \qquad (2\text{-}5)$$

## 2.5.2 Piezoelectric Membrane Sensor

A piezoelectric membrane sensor was used to develop sleep monitoring technique and carry out the experimental work required for this dissertation. Figure 2.6 shows a photograph of the piezoelectric-ceramic flexible sensor that was developed by Industrial Materials Institute (IMI), National Research Council (NRC) Canada [10]. A schematic of the configuration of the membrane sensor is shown in the Figure 2.7. The sensor consists

of a thin metallic substrate, a ceramic piezoelectric film and a top electrode. The stainless steel foil was used as a substrate, which served as the bottom electrode as well.

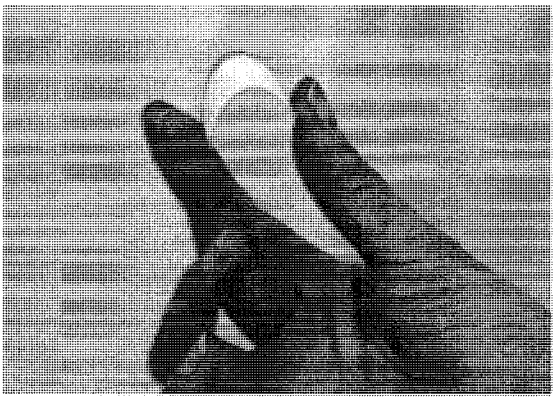

Figure 2.6: Piezoelectric ceramic flexible membrane sensor developed at IMI, NRC Canada.
[Reproduced from "A piezoelectric membrane sensor for biomedical monitoring"], [10].

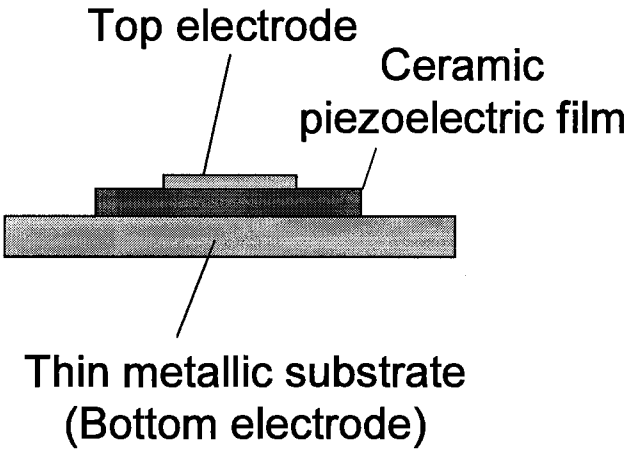


Figure 2.7: Configuration of the piezoelectric flexible sensor.

The sensor fabrication process is based on a sol-gel composite spray method that has been developed previously by IMI, NRC [9]. This method eliminates the need for a bonding layer between the piezoelectric film and the substrate. Lead zirconate titanate

(PZT) was used as piezoelectric material, and the PZT sol-gel composite was sprayed directly onto the stainless steel foil. The flexibility of the sensor is achieved due to the porosity in the piezoelectric film and the thin metallic membrane substrate.

During the fabrication process of the bending sensor, multiple PZT layers are sprayed on the stainless steel foil. Each PZT layer is approximately 5-15μm in thickness. This layered approach provides a mechanism of controlling the thickness of the piezoelectric layer and optimizing the sensor design for specific applications. Desired thickness of the PZT layer with respect to the substrate thickness will be further discussed in section 3.2. This fabrication approach could also provide freedom for the selection of substrate material and the material thickness to best optimize the sensor design.

# 2.6 Summary

Undiagnosed sleep apnea can lead to many life threatening diseases including chronic fatigue, depression, high blood pressure and cardiac diseases. Polysomnogram is the current gold standard for diagnosis of sleep apnea, requiring patients to overnight at a sleep clinic. The expense associated with conducting a polysomnogram makes it a scarce resource and sleep clinics usually have long waiting lists for patients requiring the test.

A low cost home based device that can be used as a simple, initial diagnostic test is an attractive solution to overcoming some of these challenges and it would assist the medical profession to better allocate these scarce resources. Most of the current home based sensors for apnea detection utilize thermistors/thermocouples. These devices have a slow response time and underestimate flow reductions.

The experimental work for this thesis has been conducted using a unimorph bending sensor consisting of a piezoelectric membrane film which will be developed in Chapter 4, for sleep monitoring. Based on the principles of piezoelectric materials described in this chapter, the next chapter will discuss the measurement principle and mathematical models for quantifying airflow using the unimorph bending sensor.

# Chapter 3
# Mathematical Model for Airflow Measurements

## 3.1 Overview

This Chapter provides the measurement principle and mathematical models that will be used to compare the experimental results to the theoretical models. Mathematical models will use the principles of piezoelectric unimorph bending sensor as well as Bernoulli's theorem for laminar flow. A unimorph sensor consists of one piezoelectric layer and one metallic or substrate layer. Theory from literatures regarding piezoelectric unimorph will be used for the design guidelines of the sensor configuration. Electromechanical coupling coefficient is one such parameter that will be used to provide guidelines for sensor deign. Electromechanical coupling coefficient is the efficiency with which piezoelectric materials convert between electrical and mechanical energy.

## 3.2 Measurement Principle

A piezoelectric unimorph sensor consists of one piezoelectric layer and one substrate (metal) layer which are bonded together. The metal layer also serves as the bottom electrode and a thin top electrode layer is deposited on the piezoelectric layer.

Figure 3.1 provides a structure of the unimorph bending sensor developed in this thesis. One end of the sensor is fixed and the other end is free for movement. When force

normal to the sensor surface is applied at the free end of the sensor, the sensor bends. The solid metal substrate layer resists its dimension change, thus the piezoelectric layer is driven to expand or contract along the length direction. Such dimension change causes stress inside the piezoelectric layer as illustrated in Figure 3.2, which produces electric charge as discussed in the chapter 2. The amount of electric charge excited is associated with the stress applied and can be measured using electronic devices, such as an oscilloscope, voltmeter and data acquisition unit, connected to the top and bottom electrodes of the sensor.

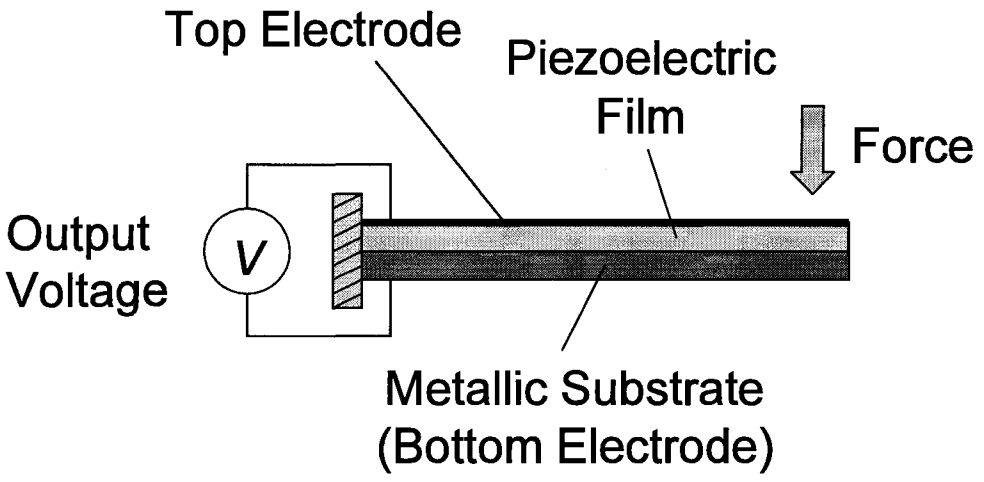


Figure 3.1: Configuration of unimorph bending sensor.

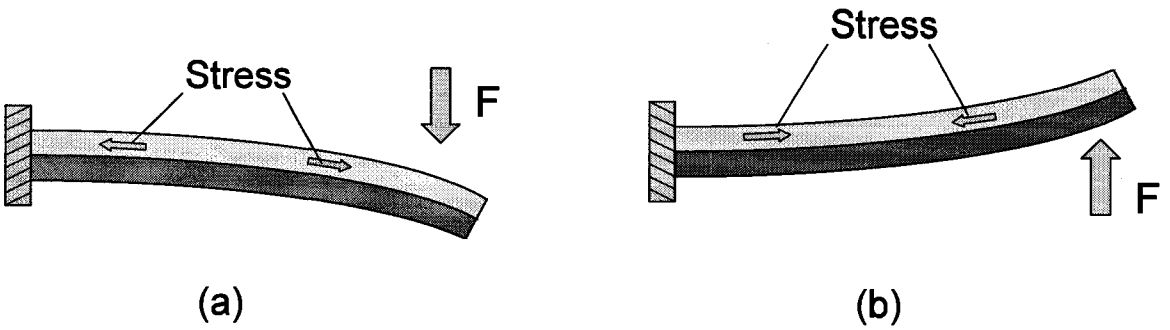


Figure 3.2: Expansion (a) and contraction (b) stress induced in piezoelectric layer due to force F applied on a free end of unimorph bending sensor.

The metal (substrate) layer in the unimorph sensor also increases the mechanical reliability of the sensor. An electromechanical coupling coefficient of the unimorph sensor, which is the efficiency with which a material converts electrical to mechanical energy, is associated with Young's modulus ratio and thickness ratio of the elastic layer and piezoelectric layer [32]. As we will discuss in section 3.3, maximum electromechanical coupling coefficient can be achieved by adjusting the thickness ratio of the elastic substrate layer and piezoelectric layer.

# 3.3 Mathematical Model

## 3.3.1 Piezoelectric Effect

Unlike the bimorph structure, which has two piezoelectric layers sandwiching a metallic layer, a unimorph sensor has a non-symmetrical structure, and because of the difference in Young's Modulus of the passive substrate layer and the piezoelectric layer, the neutral axis is not at the mid-plane of the composite structure. Therefore, when electrical field is applied on the piezoelectric layer, not only bending deformation occurs,

but extensional deformation will also be produced. Steel *et al* [33] discussed the tip bending deflection and stretching of a unimorph actuator as a function of applied electric voltage [34].

If a unimorph sensor is subjected to an applied electrical voltage (V) and an external force (F) is applied on the tip of the sensor perpendicular to the length direction, then the generated tip deflection and electrical charge can be expressed as follows [35-38].

$$\begin{pmatrix} \delta \\ Q \end{pmatrix} = \begin{pmatrix} \dfrac{4s_p s_m (s_p t_m + s_m t_p) L^3}{Kw} & \dfrac{3d_{31} s_p s_m t_m (t_m + t_p) L^2}{K} \\ \dfrac{3d_{31} s_p s_m t_m (t_m + t_p) L^2}{K} & \dfrac{Lw}{t_p}\left(\varepsilon - \dfrac{d^2{}_{31} t_m (s_m t^3{}_p + s_p t^3{}_m)}{K}\right) \end{pmatrix} \begin{pmatrix} F \\ V \end{pmatrix} \quad (3\text{-}1)$$

where $\delta$ and $Q$ are the tip deflection and charge, $s_p$ and $s_m$ are the elastic compliance of the elastic layer and the piezoelectric layer, $t_m$ and $t_p$ are the thickness of the elastic (metal) layer and piezoelectric layer, $L$ and $w$ are the length and width of the sensor respectively, $d_{31}$ is the transverse piezoelectric coefficient, and $\varepsilon$ is the dielectric permittivity.

$$K = (s_m)^2 (t_p)^4 + 4s_m s_p t_m (t_p)^3 + 6s_m s_p (t_m)^2 (t_p)^2 + 4s_m s_p t_p (t_m)^3 + (s_p)^2 (t_m)^4 \quad (3\text{-}2)$$

From [35], equation (3-1) can also be written as

$$\delta = aF + bV \quad (3\text{-}3)$$

$$Q = bF + cV \quad (3\text{-}4)$$

where

$$a = \frac{4s_p s_m (s_p t_m + s_m t_p) L^3}{Kw} \tag{3-5}$$

$$b = \frac{3d_{31} s_p s_m t_m (t_m + t_p) L^2}{K} \tag{3-6}$$

$$c = \frac{Lw}{t_p}\left(\varepsilon - \frac{d^2{}_{31} t_m (s_m t^3{}_p + s_p t^3{}_m)}{K}\right) \tag{3-7}$$

For simplicity, we will define the following:

$$A = \frac{s_p}{s_m} = \frac{E_m}{E_p}, B = \frac{t_m}{t_p}$$

where $E_m$ and $E_p$ are Young's modulus of metal (substrate) layer and piezoelectric layer respectively.

Equations (3-5), (3-6) and (3-7) can then be re written as (3-8), (3-9) and (3-10), respectively [35]:

$$a = \frac{4s_p L^3}{wt^3{}_p} \frac{AB+1}{1+4AB+6AB^2+4AB^3+A^2B^4} \tag{3-8}$$

$$b = \frac{3d_{31} L^2}{t^2{}_p} \frac{AB(1+AB^3)}{1+4AB+6AB^2+4AB^3+A^2B^4} \tag{3-9}$$

$$c = \frac{Lw\varepsilon}{t_p}\left[1 - k^2{}_{31} \frac{AB(1+AB^3)}{1+4AB+6AB^2+4AB^3+A^2B^4}\right] \tag{3-10}$$

where $k^2{}_{31} = d^2{}_{31} / \varepsilon s_p$.

From equation (3-2), the relationship between perpendicular force F applied to the tip of the sensor and the output voltage V can be obtained as follows: [35].

$$V = F\frac{a}{b} = \left(\frac{F}{d_{31}}\right)\left(\frac{4s_p L}{3wt_p}\right)\left(\frac{(AB+1)}{AB(B+1)}\right) \tag{3-11}$$

In conjunction with the above relationship, Bernoulli's theorem explains that when an incompressible and non viscous fluid, including gases and liquids, moves in a closed system, such as a pipe, the fluid undergoes a change in speed ($V_f$) as it moves into regions having different cross sectional area ($A$). The product $AV_f$ remains constant.

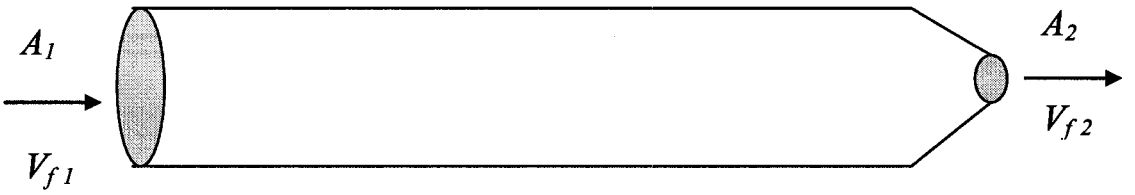


Figure 3.3: Bernoulli's Theorem.

$$A_1V_{f1} = A_2V_{f2} \qquad (3\text{-}12)$$

For the speed to undergo change there must be a change in force, which results in change in pressure. The pressure exerted by an incompressible fluid varies inversely with the square of the speed of the fluid. Bernoulli's equation allows us to understand the flow of fluids in systems with different pressures and heights and provides a relationship between induced differential pressure and flow velocity for laminar flow as follows [39] [40]:

$$\Delta P = \tfrac{1}{2}\rho V_f^2 \qquad (3\text{-}13)$$

where $V_f$ is flow speed, $\rho$ is fluid density and $\Delta P$ is induced differential pressure.

At the same time, we should also investigate the relationship between the discharge rate $Q_d$ of the pump, which is defined as the volume of fluid which emerges through the piston pump per unit time, when the force $F$ is applied to the piston. When one first applies force, the piston and fluid immediately in contact with it will accelerate. Soon after, if the force is kept constant, they reach a steady state in which their speed is constant. Immediately in front of the piston, there exists an isotropic pressure, which is greater than the atmospheric pressure. The force F applied to the piston can therefore be related to the change in pressure (between the isotropic pressure and the atmospheric pressure) and the area (A). The problem can therefore be looked at as a relationship between the Flow rate ($Q_d$) and the change in pressure. From equation (3-13), we can therefore find a relationship between flow velocity and the flow rate as per equation (3-14) [39]. This equation will be used to convert flow rate to flow speed in chapter 5 of the dissertation.

$$V_f = Q_d / A_r \qquad (3\text{-}14)$$

where $Q_d$ is the flow rate (discharge rate) and $A_r$ is the area of the tube encompassing the sensor.

One of the general principles of fluid dynamics is that in circumstances where Bernoulli's theorem is applicable in the form of (3-13), the compressibility of the fluid can always be ignored, even if the fluid is a gas, provided that the velocity is less than the velocity of sound by a factor of five or so. From Equation (3-11) and (3-13) we therefore have

$$V = \tfrac{1}{2}\rho V_f^{\,2} A_r \frac{-4 s_p L}{3 w t_p} \frac{(AB+1)}{AB(B+1)} d_{31} \qquad (3\text{-}15)$$

From equation (3-15), all parameters on the right side of the equation are a constant except for the flow velocity ($V_f$). Therefore, it is shown that output voltage V of a unimorph bending sensor is related to the square of flow speed $V_f$.

### 3.3.2 Pyroelectric Effect

The unimorph bending sensor used for this thesis also exhibits pyroelectric effects which is the generation of electrical charge in response to heat flow. It is important to note that pyroelectric effect generates electric charge in the piezoelectric layer in response to change in temperature and because change in temperature requires propagation of heat, pyroelectric devices are heat flow detectors as well as heat detectors. The material is considered pyroelectric if it exhibits a spontaneous temperature dependent polarization. Manufacturing of pyroelectric materials is similar to manufacturing of piezoelectric material and most materials that exhibit piezoelectric effects also exhibit pyroelectric effects and vice versa.

Pyroelectric effects can be used for qualitative analysis to detect the presence or absence of flow. In this section, pyroelectricity of unimorph sensor will be discussed. When subjected to changes in temperature, a piezoelectric material exhibits primary and secondary effects. Primary pyroelectric effects which are caused by temperature variations include changes in length of individual dipoles as well as changes to the randomness of dipole orientations due to thermal agitation. Voltage produced by temperature increase (or decrease) in a given piezoelectric layer of area A and thickness $t_p$ and permittivity $\varepsilon$ is determined by the pyroelectric coefficient, $\rho_y$ [27].

$$V = \frac{\rho_y t_p \Delta T}{\varepsilon} \qquad (3\text{-}16)$$

However there are also secondary pyroelectric effects which are induced as a result of piezoelectric effects. These piezoelectric effects are due to strain that is developed in the material as a result of thermal expansion and contraction [27]. Any change in the temperature induces charges on the surface of the material, inducing an electric field, which generates transverse strain and bending deformation (Figure 3.4) [40].

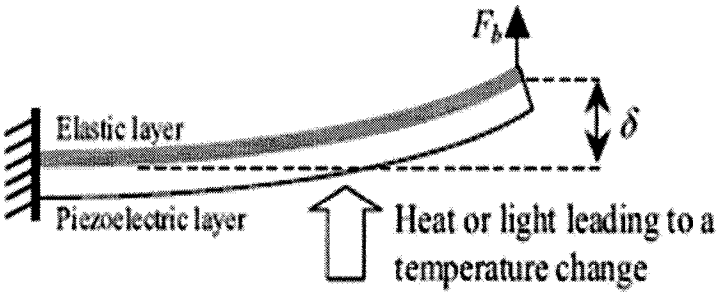


Figure 3.4: Operation of a pyroelectric unimorph sensor subjected to temperature change. Reproduced from "A pyroelectric-piezoelectric valve for integrated microfluidics", [40].

The induced electric field due to pyroelectric effects is much larger than the induced electric field due to piezo effects resulting in much larger deflection of the sensor as a result of pyro effects. In this thesis work, quantitative airflow rate monitoring is of interest, however, relationship between airflow and temperature is not straightforward mathematically since it is highly dependent on temperature environment around the sensor. In chapter 5, we will further investigate pyroelectric effects on sensor output signals experimentally and the relationship between flow speed and temperature.

# 3.4 Electromechanical Coupling Coefficient

To better understand sensor design criteria such as material selection and sensor dimensions, it is important to understand characteristic parameters of the sensor. The electromechanical coupling coefficient is one such parameter, which is the efficiency with which piezoelectric materials convert between electrical and mechanical energy. A unimorph sensor has one piezoelectric layer and one elastic layer that are bonded together as is the case with the membrane sensor used here. Since the top electrode is usually much thinner and lighter than piezoelectric and substrate layers, it's effects on electromechanical coefficient is ignored in the following discussion. An elastic substrate material also contributes to increasing the reliability of the sensor. When the piezoelectric layer is made to expand or contract as a result of external force, the substrate layer resists this change in dimension leading to stress in the piezoelectric layer [32].

From the work done by Wang *et al* [32], $k_{31}$, which is the transverse electromechanical coupling coefficient of the piezoelectric layer, is given as follows:

$$k_{31} = d^2_{31} / \varepsilon s^p \qquad (3\text{-}17)$$

where $d_{31}$ is the transverse piezoelectric coefficient, $\varepsilon$ is the permittivity and $s^p$ is the elastic compliance of the piezoelectric layer. Measured piezoelectric constants for the piezoelectric PZT sol-gel ceramic used in this dissertation, $d_{33}$ (longitudinal) and $d_{31}$ (transverse) are $37 \times 10^{-12}$ m/V at 10 kHz and $-27 \times 10^{-12}$ m/V at 1Hz respectively [10].

For analyzing the effect of the elastic substrate layer on the unimorph sensor performance, the following definitions are used [32].

$$A = \frac{E_m}{E_p} \qquad (3\text{-}18)$$

where $E_m$ and $E_p$ are Young's modulus of the elastic metal layer and piezoelectric ceramic layer respectively.

$$B = {}^{t_m}\!/_{t_p} \qquad (3\text{-}19)$$

where $t_m$ is the thickness of the metal layer and $t_p$ is the thickness of the piezoelectric layer.

Wang *et al* [18] derived the electromechanical coupling coefficient ($k^2_u$) of the unimorph structure as a function of Young's modulus ratio and the thickness ratio of the elastic and the piezoelectric layer.

$$k_u^{\,2} = \frac{9k^2_{31}}{4} \frac{A^2B^2(1+B)^2}{\left[A^2B^4 + 2A(2B+3B^2+2B^3) + 1 - k^2_{31}AB(1+AB^3)\right](AB+1)} \qquad (3\text{-}20)$$

In the case of a unimorph sensor such as the one used for the purposes of this dissertation, the electromechanical coupling coefficient is dependent on the ratio of the Young's modulus as well as the thickness ratio of the elastic and piezoelectric layers. As the above equation would indicate, the use of high $k_{31}$ material for a unimorph sensor will lead to high electromechanical coupling coefficient for the sensor. The electromechanical coupling coefficient was calculated and plotted with respect to the thickness ratio *(B)*. Figure 3.5 shows calculated results of $k^2_u$ using equation (3-20). Material parameters for the substrates and the piezoelectric material used in the calculation are given in Tables A-1 and A-2, respectively, in Appendix A.

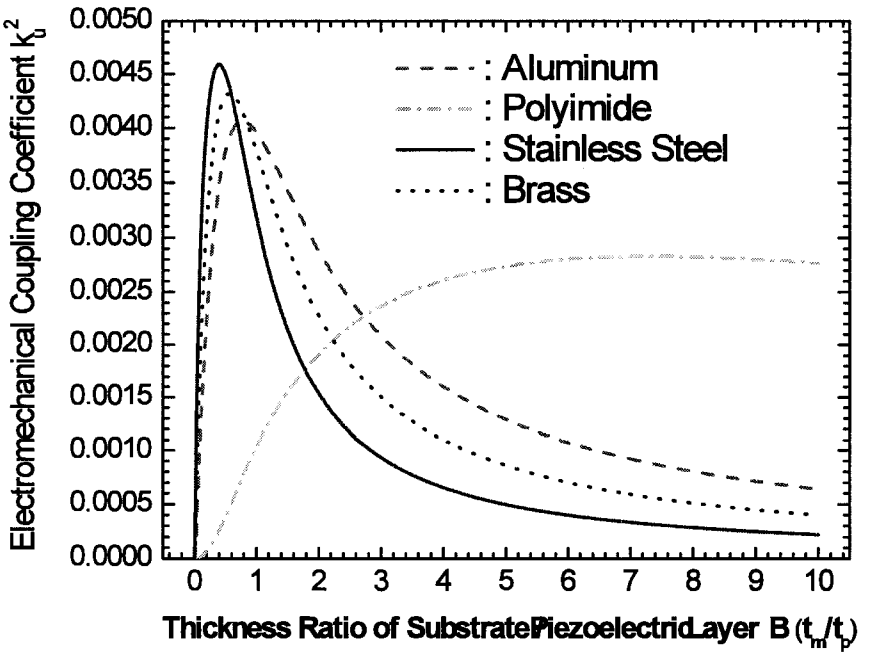


Figure 3.5: Electromechanical coupling coefficients with respect to the thickness ratio (B).

Two observations can be made from Fig. 3.5: The first one is that for this sensor configuration, the stainless steel substrate is an appropriate metal among the materials considered in the calculation to use for this sensor, as it provides the largest electromechanical coefficient. The second observation is that the maximum electromechanical coefficient occurs when the thickness ratio is 0.41 providing the $k^2_u$ value of 0.00459. In the chapter 4, we will endeavor to design the sensor as closely as possible according to this calculated result.

# 3.5 Summary

A piezoelectric unimorph bending sensor has been proposed for quantitative measurements of airflow variation due to breathing in this dissertation. A relationship between sensor outputs as a result of air pressure effects, i.e. flow speed, has been derived. It can be shown that output voltage (V) is related to the square of the flow speed ($V_f^2$).

The electromechanical coefficient ($k_u^2$) has also been calculated for the purposes of sensor design. It is shown that stainless steel could be the appropriate substrate layer as it provides the largest electromechanical coefficient as compared to a number of other common substrates.

Relationship between the sensor output voltage and pyroelectric effects as a result of change in temperature was also discussed.

Chapter 4 to follow will discuss the sensor development as well as the respiration simulator system used for the purposes of modeling human breathing under different circumstances such as volume and airflow cycle.

# Chapter 4

# Piezoelectric Sensor and Respiration Simulator System

## 4.1 Overview

In order to be able to carry out the experiments for this thesis, an airflow simulator that can model human breathing has been developed. The primary reason for the development of the airflow simulator is to be able to study sensor output under different airflow conditions by varying the airflow cycle and air volume through the simulator, in order to verify the measurement principle and mathematical model developed in chapter 3 for quantitative airflow monitoring. The respiration simulator also provides a mechanism to separate the piezoelectric and the pyroelectric effects of the sensor enabling the study of these two effects separately. The separation of the pyro- and piezoelectric effects is necessary to quantify the piezoelectric effects of the sensor caused by the flow pressure only and be able to isolate the thermal or temperature effects.

A miniature piezoelectric unimorph bending sensor has been developed specifically for the study of airflow monitoring. The dimension of the sensor is important due to it's placement over the nose and the mouth so as not to block the airflow. In addition, adequate thickness ratio of piezoelectric to substrate layer is achieved to provide maximum electromechanical coupling coefficient so that the sensor is sensitive enough to detect the variation of airflow speed.

# 4.2 Sensor Development

A miniature unimorph bending sensor has been developed in this thesis using a piezoelectric membrane transducer for the purposes of airflow monitoring and detection. Figure 4.1 presents a picture of the miniature sensor used in this dissertation.

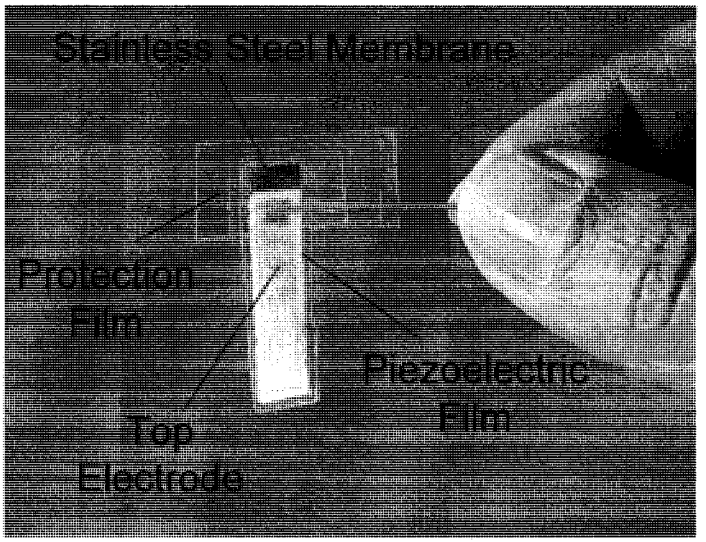


Figure 4.1: Miniature unimorph bending sensor for airflow monitoring.

The length of the piezoelectric film is 29mm and the width is 6mm, and the length of the top electrode is 22mm and the width is 4mm. As per the calculations in Chapter 3, maximum electromechanical coefficient occurs when the thickness ratio between substrate and piezoelectric layer is 0.41. The thickness of the stainless steel membrane is 40 μm and the thickness of the piezoelectric film is 60μm providing a thickness ratio of substrate to piezoelectric layer of 0.67. Future development of the sensor will focus on increasing the thickness of the piezoelectric layer to approximately 100 μm, in order to

get a ratio that is as close as possible to 0.41 to maximize the electromechanical coupling coefficient.

# 4.3 Respiration Simulator System

A piston-pump system is used to simulate breathing. The volume of air breathed during normal respiration (tidal volume) of adult, is on the average about 500 ml. Thus, the volume of the piston pump used for simulation purposes for the experiments is chosen to be 500 ml.

Figure 4.2 presents a block diagram of the respiration simulator system and Figure 4.3 provides a picture of the system developed for the experiments in this thesis. A 500ml piston pump was tightly mounted on a wooden structure to provide stability and to reduce experimental errors due to unwanted movement. [41], [42]. The pump was connected to a plastic tube which in turn was connected to a square tubing (airflow chamber) that housed the piezoelectric sensor developed. The airflow chamber was also mounted on a wooden structure to avoid movement. The airflow chamber was constructed using an acrylic pipe whose internal cross-section had a rectangular shape with the length of 2.2cm and the width of 1.1cm. The cross-sectional area of the tubing used was $2.42 \times 10^{-4}$ $m^2$. The sensor was placed in the tubing such that one end of the sensor was fixed while the other end was free moving. The fixed end of the sensor was held in the tube using an adhesive tape. A slight slit was made through the square tube where the sensor was inserted. This ensured that one end of the sensor was fixed during breathing simulation, while the other end was free. The sensor can be mounted on the airflow chamber in the following two ways; the sensor surface is normal to the airflow to

measure air pressure effects using the piezoelectric response of the sensor; and parallel to airflow to eliminate the pressure response for temperature effect measurements using the pyroelectric response. The other end of the square pipe was connected to a plastic tube and into a spirometer. A charge amplifier (Type 2635, Brüel & Kjær, Denmark) was used to amplify electric charge signals from the sensor into a usable output voltage for an analog-digital (A/D) convertor having an input range of ±10V. Nominal output voltage from the sensor is in the range of 0 to 50 mV. Depending on the pumping cycle and/or airflow volume, a gain of between 50dB and 70dB was used to amplify the signal without overloading the charge amplifier or the A/D convertor which had an input range of ±10V. For data analysis, all data were adjusted and analyzed at a common gain value of 60dB after digitization.

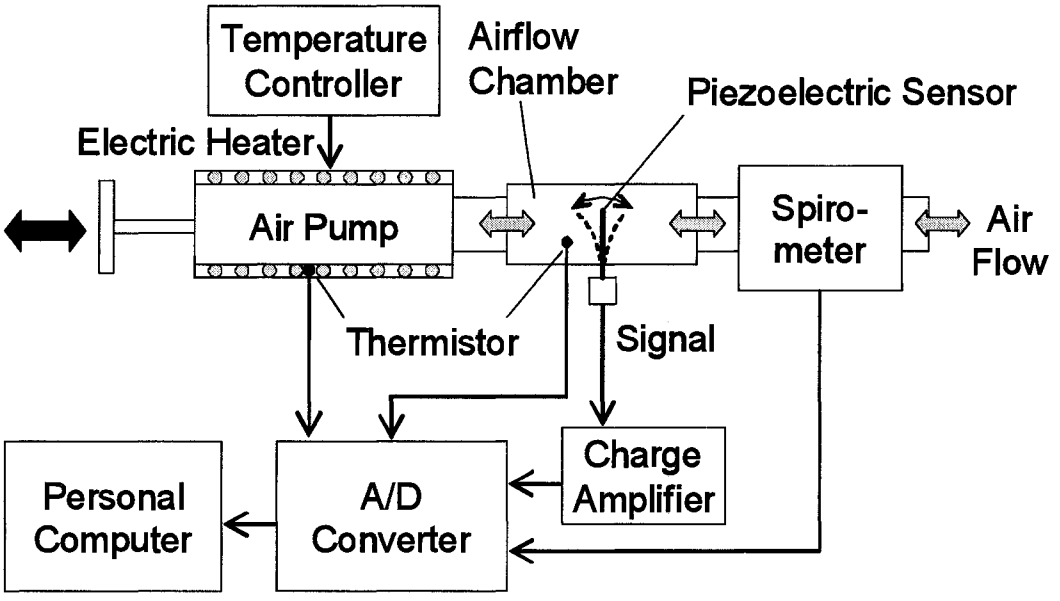


Figure 4.2: Respiration simulator system.

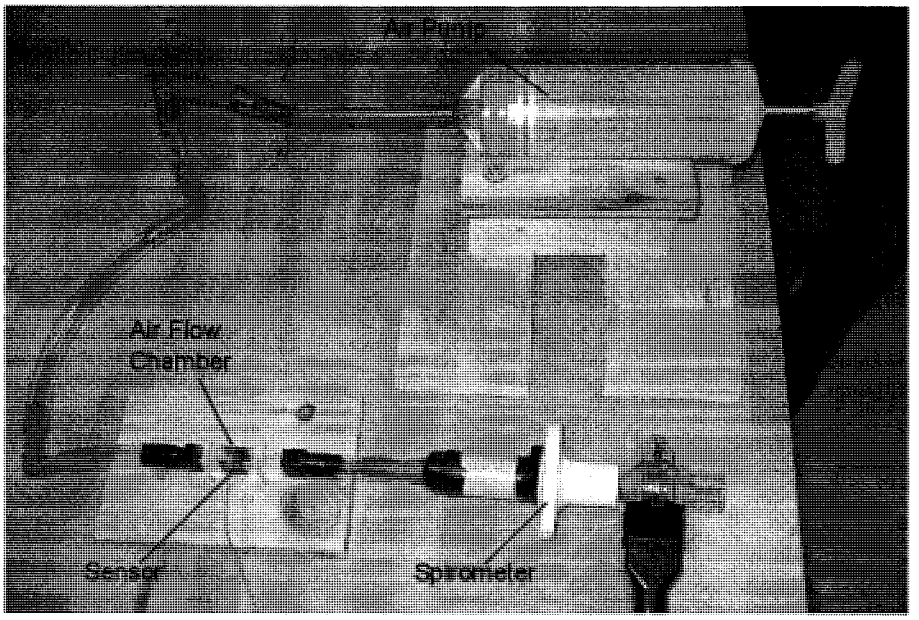


Figure 4.3: Picture of the respiration simulator system

Figure 4.3 shows a picture of respiration simulator system used in the experiments. The picture does not show the signal acquisition components such as the charge amplifier, A/D converter and personal computer as well the electric heaters that were used to introduce temperature variations to the system. Temperature variations were introduced by covering the piston pump as well as the pipe connecting the airflow chamber with the electric heaters.

Flow rate was controlled by changing the cycle and volume of air being pumped through the membrane sensor and the spirometer. At the time of the experiments for this thesis work, the pump was driven manually. Therefore, the cycles and air volume pumped were controlled using a timing alarm and the scale on the pump, respectively. In future work, a mechanical translation stage driven with an electric motor would be equipped with the pumping system so that more accurate airflow control could be realized and the need for manual pumping can thus be eliminated.

A spirometer (Vernier Software & Technology, USA) was used to measure the airflow rate, in order to compare the sensor output signals with the flow speed inside the airflow chamber where the sensors is installed. The flow speed ($V_f$) can be calculated by

$$V_f = \frac{Q}{A} \qquad (4\text{-}1)$$

Where Q is the airflow rate (provided by the spirometer) and A is the area of the airflow chamber.

The spirometer is composed of a removable flow head and a differential pressure transducer. The flow head of the spirometer consists of a plastic housing through which air is forced. In the center of the flow head is a mesh screen. As air is forced through the flow head a slight difference in pressure occurs between the front and the back surface of the screen. A tube in front of the screen and a tube behind the screen pass the pressures to a differential pressure transducer. Airflow rate can thus be measured directly [18]. The change in air volume can then be inferred from the integrated airflow signal over time. The above set up provided with a mechanism to quantify piezoelectric effects only as no change in temperature was introduced during the first stage of the experiments. The spirometer used was set to match the stored calibration before shipping and the vendor does not recommend any calibration process.

In actual breathing, the temperature beneath the nose or above the mouth varies periodically due to inhalation of surrounding air and exhalation of warm air from the body. Therefore, the second stage of the experiments introduced changes in temperature to the above setup. Changes in temperature generate pyroelectric response of piezoelectric sensor. To introduce changes in temperature to the air in the airflow chamber in the simulator, the piston pump was covered with the electric heater as

indicated in the figure 4.2. The heater has the ability to increase and control the temperature up to 70°. In our experiments, the actual air temperature in the air chamber reached up to around 40° but not 70° due to large air volume and poor heat conductance of the pump material (plastics). The temperature control up to 40° is enough and appropriate to simulate the temperature of actual breathing air. Two thermistors were inserted inside the air chamber and between the pump housing and the heater, respectively, in order to monitor and control the air temperature beside the piezoelectric sensor.

One could argue that since the spirometer is used to measure airflow in these experiments, that we could equally well use the spirometer to measure airflow for detection of apneic episodes. While the spirometer can be used to measure airflow, these measurements usually extend over a short period of time covering a few breathing cycles. Spirometer cannot be used reliably as a breathing monitoring device, since that would require a stable operation of the spirometer over an extended period of time. For a number of reasons as covered by the work done by Zhang *et al* [21] [22], the spirometer signal usually drifts away significantly from its original baseline and thus impairing its ability to be used for breathing monitoring for a long time. In order to prevent drifting of the spirometer signal, the spirometer must be held vertically and very still for the duration of the use, which is not possible during sleep. In addition, wearing a spirometer during sleeping may not be comfortable, thus it is not suitable as a home device.

A data collection device (Labpro from Vernier Systems) was used as part of data acquisition system. The Labpro used was equipped with six input channels which allowed for simultaneous data collection. The piezoelectric sensor, the spirometer and the

two thermistors were connected to Labpro. The Labpro has a 12 bit analog to digital convertor and capable of collecting up to 50,000 samples per second. The Labpro data collection system running on a desktop allowed for simultaneous data collection from these sensors. The data collected included time, output voltage signals from the sensor, airflow rate from the spirometer as well as temperatures from the thermistors.

Airflow applied to the piezoelectric sensor through the pumping action of the piston generated voltage in the sensor resulting from the bending deformation of the sensor. The flow rate was measured by the spirometer and the voltage generated was measured directly using a voltage probe. In the case where temperature changes were introduced, a thermistor was also used to measure the temperature of the air in the respiratory simulation system.

# 4.4 Summary

The main benefit of using a flow simulator developed in this thesis is to provide a mechanism to simulate human breathing under different conditions such as different breathing cycles as well as different air volume. The simulator also enables to isolate piezoelectric and pyroelectric effects of breathing and study each of these effects independently. A 500ml piston pump was used to simulate airflow due to breathing. The volume and cycle of flow rate are varied to study the sensitivity of the sensor to volume and breathing cycle, which will be discussed in chapter 5. Pyroelectric effects are also studied by introducing temperature change in the air chamber where the piezoelectric sensor is installed. A data acquisition device along with the data acquisition software is

used to provide simultaneous data collections of the sensor output voltage, flow rate and temperature for different airflow volumes and cycles.

# Chapter 5

# Simulation Experiments and Discussion

## 5.1 Overview

The purpose of this chapter is to investigate experimentally the piezoelectric response of the unimorph bending sensor caused by airflow due to breathing as well as pyroelectric response by the temperature variation, in order to quantify airflow variations using the unimorph bending sensor developed. For such purposes the airflow (breathing) simulator constructed in Chapter 4 is used for the experiments. The simulator provides a mechanism of understanding sensor output under varying airflow conditions including variations in airflow volume and breathing (expiration and inhalation) cycle. The simulator also provides the capability of studying the effects of pressure and temperature variations separately and in isolation from each other.

As mentioned previously, the objective of the experiments is also to verify the measurement principle and mathematical model developed in chapter 3, in order to quantify airflow using the output voltage signal of the sensor. Because normal breathing is composed of both variations in airflow rate and air (breath) temperature, it is important to understand each of these effects in isolation. As described in Chapter 3, a mathematical model has been developed that provides for a direct relationship between the output voltage and airflow speed. However, the relationship between change in temperature and

output voltage is an indirect one since correlation between airflow speed and temperature variations is highly dependent on the surrounding temperature environment. As mentioned in Chapters 1 and 2 of the thesis, quantification of airflow is necessary for detection of hypopnea. Thus, an electric heater was also added to the simulator to understand pyroelectric response of the sensor resulting from the change in temperature.

Experiments were carried out in two main phases; the first phase was to understand piezoelectric effects of the sensor by applying air flow pressure through the simulator at a constant temperature. The sensor was subjected to varying airflow speeds which were applied by varying pumping cycles and air volumes. The second phase of the experiments introduced temperature changes to the airflow and again varying airflow speed were applied at different pumping cycles and air volume. In this phase the sensor was placed parallel to the flow, such that there were no piezoelectric effects resulting from the pressure of the airflow, however there could be secondary piezoelectric effect that resulted from the thermal expansion of the sensor caused by temperature changes as discussed in chapter 3.

# 5.2 Pressure Response of Sensor

## 5.2.1 Airflow variations of Actual Breathing

Before conducting experiments using the flow simulator, it would be interesting to understand the baseline of actual human breathing in terms of flow rate and flow speed under different breathing conditions.

Airflow rate under different conditions was measured using a spirometer. A 40 year old male subject breathed into the spirometer under three different breathing cycles, fast (45 breaths per minutes: bpm) medium (20 bpm) and slow (10 bpm). These three conditions may be rather subjective, but provide enough variations in the breathing conditions as accounted in the experiments conducted. Figure 5.1 (a) provides the flow rates for a 40 year old male subject breathing into the spirometer under these three different breathing conditions. The positive flow rate corresponds to exhalation and the negative one to inhalation. The sensor handle was held manually and the subject was required to both inhale and exhale through the spirometer. To ensure that the subject is only breathing through his mouth, the subject held on to his nose. The spirometer was held vertically and still during the measurements to ensure that the "zero" point of the spirometer is not altered.

One possible configuration for monitoring breathing using the unimorph bending sensor developed, is to attach the sensor underneath the nasal opening. Therefore, the diameter of the subject's nasal opening was measured and its area ($A_{nose}$) was calculated, in order to estimate the flow speed ($V_f$) beneath the nose by $V_f = Q/ (A_{nose})$, where Q is the airflow rate (liter) per second. The flow rate from the spirometer which is provided in L/s is converted to $m^3/s$ using the conversion of 1 $m^3$ is equal to 1000 Liters. The area of the subject's nose was calculated to be $1.77 \times 10^{-4}$ $m^2$. Figure 5.1 (b) presents airflow speeds beneath the nose estimated from the result of measured flow rates shown in Figure 5.1 (a), assuming that the $A_{nose} = 1.77 \times 10^{-4}$ $m^2$ as discussed above. From these results, the maximum airflow speed beneath the nose due to breathing is estimated within the range of ±4 m/s in these experimental conditions. The goal of the experiment was to get an

estimate range of actual flow speeds to ensure that the range of flow speed is covered within the experimental conditions.

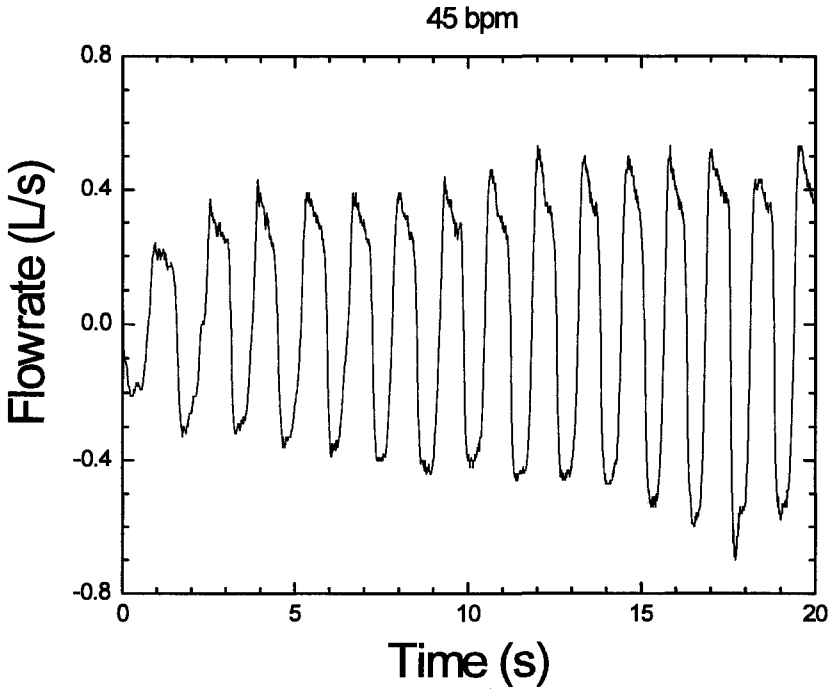


Figure 5.1a: Measured airflow rates of actual breathing of a male subject using spirometer with breathing conditions of fast (45 bpm). (Continued on next page)

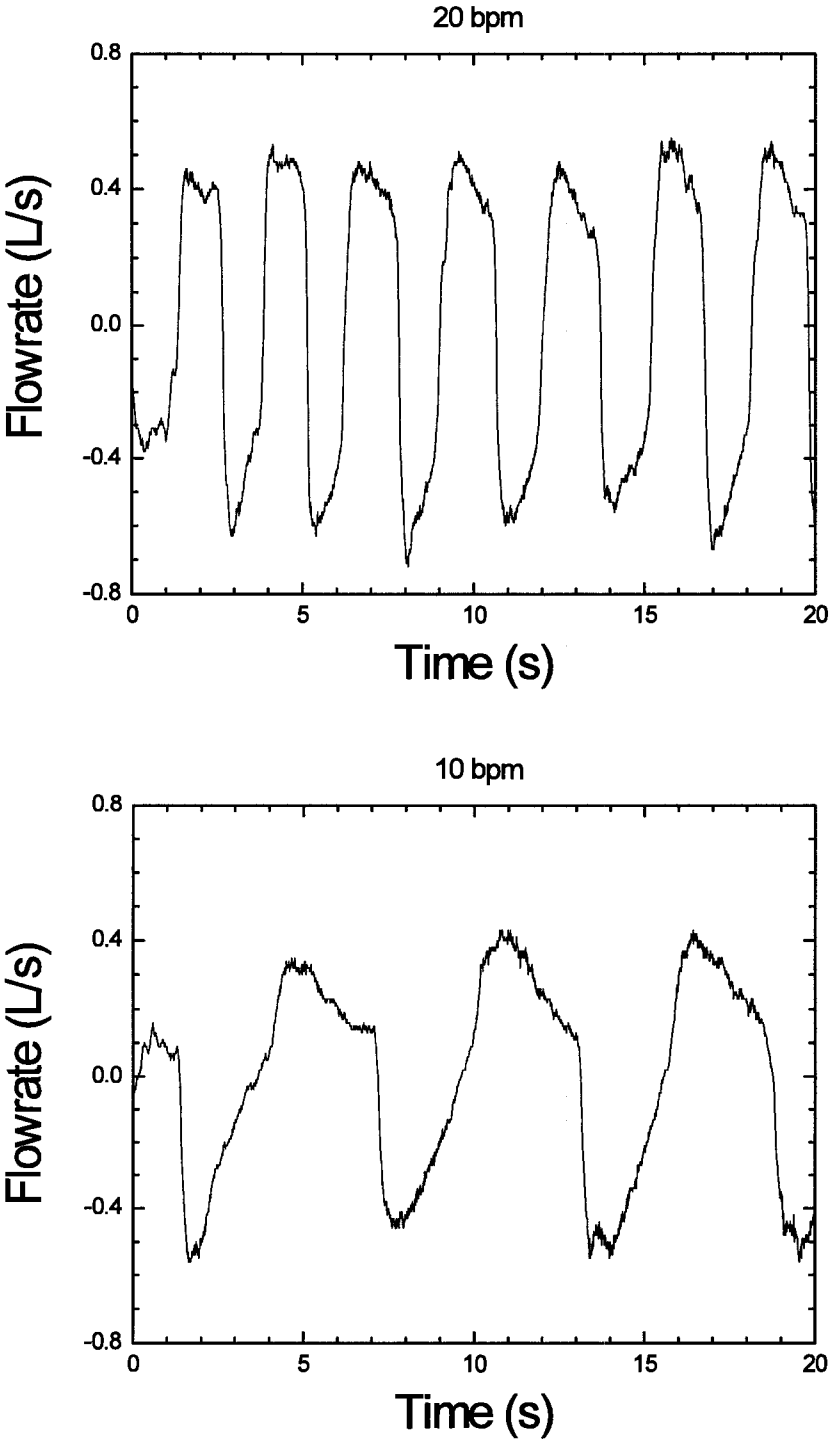


Figure 5.1a: Measured airflow rates of actual breathing of a male subject using spirometer with breathing conditions of fast medium (20 bpm) and slow (10 bpm).

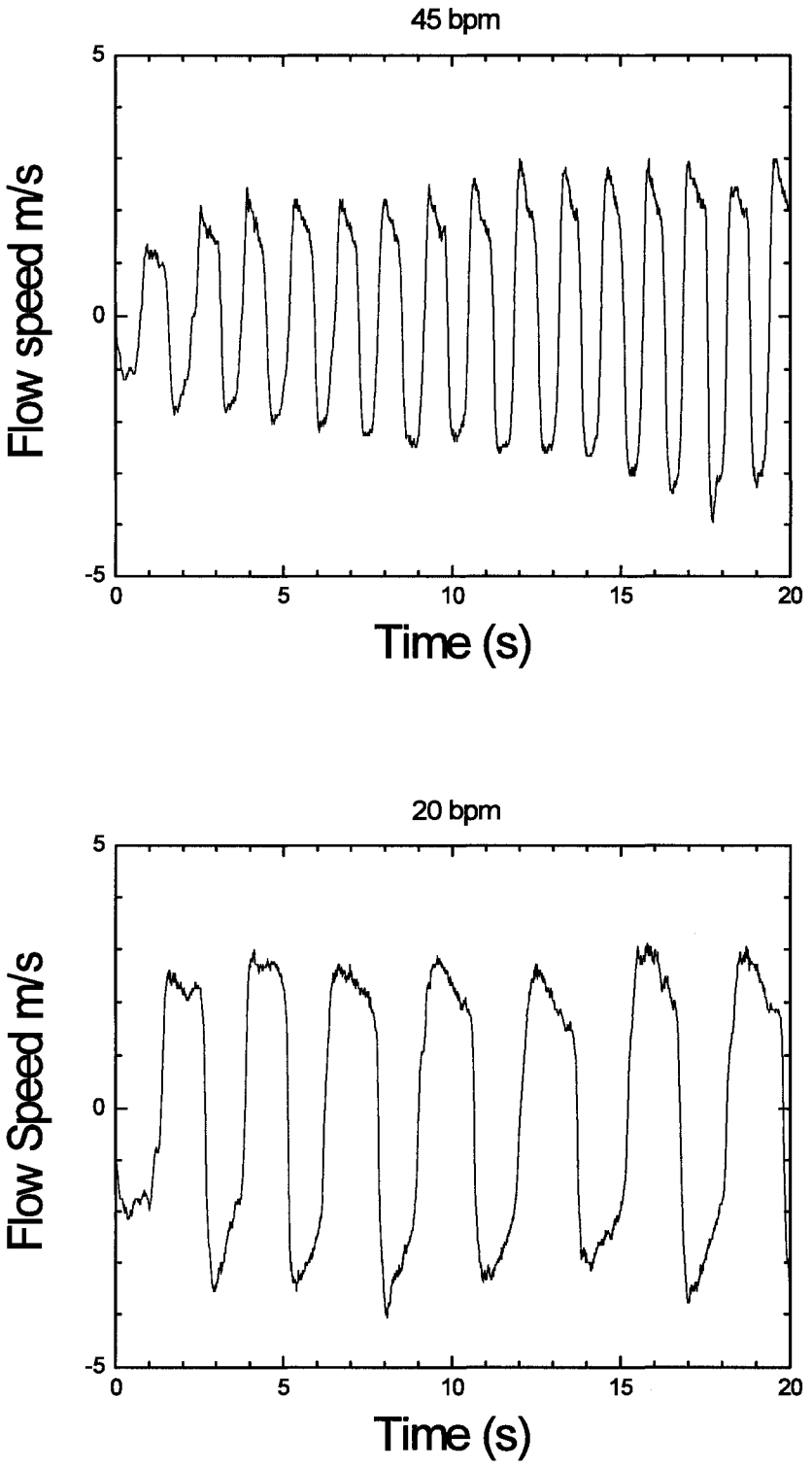


Figure 5.1b: Airflow speed of actual breathing of an adult male subject using spirometer with breathing conditions of fast (45 breathing per minutes: bpm), medium (20 bpm
(Continued to next page)

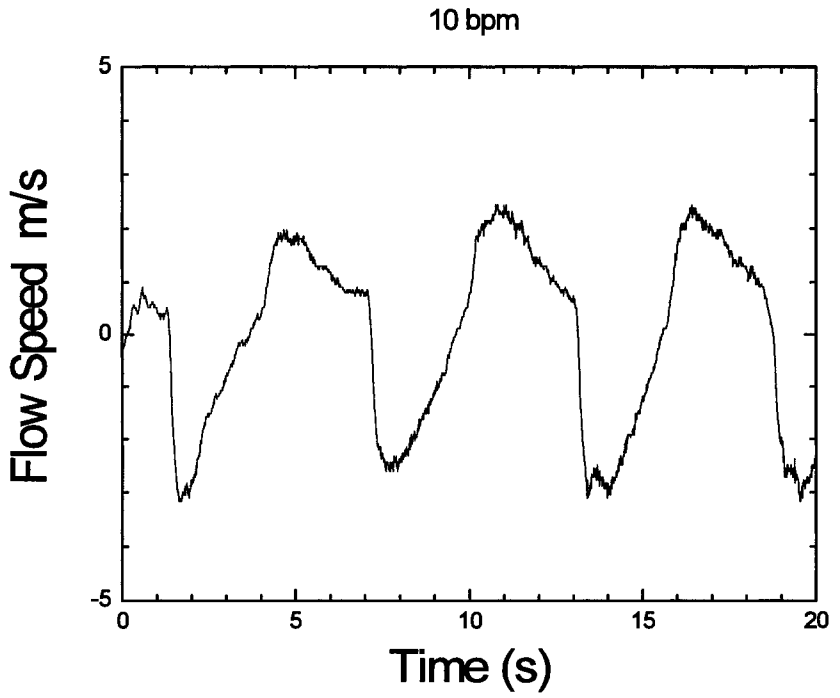


Figure 5.1b: Airflow speed of actual breathing of an adult male subject using spirometer with breathing conditions of fast (45 breathing per minutes: bpm), medium (20 bpm) and slow (10bpm).

## 5.2.2 Experiments and Results

Piezoelectric response of piezoelectric unimorph bending sensor with airflow pressure (speed) was investigated using the respiration simulator system described in chapter 4. The piezoelectric unimorph bending sensor was placed so that its surface is perpendicular to the direction of the airflow to ensure that airflow pressure is being applied normal to the sensor. Such placement of the sensor is important in order to produce stress in the piezoelectric layer in its length direction when the sensor bends due to airflow pressure applied, resulting in voltage signal output from the sensor. The reciprocal airflow was provided using the piston pump. Both the voltage signal from the sensor and the airflow rate measured by the spirometer were acquired simultaneously via

the data acquisition system. In this experiment, the electric heater is off so that air temperature is kept constant during the experiments. Therefore, the output voltage signal from the sensor is solely due to piezoelectric response of the sensor.

A voltage probe is attached to the sensor electrodes to measure the output voltage signals from the charge amplifier. A gain of between 50dB to 70dB was applied to the output voltage of the sensor. The applied gain was dependent on getting a quality signal without overloading the charge amplifier or exceeding input range (±10V) of the A/D convertor. However for data analysis purposes, all data was adjusted to the same gain values after digitization. The flow rate through the airflow chamber where the sensor was installed was also measured using a spirometer. Both the spirometer and the voltage probe were connected to the data acquisition system allowing both data sets to be captured at the same time. Both pumping cycle and volume of the airflow were varied in the experiments. Two kinds of experiments were conducted with the following experimental conditions: (1) different pumping cycles with a constant airflow volume; (2) different airflow volumes with a constant pumping cycle. The volume was varied from 100 ml to 500 ml in increments of 100 ml. The cycle was varied from 15 cycles per minute (cpm) to 90 cpm in increments of 15 cpm.

Breath cycle of 30 cpm is deemed to be typical of human breathing with a tidal volume of 500ml. Figure 5.2 provide sensor output voltage and flow speed with respect to the measurement time with a pumping cycle of 30 cycles per minute (cpm) while varying the airflow volume from 500ml to 100ml. Data for 15, 45, 60, 75 and 90 cycles per min (cpm) are provided in the appendix B. From the results in Figure 5.2, the output voltage of the piezoelectric sensor with respect to the airflow speed at the cycle of 30

cmp is obtained. All data are adjusted to the same gain value of 60dB. The output voltage is obtained directly from the voltage probe connected to the sensor via the charge amplifier and the flow rate is obtained from the spirometer in L/s. The flow rate is converted to $m^3/s$ and divided by the cross-section area of the tubing to obtain flow speed at the bending sensor inside the tubing.

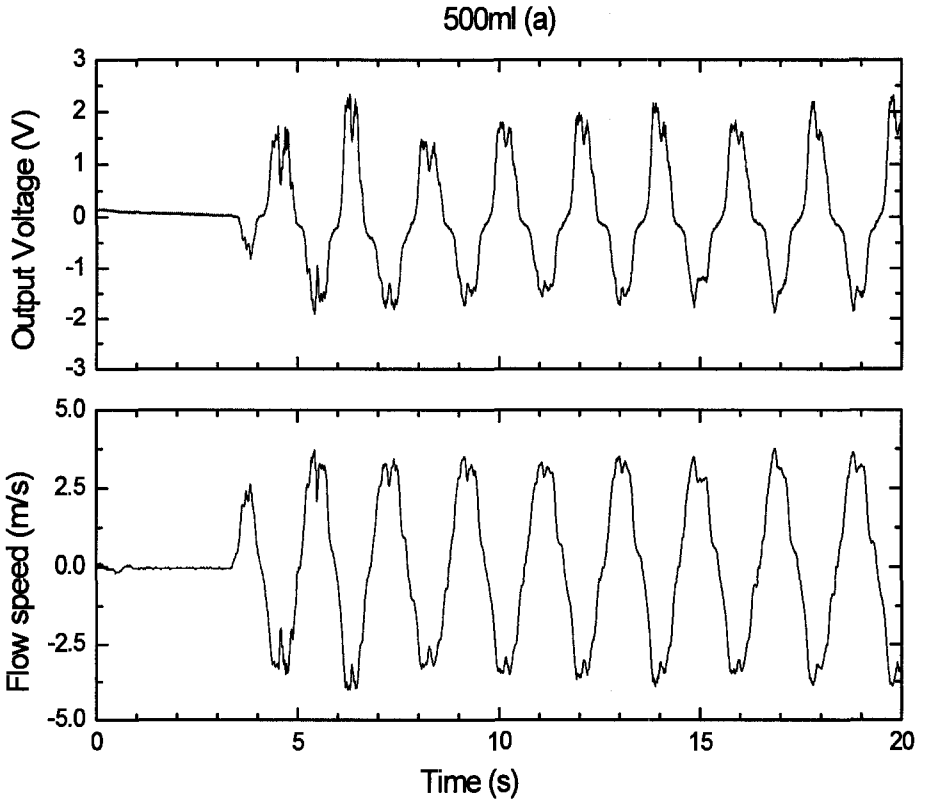


Figure 5.2: Output voltages of piezoelectric sensor and flow speed obtained from spirometer with respect to the time at a constant pumping cycle of 30 cycles per minute for volume 500 ml (a). (Continued to next page).

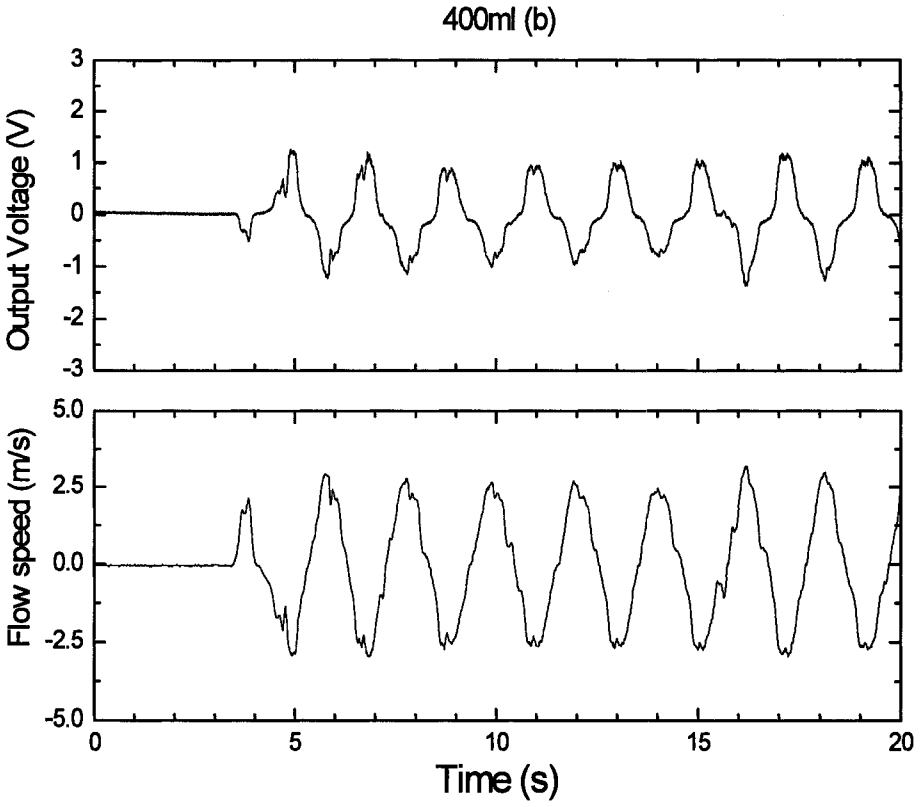


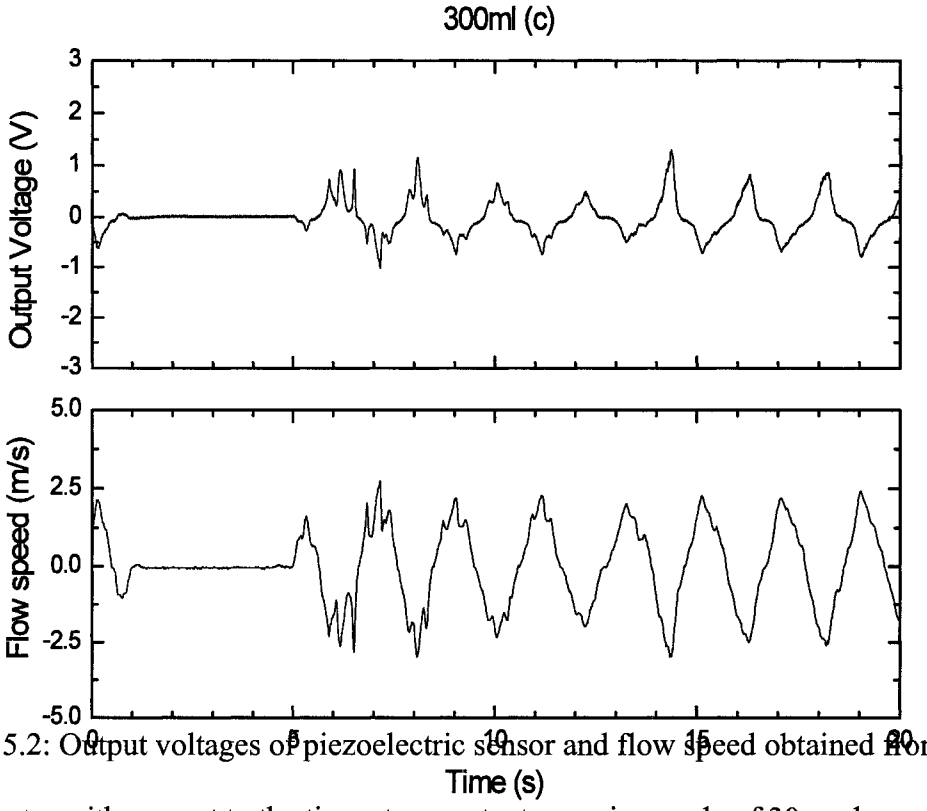


Figure 5.2: Output voltages of piezoelectric sensor and flow speed obtained from spirometer with respect to the time at a constant pumping cycle of 30 cycles per minute for volumes 400 ml (b), 300 ml (c). (Continued to next page).

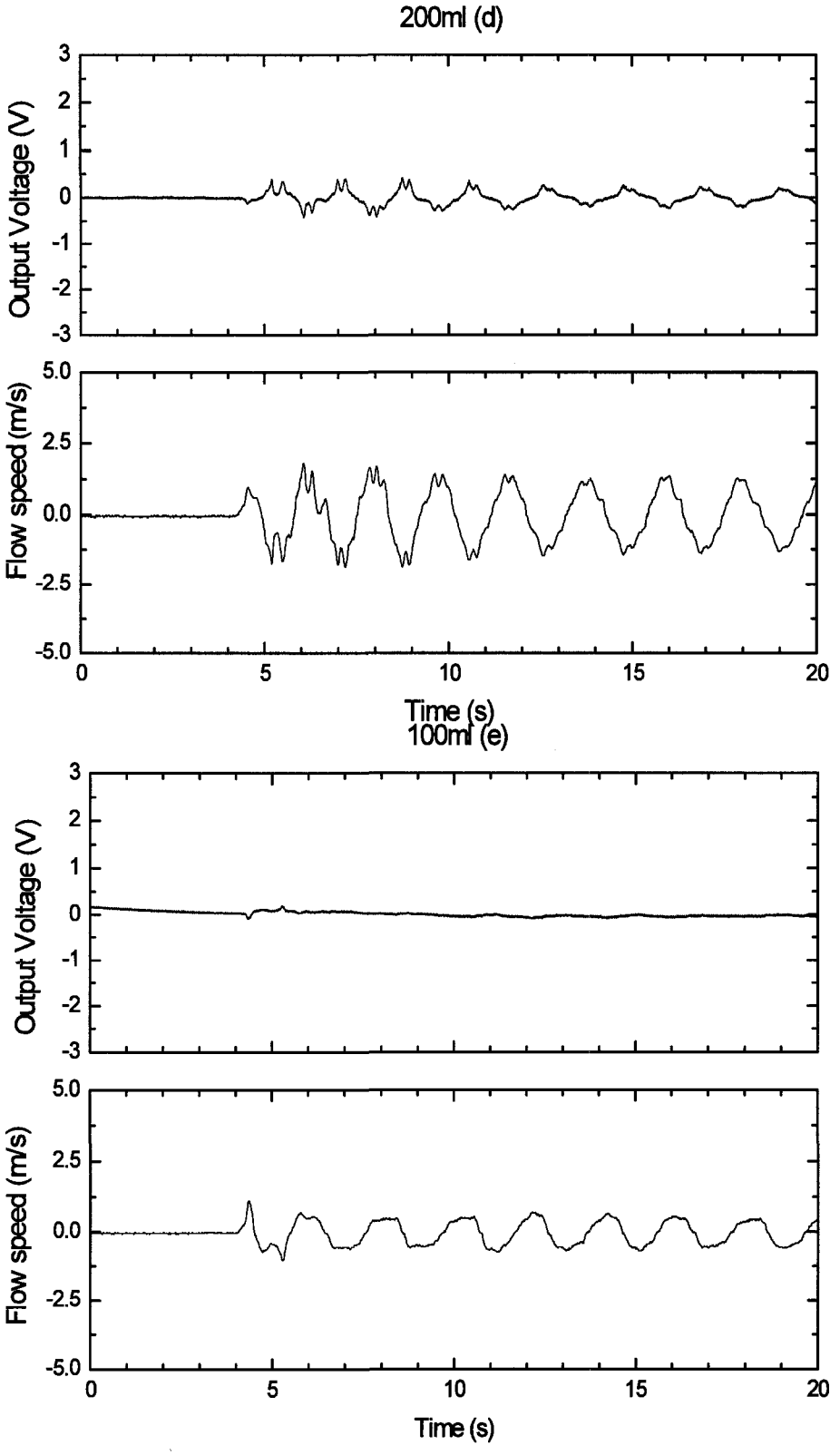


Figure 5.2: Output voltages of piezoelectric sensor and flow speed obtained from spirometer with respect to the time at a constant pumping cycle of 30 cycles per minute for volumes 200 ml (d) and 100 ml (e).

Figure 5.3 provides the results of the output voltage with respect to the flow speed obtained from the results in Figure 5.3 under the experimental conditions employed. For each instance of time, the output voltage was plotted against the flow speed. The flow speed was calculated from the flow rate that was acquired from the spirometer. All data was adjusted with a common gain of 60dB. One can note that all the experimental data for various air volumes fall onto one curve.

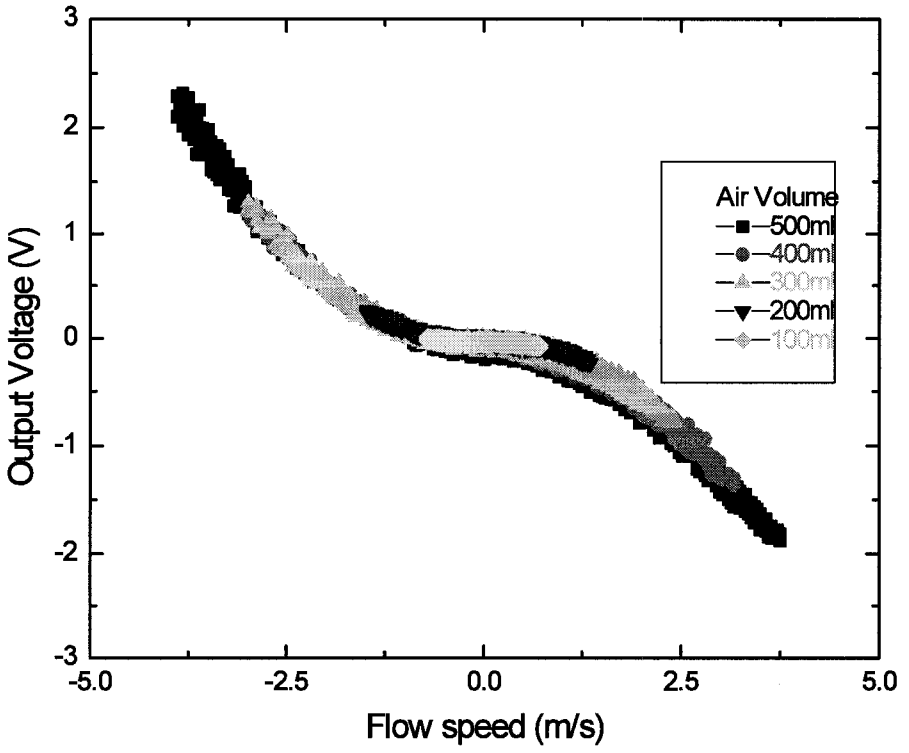


Figure 5.3: Output voltage of the piezoelectric sensor with respect to the airflow speed at a constant pumping cycle of 30 cpm, obtained from the results in Figure 5.2.

Figure 5.4 provide sensor output voltage and flow speed with respect to the measurement time with a constant volume of 500ml while varying the pumping cycles. Data for the other volumes are presented in the appendix B.

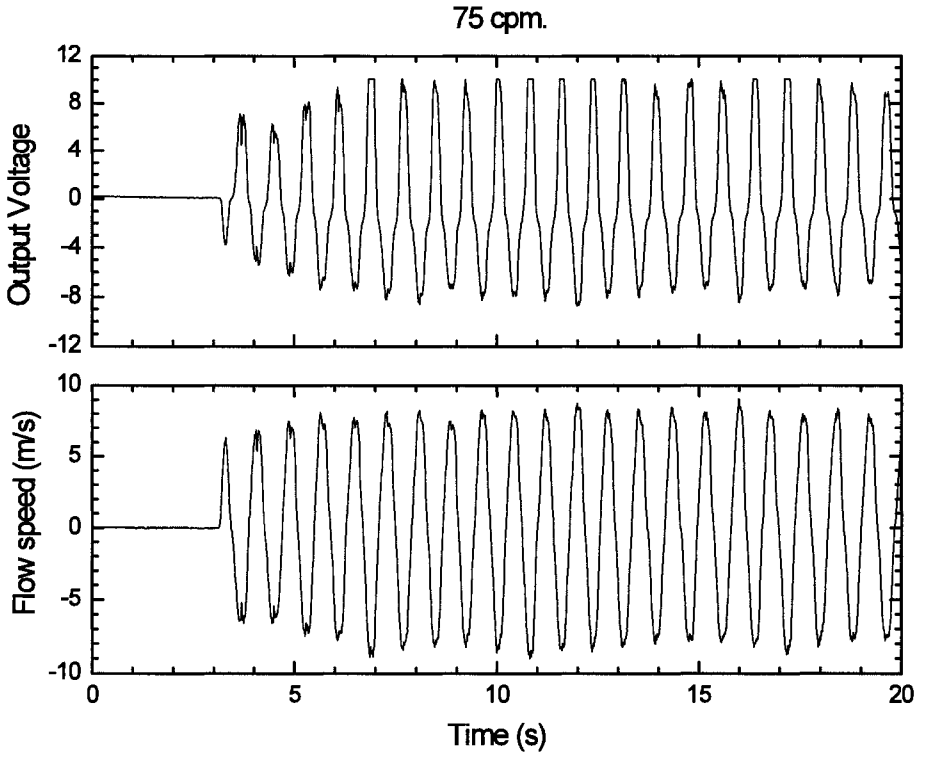


Figure 5.4: Sensor output voltage and flow speed with respect to the measurement time with a constant volume of 500ml for pumping cycles from 75 cpm to 15 cpm with a step of 15 cpm. (Continued to next page)

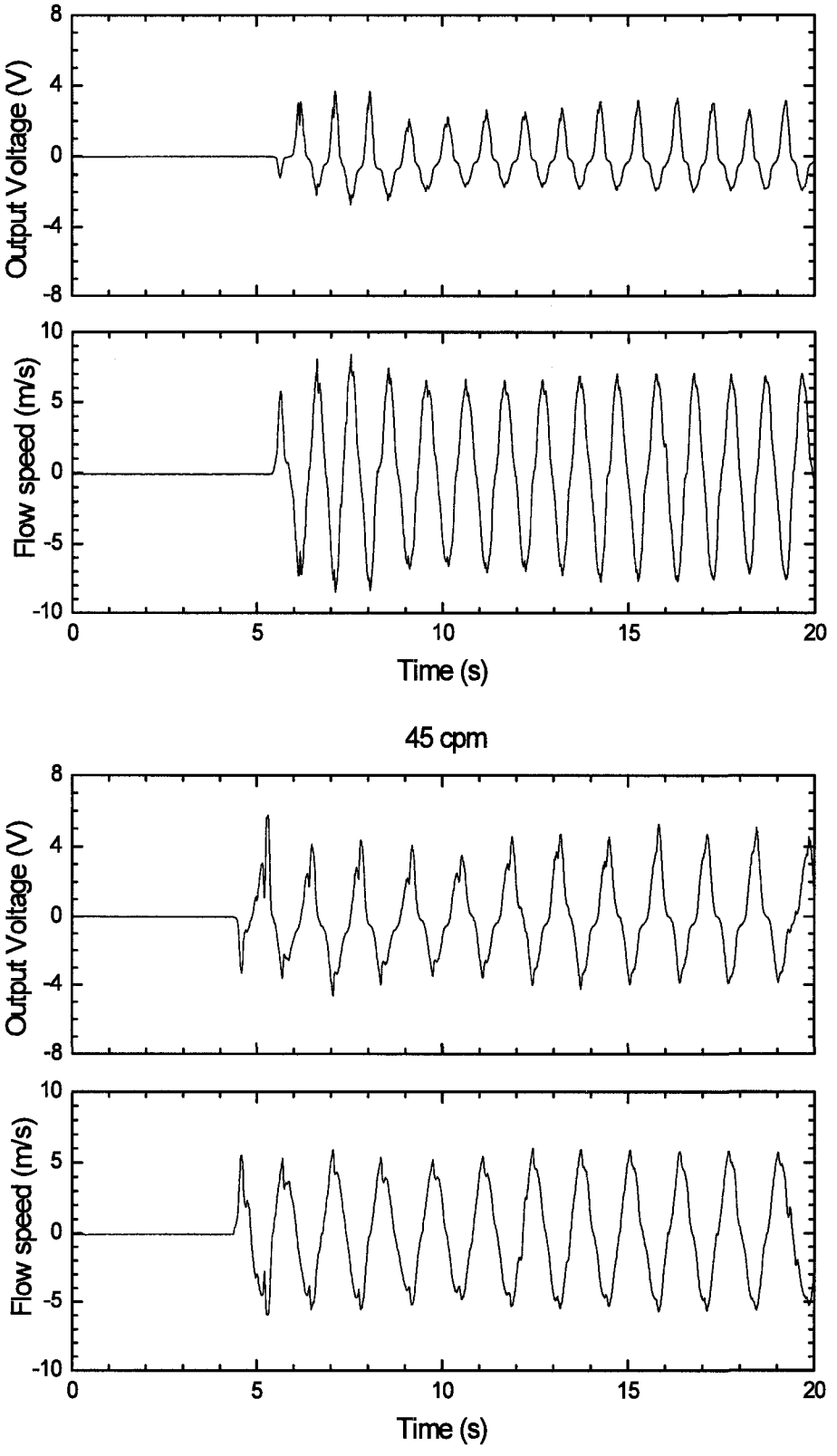


Figure 5.4: Sensor output voltage and flow speed with respect to the measurement time with a constant volume of 500ml for pumping cycles from 75 cpm to 15 cpm with a step of 15 cpm. (Continued to next page)

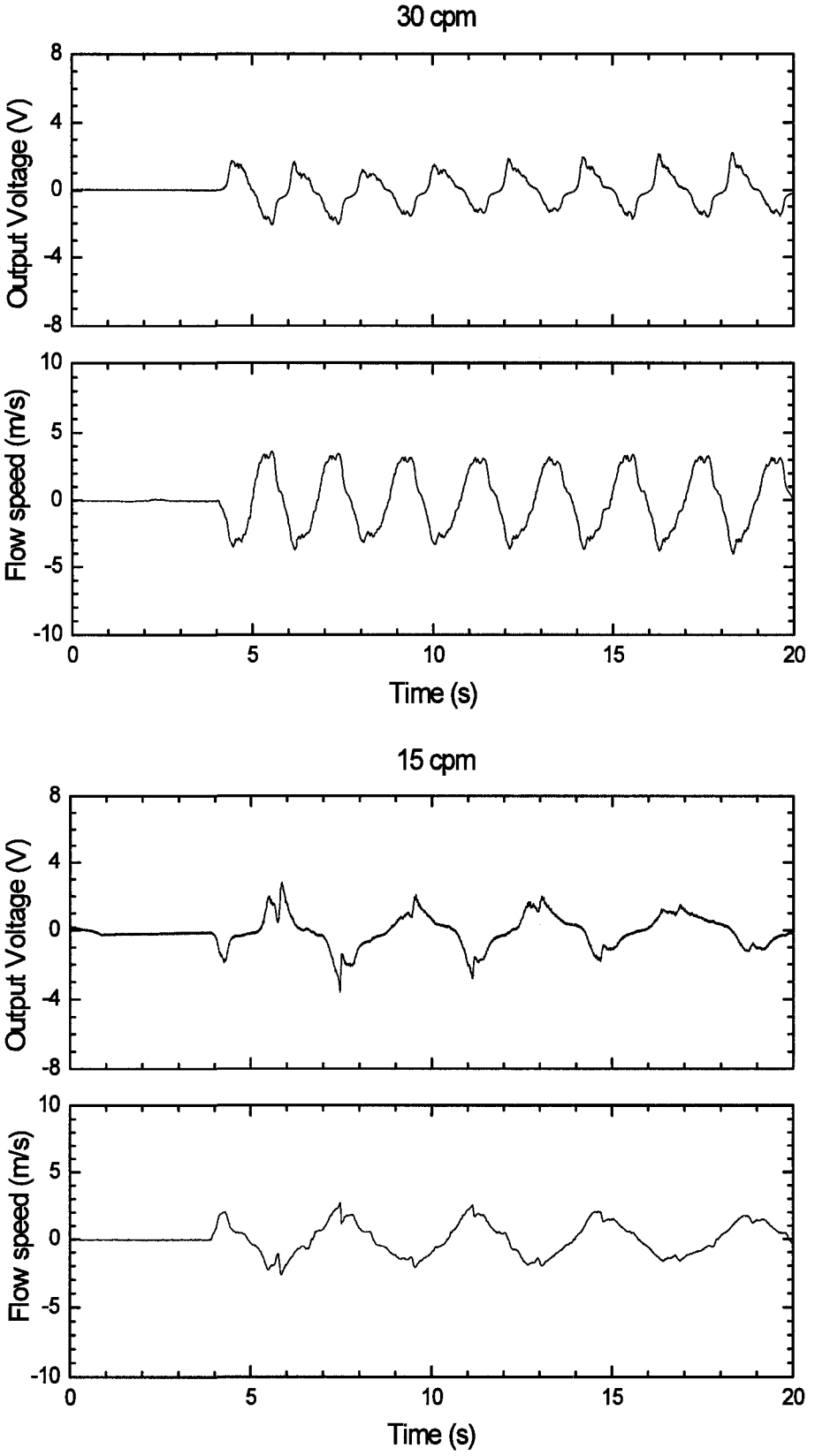


Figure 5.4: Sensor output voltage and flow speed with respect to the measurement time with a constant volume of 500ml for pumping cycles from 75 cpm to 15 cpm with a step of 15 cpm.

Figure 5.5 represents the output voltage of the piezoelectric sensor with respect to the airflow speed at various pumping cycles. All data was converted to a common gain of 60dB. All experimental data fall on the same curve as in Figure 5.3. Output voltage can therefore be used to uniquely determine airflow speed independent of pumping air volume and cycle.

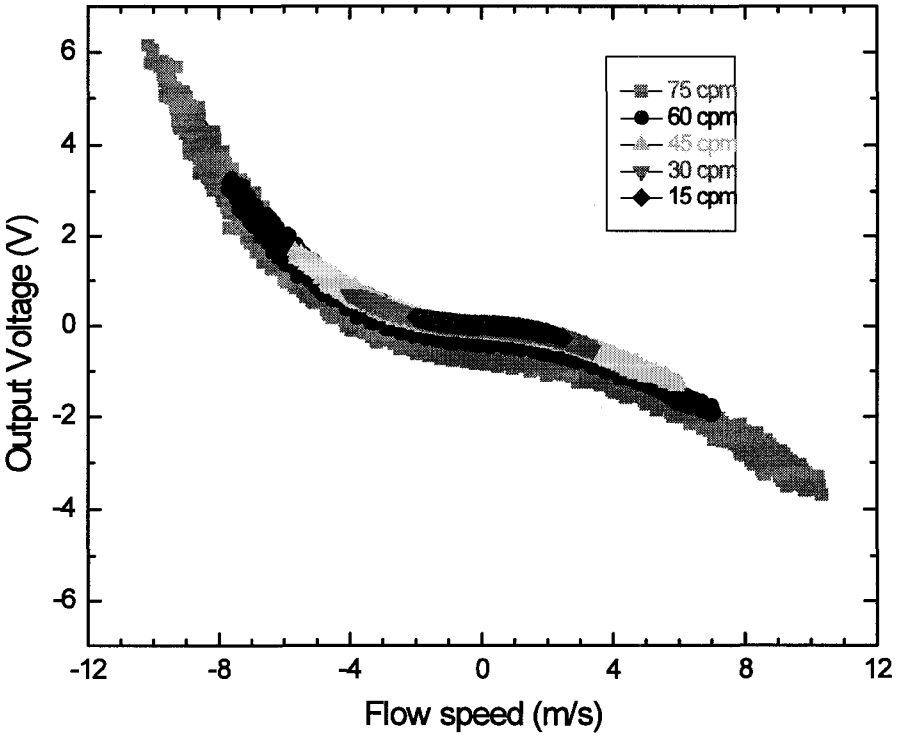


Figure 5.5: Output voltage of piezoelectric sensor with respect to airflow speed at a constant volume of 500ml, obtained from results in figure 5.4.

### 5.2.3 Discussions

Figures 5.1 (b) indicates that the airflow speed beneath the nose of a healthy 40 year old male could be in the range of ±2m/s to ±4 m/s for fast (45 bpm), medium (20 bpm) and slow (10 bpm) breathing. The experimental results with the simulator in Figure 5.3 also cover the airflow speeds ranging from -4m/s to about 4m/s. The output voltage signal varies with the flow speeds, with higher airflow speeds producing larger output voltage.

Figure 5.6 shows the result with the flow volume of 500 ml and the cycle of 30 cpm, extracted from the results in Figure 5.3. The two solid lines are the second order polynomial fitting curves obtained from the data covering the range of negative and positive flow speeds respectively. The output voltage (V) of the sensor and the square of the flow speed ($V_f^2$) are related by a second order equation as indicated in equations (5-1) and (5-2). The second order polynomial curve fitting will enable us to determine a calibration curve that can be used to determine the flow speed and hence air volume based on a given output voltage from the sensor. The determined air volume can then be of assistance in preliminary diagnosis of apnea or hypopnea.

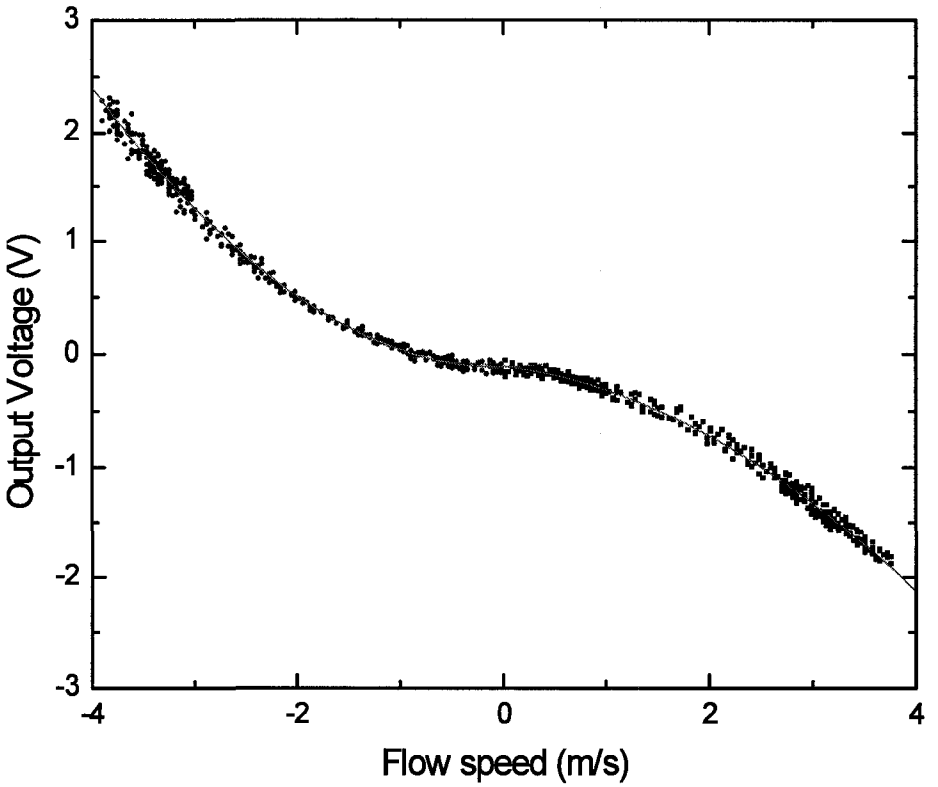


Figure 5.6: The experimental result with the flow volume of 500 ml and the cycle of 30 cpm, extracted from the results in Figure 5.3. The two solid lines are the second order polynomial fitting curves obtained from the data in negative and positive airflow speeds respectively.

In Figure 5.6, the equations of the curve fitting given by the solid lines indicate the relationship between output voltage and flow speed in this experimental condition as follows.

$$V = -0.0998V_f^2 - 0.107V_f - 0.106 \qquad (V_f > 0) \qquad (5\text{-}1)$$

$$V = 0.160V_f^2 + 0.00816V_f - 0.116 \qquad (V_f < 0) \qquad (5\text{-}2)$$

As one may note that the equation for negative flow speed ($V_f < 0$) is different from that for positive flow speed ($V_f > 0$), i.e. the coefficients are different. This is due to the asymmetrical structure of the unimorph sensor. The graph also indicates that even

when the flow speed is zero, there is a minor offset in the curve; the output voltage would ideally be zero, when flow speed is zero. The reason for this offset value is currently not well understood and needs to be investigated in future work. These fitting curves could be used as a calibration curve to determine the flow speed from the output voltage measured.

It should also be noted from Figure 5.5 and 5.6 that flow speed variations in the range of ±1m/s may not be detectable due to the reproducibility of about 0.2V for output voltage measurement when flow speeds for different volumes are plotted on the same curve.

During sleep, an average person breaths approximately 10 breaths/min with a tidal volume of 250ml per breath. This would result in an approximate air volume of 42 ml/sec. If hypopnea is defined as a minimum reduction of 30% or more in airflow volume, then the sensor should be able to detect at least 30 ml/sec (30% reduction from 42 ml/sec) or an equivalent of $3x10^{-5}$ $m^3/s$. The area of subject's nostril has a cross-sectional area of $3.54x10^{-4}$ $m^2$ (= $A_{nose}$ x 2) and therefore the sensor should be able to detect flow speeds of 0.09 m/s or less. Analyzing the data in Figure 5.7, which is the experimental condition of pumping volume of 100ml and pumping cycle of 15cpm, the average of the noise level, is calculated to be 0.04V and the standard deviation ($\sigma$) to be 0.01V. This is calculated using the data in Figure 5.7, when no airflow is presented (0-5 sec).

The sensor sensitivity was therefore determined from Figure 5.7 as 2.3 (m/s)/V. This was determined from dividing the average peak-to-peak flow speed attained at 15 cpm and 100ml by the average peak-to-peak voltage attained. Applying 4σ of 0.04V as the voltage measurement resolution and the sensor sensitivity of 2.3 (m/s)/V, the resolution of the flow speed measurement is estimated to be 0.09 m/s. This resolution is comparable to the requirement to detect a minimum level of hypopnea at 30% flow reduction with a tidal volume of 250ml. Levels of flow reductions of greater than 30% would require improvement in sensor sensitivity/resolution to realize a measurable variation in output voltage.

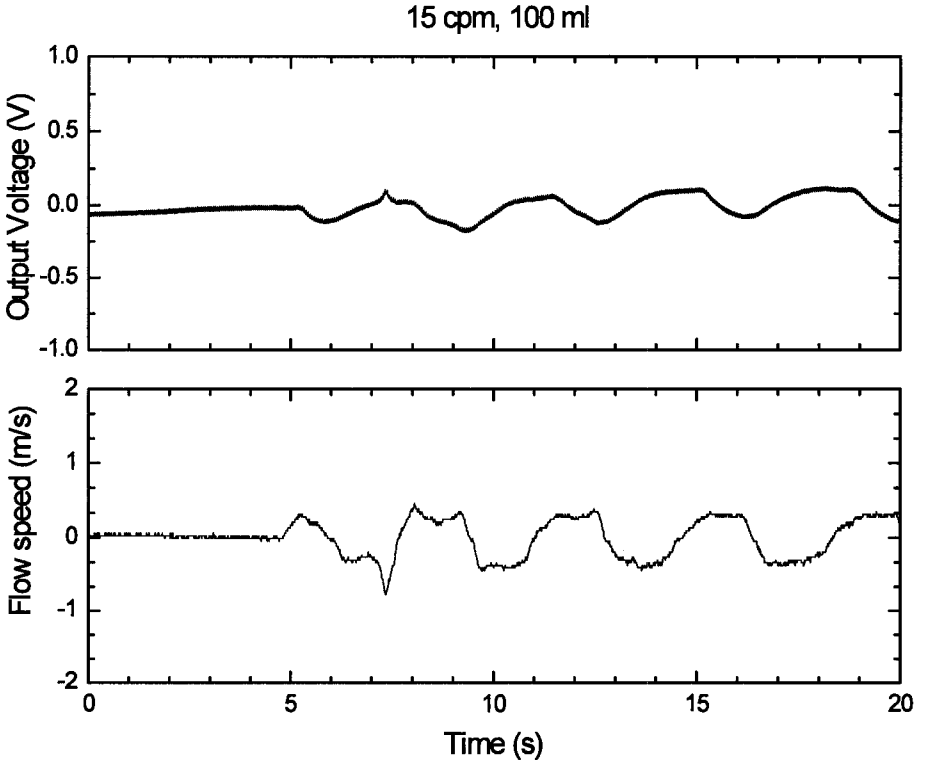


Figure 5.7: Sensor output voltage for 15 cpm, and airflow volume of 100ml

Increasing the sensitivity of the sensor would be an important area for future work, but at the same time reducing or eliminating sources of errors in the experimental conditions as well as actual measurements with human subjects would also improve the accuracy of the results. Sensor sensitivity could be improved by optimizing the thickness ratio between the substrate layer and the piezoelectric layer as discussed in section 3.4. Optimizing the thickness ratio will improve the efficiency with which the sensor converts between mechanical and electrical energy.

Some sources of errors in the experimental results could be due to the respiration simulation set up. The distance between piston pump and the spirometer should be kept as short as possible to minimize the "dead space". Physiologically, the dead space is the space in the trachea, bronchi, and other air passages which contain air that does not reach the alveoli during respiration [22]. In the experimental set up, this would be the air that would not reach the sensor or the spirometer due to leakage in the set up. Minimizing the "dead space" would improve the accuracy of measured flow rates and improved variations in the output voltage.

During the experimental setup, one end of the unimorph bending sensor was fixed on the airflow chamber using an adhesive tape, while the other end was free to move in response to the airflow. While every attempt was made to ensure that the fixed end of the sensor does not move with the applied airflow, it is quite conceivable that there could be some movement of sensor at the fixed end. The movement of the fixed end of the bending sensor would reduce the overall displacement in the sensor and hence reduce the output voltage of the sensor. The reduction in output voltage could be significant if there

is a significant amount of movement. A stable alternative to fix one end of the sensor should be investigated for future work.

Other sources of errors in the experimental set up include errors due to vibration caused by the manual pumping of the piston pump to simulate breathing. Even though the piston pump was mounted on and clamped on a wooden structure, the handling of the piston pump during the pumping action could result into the vibration of the set up introducing noise in the sensor output.

The wires connecting the unimorph sensor to the electronics such as a charge amplifier are quite susceptible to the 50Hz/60Hz electrical noise interference. While fairly short wires were used to minimize this interference, future experiments should investigate the possibility of using shielded or coaxial cable though such an effect was not observed in the experimental results presented.

For experiments carried out on human subjects, main sources of noise include, artifacts induced by body movement. The subject's movement may change the position of the sensor and the resulting data may not be from the same position as at the beginning of the experiment. Body movement may also contribute to noise in the sensor output voltage as the stress applied on the sensor may also increase and real signal from respiration will need to be isolated from the accompanying noise artifact [43]. An effective way to attach the sensor on human subject should be investigated.

Another source of error with human experiments could be loss of sensor signal. If the sensor is not positioned correctly under the nose and the mouth, the pressure variations due to airflow cannot reach the surface of the sensor. This will significantly influence the detection of respiration. This problem can be overcome by mechanism such

as elastic band that strongly binds the sensor and holds it in place when positioned over the nose or the mouth.

Snoring could also be another source of noise since it may create additional vibration on the sensor. A mechanism to separate the snore signal from the airflow signal will be required to determine the output voltage due to breathing airflow only.

Environmental conditions can also introduce errors in the sensor output. If for example, a subject is sleeping with a fan blowing on the subject's face, the air flow from the fan will introduce additional stress on the sensor and the output voltage of the sensor may be a combination of the subject's respiration as well as airflow from the fan and not a true reflection of the subject's breathing situation.

# 5.3 Temperature Response of Sensor

The next sets of experiments were carried out to understand the effects of temperature variations on sensor output.

## 5.3.1 Temperature Variations of Actual Breathing

The purpose of this section was to estimate actual temperature variations due to breathing. Temperature variation due to breathing was measured beneath the nose to evaluate the pyroelectric response of the sensor. This part of the experiment was conducted prior to embarking upon experiments using the simulator. A thermistor was placed on the outer edge of the subject's nostril and the piezoelectric unimorph sensor was placed under the subject's nose perpendicular to the airflow. The placement of the

sensor is important to ensure that both pressure and temperature effects are being applied to the sensor. If the sensor was placed parallel to the flow, no piezo effects would be experienced by the sensor. This was also experimented and proved to be the case. The thermistor was placed on the outer edge of the subject's nostril in order to record the temperature variation resulting from breathing. The subject took deep breaths for the first half of the experiment and normal breathing for the second half of the experiment. Figure 5.8 provides temperature variations during deep and normal human breathing of a 40 year old male subject. The change in air temperature was about 2 °C and 1°C, respectively, for deep (11 bpm) and normal (17 bpm) breathing. As per the manufacturer specs (Vernier Systems), this probe does not need to be calibrated as it provides very accurate temperature readings.

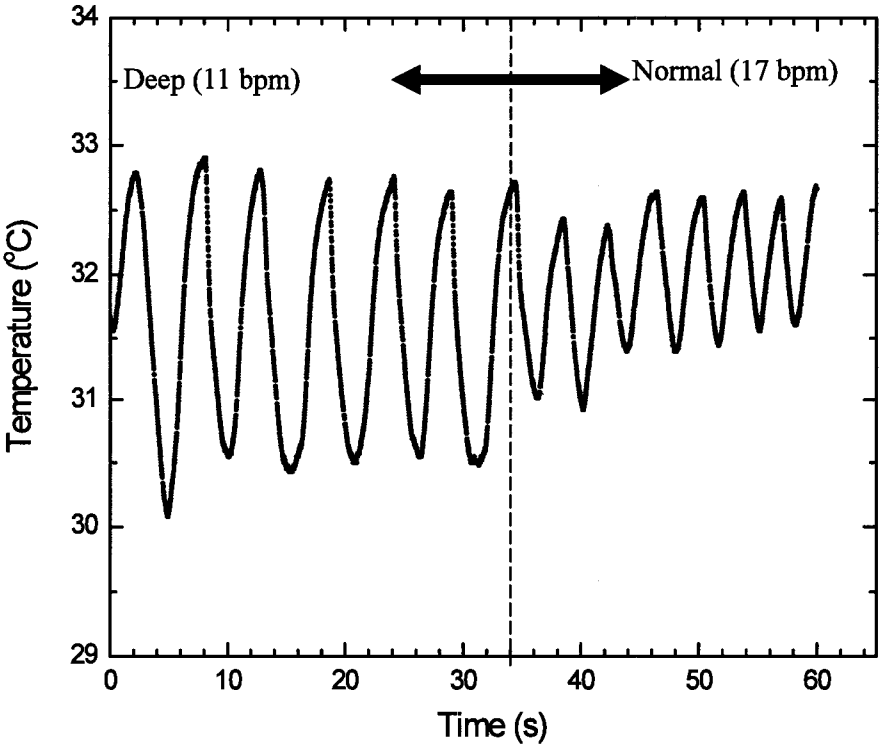


Figure 5.8: Temperature variations of a 40 year old male breathing

### 5.3.2 Experiments and Results

Temperature variation was introduced to the experimental set up. Temperature variation was measured using a thermistor; flow rate was measured using a spirometer and voltage probe for measuring output voltage from the sensor. All of these three devices were connected to the data acquisition system for simultaneous capture of temperature, flow rate and output voltage.

The piezoelectric unimorph bending sensor was placed in the air chamber of the simulator in such a way that its surface is parallel to the direction of the airflow to ensure that airflow pressure is not applied to the sensor. Such placement of the sensor is important in order to have sensor output signals only due to temperature variations of the air. The temperature variations were introduced by warming up the pump using the electric heater in the simulator. The temperature around the sensor increases when warmed air flows into the air chamber from the pump by pushing the piston while it decreases when room temperature air flows into the chamber by pulling the piston.

To understand temperature effects using the respiration simulator shown in Figure 4.2, two sets of experiments were carried out. The first set consisted of varying the air volume while keeping the pumping cycle fixed. The second set of experiments consisted of keeping the volume fixed while varying the pumping cycle. Figure 5.9 provides results of sensor output voltage, temperature and flow speed with respect to the time for fixed pumping cycle of 30 cycles per minute with different volumes of 500ml (a), 300 ml (b) and 100ml (c).

Figure 5.10 illustrate relationships between output voltage and flow speed (a), output voltage and temperature (b) and temperature and flow speed (c) derived from Figure 5.9.

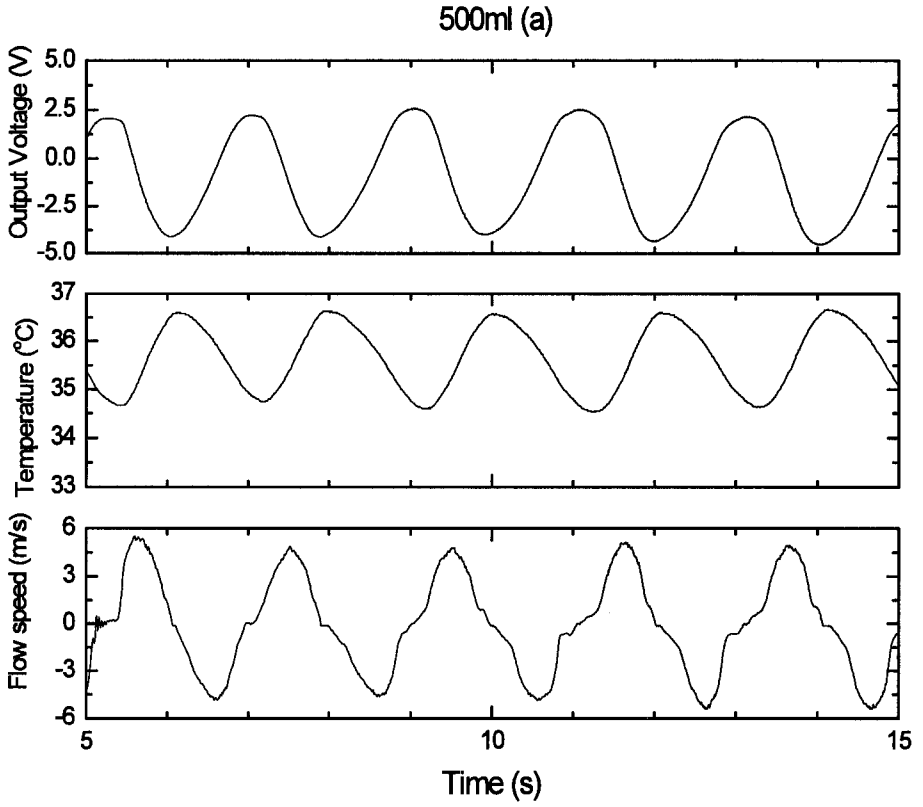


Figure 5.9: Sensor output voltage, temperature and flow speed with respect to the time for fixed pumping cycle of 30 cycles per minute with different volume of 500ml (a), 300 ml (b) and 100ml (c). (Continued on next page)

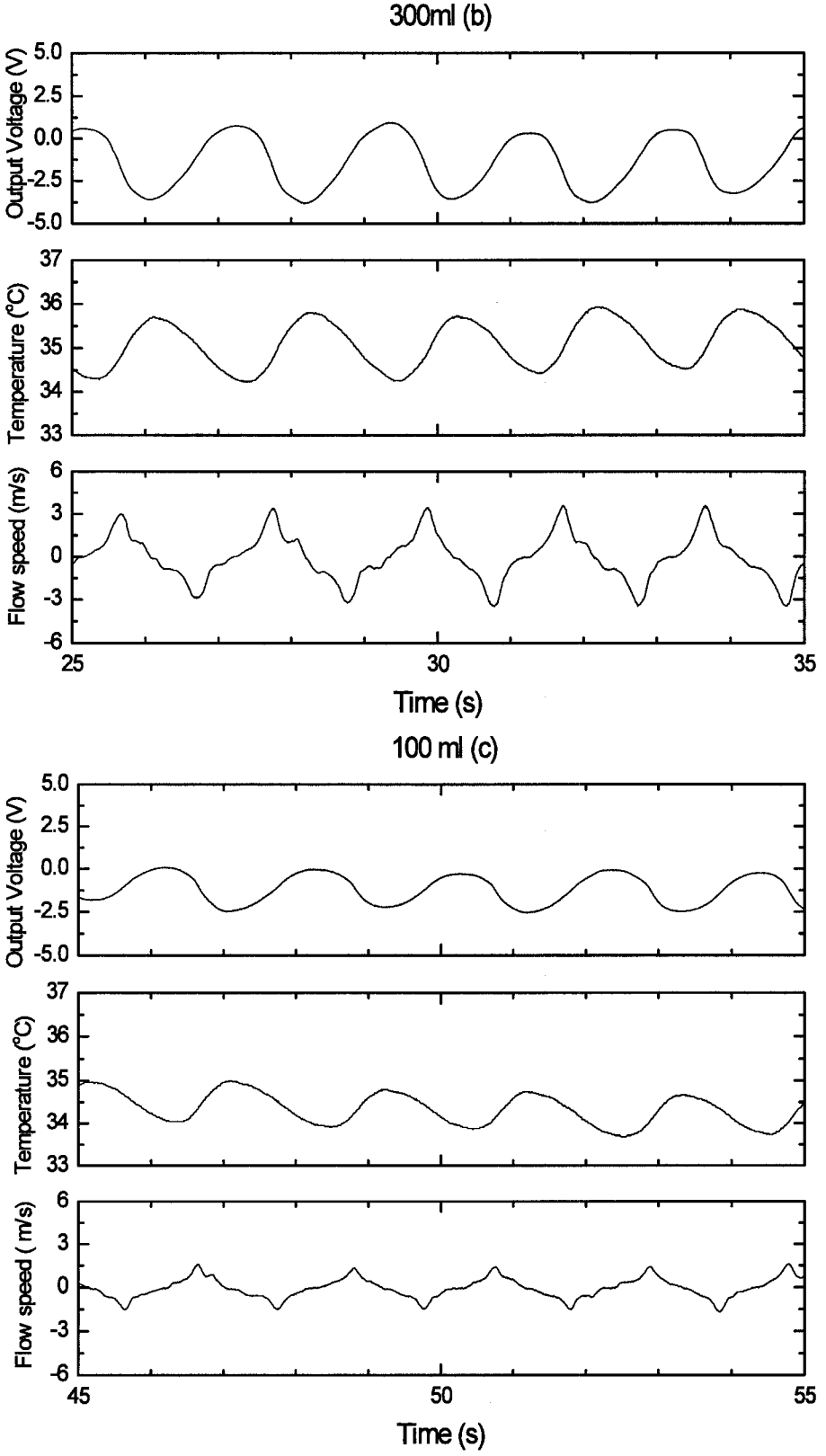


Figure 5.9: Sensor output voltage, temperature and flow speed with respect to the time for fixed pumping cycle of 30 cycles per minute with different volume of 500ml (a), 300 ml (b) and 100ml (c).

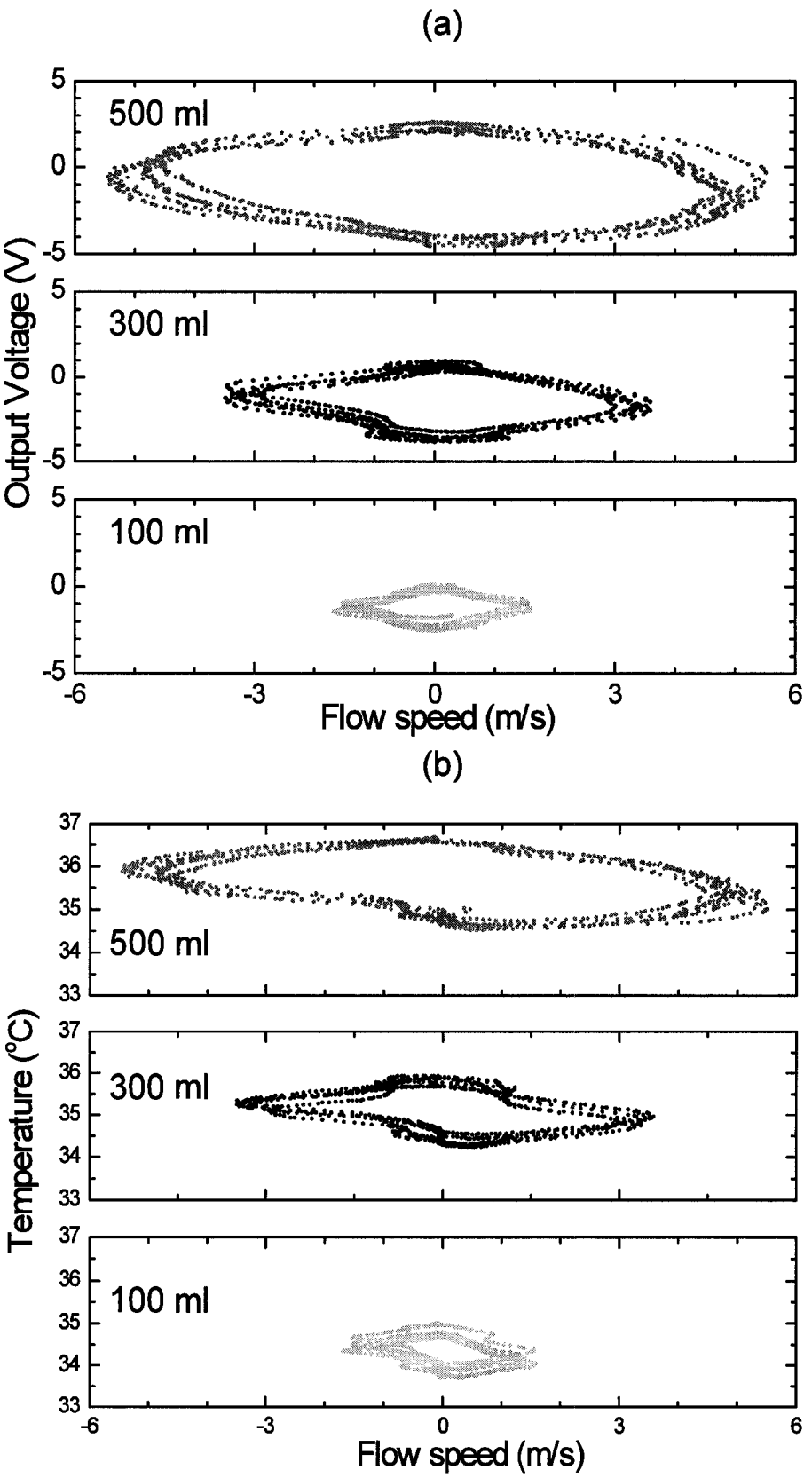


Figure 5.10: Output voltage vs. flow speed (a), temperature vs. flow speed (b) and output voltage vs. temperature (c) for fixed breathing cycle of 30 cpm with volume of 500 ml, 300ml and 100ml, derived from Figure 5.8. (Continued on next page).

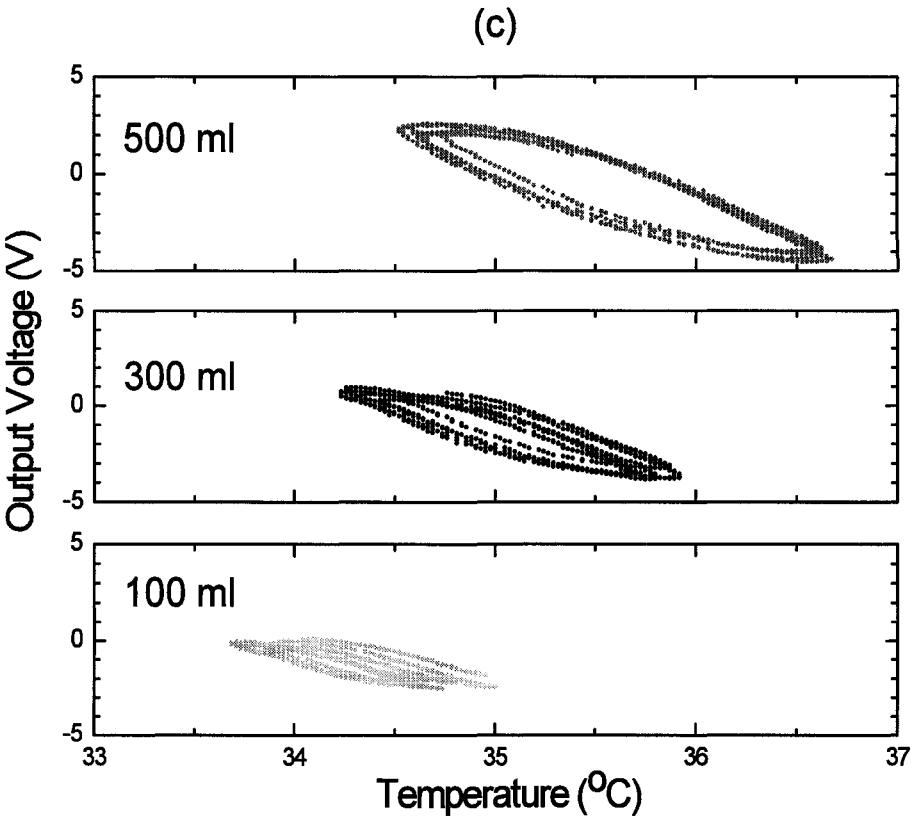


Figure 5.10: Output voltage vs. flow speed (a), temperature vs. flow speed (b) and output voltage vs. temperature (c) for fixed breathing cycle of 30 cpm with volume of 500 ml, 300ml and 100ml, derived from Figure 5.8.

The second set of experiments consisted of keeping the volume fixed at 500ml while varying the pumping cycles of 60, 48, 30 and 18 cpm. Figure 5.11 provides the sensor output voltage, temperature and flow speed for fixed volume of 500ml and varying pumping cycle from 60 cpm (a), 48 cpm (b), 30 cpm (c) and 18 cpm (d). Figure 5.12 shows the relationship between output voltage and flow speed (a), temperature and flow speed (b) and output voltage and temperature (c), as derived from Figure 5.11.

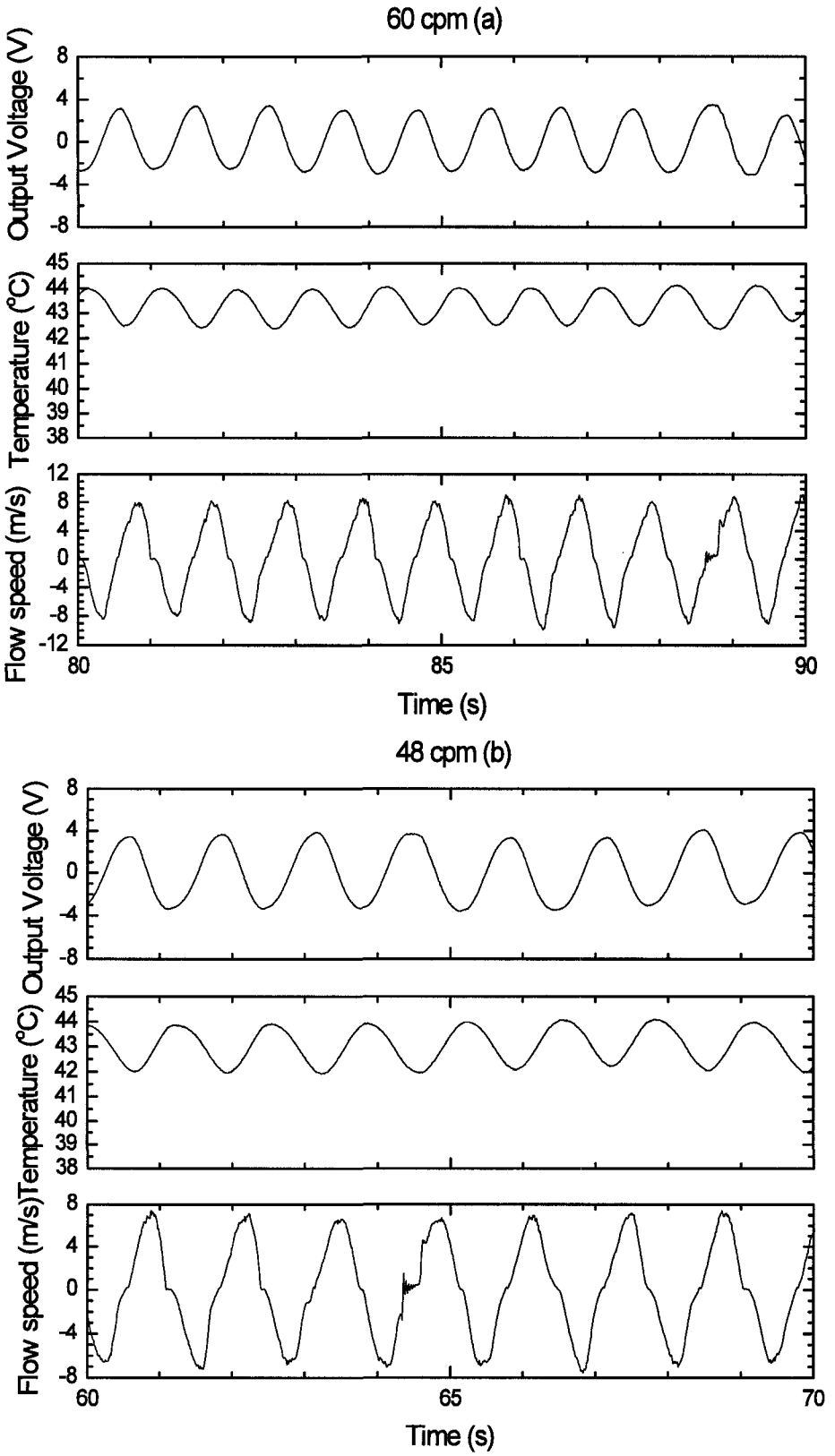


Figure 5.11: Sensor output voltage, temperature and flow speed for fixed volume of 500ml and varying breathing cycle from 60 cpm (a), 48 cpm (b), 30 cpm (c) and 18 cpm (d). (Continued on next page).

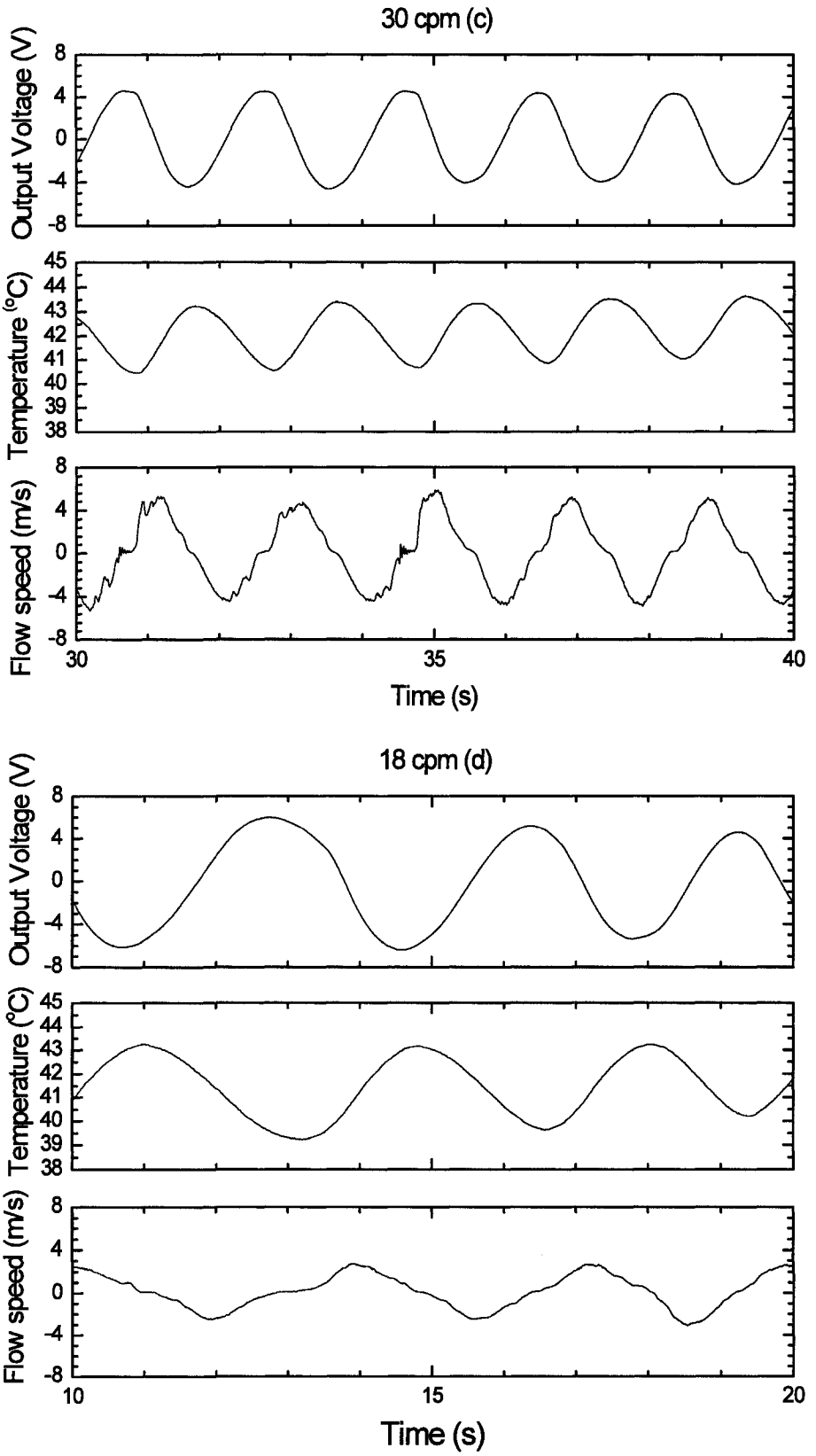


Figure 5.11: Sensor output voltage, temperature and flow speed for fixed volume of 500ml and varying breathing cycle from 60 cpm (a), 48 cpm (b), 30 cpm (c) and 18 cpm (d).

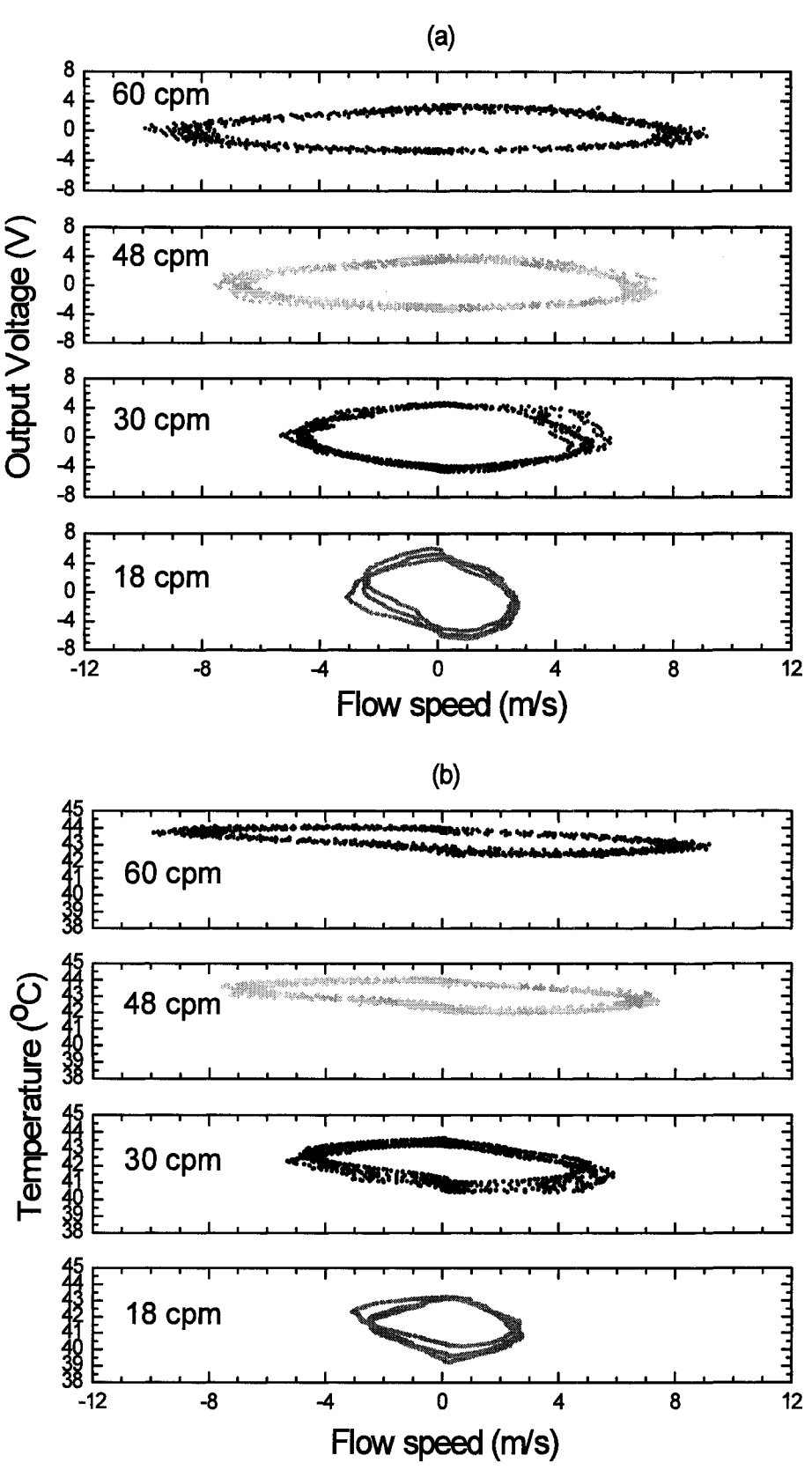


Figure 5.12: Output voltage vs. Flow speed (a), Temperature vs. Flow speed (b) and Output Voltage vs. Temperature (c), derived from Figure 5.10. (Continued on next page).

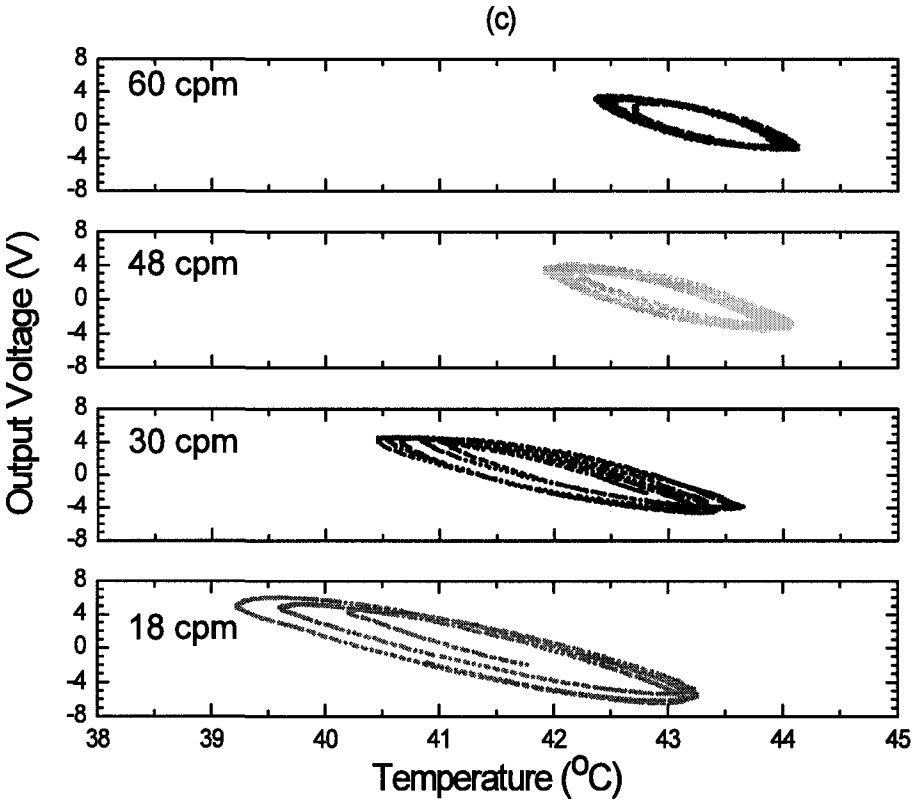


Figure 5.12: Output voltage vs. Flow speed (a), Temperature vs. Flow speed (b) and Output Voltage vs. Temperature (c), derived from Figure 5.10.

### 5.3.3 Discussions

Comparing the output voltage from the simulation experiments where pressure effects are applied to the sensor to the output voltage where temperature effects are applied, it is evident that for the same breathing cycle and volume, the output voltage for temperature effects is greater than the output voltage produced by pressure effects as discussed in the section 5.2. For example, for a pumping cycle of 30 cpm and air volume of 500 ml, when temperature effects are applied to the sensor, the output voltage ranges from -4V to +4V, compared to an output voltage of -3.5V to +2.5V for the same pumping cycle and air volume but when only pressure effects are applied. One of the reasons for this observation could be that pyroelectric response of the piezoelectric sensor employed due to the temperature variations was greater than piezoelectric response due to pressure variations under the presented experimental conditions. Another reason could be that temperature changes cause pyroelectric materials to absorb thermal energy and therefore causing these materials to expand and contract. The expansion and contraction of these materials introduce a secondary piezoelectric effect and therefore the output voltage when temperature changes are introduced consists of both the pyroelectric effects and secondary piezo-effects and therefore producing a much stronger output voltage signal from the sensor.

Figure 5.7 indicates that temperature variation is dependent on breathing air volume and cycle. Deep breathing has more temperature variations than normal breathing. This could be because with deeper and slower (11 bpm) breathing, there is more mixing of the cooler inhaled air and the warmer air in the lungs. Cooler breath will flow deeper into lungs for longer time with the deep breath, where the air is warmed up

more than that with normal breath (17 bpm). With normal, shallower breathing, cooler air comes in contact with air that is around the chest and upper body area which is not as warm as the air in the lungs and hence the temperature variation is not as large as with deeper breath.

Figures 5.9 and 5.11 indicate that output voltages due to temperature variations are dependent on both the air volume and pumping cycle. Therefore, it would be challenging to obtain a calibration curve that would quantitatively determine flow speed from output voltage due to temperature variations. Temperature variations could be also affected by the environmental conditions, such as air conditioner and/or winds, under which measurements are conducted. Therefore, using temperature variations to detect hypopnea becomes more challenging as the patient may be breathing shallowly and registering a temperature variation, but the quantity of airflow may be very small. Detection of apnea on the other hand may be possible using temperature effects since apnea is complete cessation of breathing.

For pressure effects only, as we saw in the section 5.2, within the experimental constraints, we were able to determine a one to one relationship between output voltage and flow speed/rate which would enable us to determine air volume. This is not the case where we have pyroelectric effects and secondary piezoelectric effects, because the output voltage is not just dependent on temperature variation and there is not a straight forward relationship between output voltage, temperature variation and flow speed.

Since actual human breathing would cause both pyroelectric and piezoelectric effects of the sensor, in order to use this sensor effectively to calculate air flow speed when both of these effects are present, it would require the ability of separating these two

responses. Some work has been done by Castro *et al* [44], and they have provided two approaches for separation of pyroelectric and piezoelectric responses produced by temperature and pressure changes respectively. The first method involves signal processing to separate these two responses. This method analyses the signal consisting of both the pyroelectric and piezoelectric responses of a unimorph sensor in the frequency/time domains by means of signal processing that allows the separation of these signals. This work suggests that the spectral response of material when only pressure is applied has a much lower bandwidth when compared to the spectral response of the material when only temperature is applied. This different spectral bandwidth of the signals would enable the separation of the pressure and temperature responses by means of filters. This would be interesting future work to determine if that can indeed be achieved for the unimorph bending sensor used in this dissertation.

The second approach presented by Castro *et al* [44], is to use a bimorph sensor that has two piezoelectric layers sandwiched by a metal layer. Experiments conducted in this work indicate that the piezoelectric response is equal in each of the layer, while the pyroelectric response dominates in the layer exposed to the temperature variations. The paper suggests that piezoelectric response can be obtained directly from the lower layer whereas the pyroelectric response can be obtained by subtracting the signals of the two layers.

While both of these methods would be feasible for the sensor used in this dissertation, to employ the second approach, the sensor would need to be redesigned from the existing unimorph sensor to a bimorph sensor. However both of these approaches and others should be investigated as part of future work to determine the best method of

extracting piezoelectric signal from the output signal that includes both pyroelectric and piezoelectric responses that would be produced as a result of human breath.

# 5.4 Sensor Response to Human Breathing

Experiments were also conducted on human subject breathing through the sensor. The sensor was placed under the nose of a forty year old male subject. The placement of the sensor was such that both the pressure effects as well as the thermal effects were being applied to the sensor. Figure 5.13 shows the sensor placement on the subject's nose using a clip.

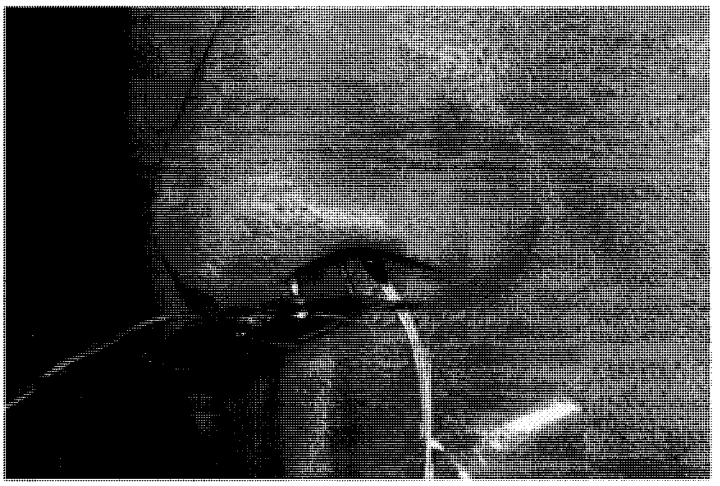

Figure 5.13: Sensor placement on human subject.

The sensor output voltage due to breathing of a forty year old human subject is provided in Figure 5.14. The subject took deep breaths for the first twenty seconds, followed by normal breaths. The peak-to-peak output voltage due to breathing is around 8V for deep breathing and 5V for normal breathing.

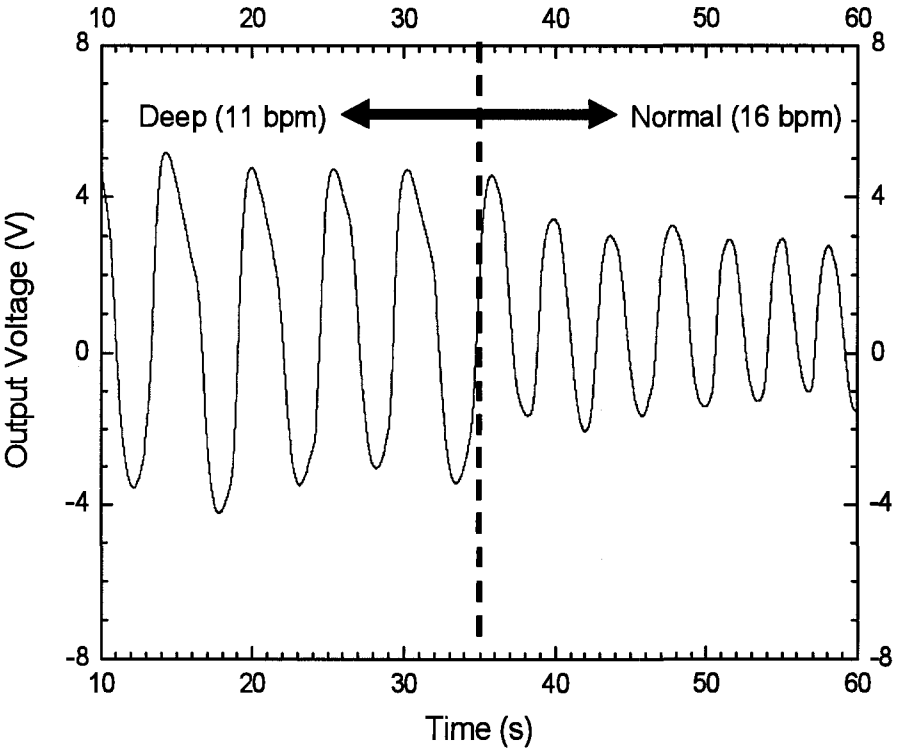


Figure 5.14: Sensor output voltage of a 40 year old male breathing (deep and normal)

Table 5-1 provides the average peak-to-peak output voltages obtained from the experimental results shown in Figures 5.2 (a), (c) and (e) due to pressure effect only and those obtained from the result in Figures 5.9 (a), (b) and (c) due to temperature effect only with airflow volumes of 500, 300 and 100 ml, respectively at pumping cycle of 30 cmp. Only the results that were obtained with the same experimental conditions are chosen. From these results, the total output voltage is estimated when both pressure and temperature effects are present.

Table 5-1: Output voltage for pressure and temperature effects for 30 cpm

| Volume (ml) | Measured output voltage | | Estimated total output voltage (V) | Percentage of pressure effect (%) | Percentage of temperature effect (%) |
|---|---|---|---|---|---|
| | Pressure effect (V) | Temperature effect (V) | | | |
| 500 | 3.8 | 6.5 | 10.3 | 36.8 | 63.2 |
| 300 | 1.3 | 4.9 | 6.2 | 21 | 79 |
| 100 | 0.1 | 2.5 | 2.6 | 4 | 96 |

From Table 5-1, the total output voltage estimated (2.6~10V) is comparable to normal human breathing output voltage in Figure 5.14. Percentages of the output voltage due to temperature effects are higher than those due to pressure effect in these experimental conditions. The temperature effects account for roughly 60%-90% of the total output voltage and that contribution tends to increase as the airflow volume decreases. This would be the expected behavior because as the airflow volume decreases, the airflow speed decreases as well, thus the output voltage due to pressure effects decreases by square of decrease in flow speed. For example, when airflow volume changed from 500 to 100 ml, output voltage due to pressure effect decreases by 97%, on the other hand, output voltage due to temperature effect decreases by 62%. Therefore, change in airflow speed affect more on output voltage due to pressure effect than that due to temperature effect.

# 5.5 Summary

Experimental results using the airflow simulator indicates that the sensor output voltage due to piezoelectric effect caused by the airflow pressure was proportional to the square of the airflow speed, which agreed with the mathematical model developed in Chapter 3 under the experimental conditions employed. A calibration curve between the airflow speed and the output voltage was obtained experimentally, which enables to measure airflow variations quantitatively.

Temperature effects are more complicated to use to quantify airflow because the output voltage of the sensor depends not only on airflow speeds but also on breathing cycles. In addition, temperature variations cause primary and secondary effects on the sensor and sensor output signals resulting from changes in temperature has multiple and interdependent factors. Changes in temperature can still be used effectively to qualitatively understand presence or absence of flow.

Sensor output voltage due to pressure effects and temperature effects were analyzed. The contribution of temperature effects to the total output voltage is higher than the contribution of the pressure effects. The total output voltage in the simulation experiments is comparable to the total output voltage of actual human breathing.

Since human breathing causes both pyroelectric and piezoelectric effects of the piezoelectric sensor, one of future works is to find a way to separate these two responses by either using signal processing or redesigning the sensor with different configurations such as a bimorph sensor, for example. For the purposes of quantifying hypopnea,

piezoelectric response may be more useful since the mathematical model developed in chapter 3 could be used to estimate flow speed based on the output voltage.

The unimorph sensor developed shows good feasibility and can be used as a sensor to detect occurrences of apnea and/or hypopnea. Based on the output voltage produced from the sensor, one could use the equations provided to calculate flow speed. However, as the simulation experiments indicate, with in the flow speed range of $\pm 1$m/s, current sensitivity of the sensor may not be sufficient to detect small changes in air volume and hence the corresponding output voltage. This would be important for future work as the conditions of apnea and hypopnea by their very nature involve low volumes of airflow.

# Chapter 6
# Conclusions

## 6.1 Summary

Undiagnosed sleep apnea can lead to many life threatening diseases such as chronic fatigue, depression, high blood pressure and cardiac diseases. Polysomnogram is the current gold standard for diagnosis of sleep apnea, requiring patients to overnight at a sleep clinic. The expense associated with conducting a polysomnogram makes it a scarce resource and sleep clinics usually have long waiting lists for patients requiring the test.

A low cost home based device that can be used as a simple, initial diagnostic test is an attractive solution to overcoming some of these challenges and it would assist the medical profession to better allocate these scarce resources. Current home based sensors for apnea monitoring utilize thermistors/thermocouples. These devices are highly nonlinear and underestimate flow reductions which are especially important for monitoring of hypopnea.

The main objective of this thesis has been to investigate the feasibility of the piezoelectric unimorph bending sensor for monitoring apnea and hypopnea. The definition of apnea is quite straightforward i.e. complete cessation of airflow for 10 sec or longer, while monitoring for hypopnea requires more quantitative data, since it is concerned with the reduction of airflow rather than complete absence.

A relationship between sensor output voltage as a result of air pressure effects, i.e. flow speed, was derived theoretically. It can be shown that output voltage is propositional to the square of the flow speed. This relationship could be utilized to determine a calibration curve between output voltage and flow speed.

The electromechanical coefficient is one of the parameters that can be used to determine design criteria for the sensor. It is shown that stainless steel could be the appropriate substrate layer as it provides the largest electromechanical coefficient as compared to a number of other common substrates such as aluminum, brass and polyimide.

A respiration simulator system has been developed that was utilized for the experiments. The simulator provided two important functions; the first one was that it provided for the capability to study the response of the sensor under different conditions including different airflow speeds, volumes and cycles. The second function that the simulator provided was the capability to study the piezoelectric effects in isolation from the pyroelectric effects of the sensor.

Piezoelectric and pyroelectric effects were studied separately using the respiration simulator. The sensor output voltage due to piezoelectric effect caused by the airflow pressure was proportional to the square of the airflow speed, which agreed with the mathematical model developed under the experimental conditions employed. A calibration curve between the airflow speed and the output voltage was obtained experimentally, which enables to measure airflow variations quantitatively. Temperature effects are more complicated to use to quantify airflow because the output voltage of the sensor depends not only on airflow speeds but also on breathing cycles. Changes in

temperature can still be used effectively to qualitatively understand presence or absence of flow. The developed unimorph sensor provides many advantages such as flexibility and low cost and can be used as a cost effective home based apnea monitoring device.

## 6.2 Contributions

This thesis makes a number of contributions to the understanding of the behavior of the piezoelectric unimorph sensor and the feasibility of this sensor as a monitoring device for apnea and hypopnea.

The first contribution that this thesis makes to the knowledge of home based diagnostic devices for apnea is to propose using the piezoelectric ceramic film as an airflow monitoring device. The cost effectiveness, the flexibility and the size and the sensitivity of this sensor makes it a very attractive alternative given the challenges of the current technologies used in existing home based apnea monitoring devices.

The second contribution is development of the piezoelectric unimorph bending sensor using piezoelectric membrane, measurement principle and mathematical model for quantitative measurement of airflow. The sensors use the piezoelectric response caused by air pressure for the quantitative measurement of airflow. Current thermal sensors available commercially can detect the absence of breathing but are not capable of providing quantitative information of breathing such as air volume or airflow speed.

The third contribution of this work is the development of the respiration simulator. The simulator enabled the modeling of human breathing under different conditions as well as a capability of separating pyroelectric response and piezoelectric

response of the sensor. The pyroelectric response of piezoelectric material can also become noise source for measurements and therefore it is desirable to separate out the pyroelectric response. While there are methods that can eliminate the pyroelectric response, these methods would require redesign of the existing unimorph sensor that was used in this thesis. Therefore, in this work, piezoelectric and pyroelectric responses were separated by the development of an airflow simulator that was capable of providing pressure changes only to illicit piezoelectric response. The simulator could provide the capability of collecting sensor output that resulted from the pressure response independent of sensor output resulting from the temperature effects.

The fourth contribution of this thesis is the analysis of the data acquired and correlating the experimental data to the mathematical models. The correlation between the output signal of the sensor and the airflow speed is also obtained, which could be used as a calibration curve to quantify the flow speed.

The fifth contribution of this dissertation is to provide for design criteria for the piezoelectric unimorph sensor, such as suitable substrate material and thickness ratio of piezoelectric and substrate layers.

The sixth contribution is to provide suggestions for future improvement and development.

# 6.3 Future Research

1) Experiments with piezoelectric response of the sensor have shown that with the low flow speed in the range of around ±1 m/s, the sensor does not provide enough sensitivity. Therefore to further utilize this sensor for detection of apnea and/or hypopnea, we would need to look at ways to improve the sensitivity of this sensor at low flow speeds resulting from low breathing cycle and/or low air volume.

2) The mathematical models utilized as well as the experiments indicate that it is relatively straightforward to quantify air flow speed for piezoelectric response. However, human breathing consists of both temperature and pressure effects and we would need to find a methodology to separate these two responses from the output signal.

3) Further work is also suggested in the improvement of respiration simulator. The simulator developed in this dissertation required manual pumping of airflow which could lead to human error for pumping cycle and air volume. Mechanical translation stages driven by electric motors could be implemented to the pumping system for more accurate breathing simulation.

4) Trials using the sensor eventually need to be conducted using human subjects during sleeping. These trials would be important to understand sensor characteristics under actual conditions.

# References


[1] C. Guilleminault, A. Tilkian, and W.C. Dement, "The sleep apnea syndromes", Annu. Rev. Med., vol. 27, pp. 465-484, 1976,

[2] N.J. Moser, B.A. Phillips, D.T. Berry and L. Harbison, "What is hypopnea, anyway?", Chest, vol. 105, pp. 426-428, 1994.

[3] J.F. Pagel and S.R. Pandi-Perumal, *Sleep Medicine in Primary Care*, 1st ed. Totowa, NJ: Humana Press, 2007.

[4] J. K. Matheson, R. Singh, and A. Packard, *The Clinical Neurophysiology Primer,* 1st ed. Totowa, NJ: Humana Press, 2007.

[5] C. Guilleminault and V. C. Abad, "Obstructive sleep apnea", current treatment options in neurology, vol. 6, pp. 309–317, 2004.

[6] W. W. Flemons and W. T. McNicholas, "Clinical prediction of the sleep apnea syndrome", Sleep Medicine Reviews, vol. 1, pp. 19-32, 1997.

[7] R. Farré, J.M. Montserrat, M. Rotger, E. Ballester, and D. Navajas, "Accuracy of thermistors and thermocouples as flow-measuring devices for detecting hypopnoeas", Eur Respir J, vol. 11, pp. 179–182, 1998.

[8] R.B. Berry, G.L. Koch, S. Trautz, and M. H. Wagner," Comparison of respiratory event detection by a polyvinylidene fluoride film airflow sensor and a pneumotachograph in sleep apnea patients", Chest, vol. 128, pp.1331-1338, 2005.

[9] Y.M. Chang, J.S. Lee, and K. J. Kim, "Heartbeat monitoring technique based on corona-poled PVDF film sensor for smart apparel application", vol. 124-126, pp. 299-302, 2007.

[10] Y. Ono, Q. Liu, M. Kobayashi, C-K. Jen, A. Blouin, "A piezoelectric membrane sensor for biomedical monitoring", Proc. of IEEE Ultrasonics Symp., pp. 800-803, 2006.

[11] P. Kielczyrbki, W. Pajewski, and M. Szalewski, "Piezoelectric sensors for investigations of microstructures", Sensors and Actuators, vol. 65, pp. 13-18, 1997.

[12] C. –K. Jen, D.R. Franca, Z. Sun, and I. Ihara, "Clad polymer buffer rods for polymer process monitoring", Ultrasonics, vol., 39, pp. 81-89, 2001.

[13] A. Bartolo, B. Clymer, J. Golish, and R. Burgess, "The polysomnogram assay: a method to represent the overnight polysomnogram in a condensed format", Computers and Biomedical Research, vol. 33, pp.110–125, 2000.

[14] M.H. Kryger, T. Roth, and William C. Dement, *Principles and Practice of Sleep Medicine,* 4th ed. Philadelphia, Pennsylvania: Saunders, 2005.

[15] D. Rapoport, R. Norman and M. Nielson, *Nasal Pressure Airflow Measurement*, 2001.

[16] http://www.braebon.com/

[17] E. Ballester, J. Badia, L. Hernández, R. Farré, D. Navajas, and J.M. Montserrat, "Nasal prongs in the detection of sleep-related disordered breathing in the sleep apnoea/hypopnoea syndrome", Eur Respir J, vol. 11, pp. 880–883, 1998.

[18] J.G. Webster, *Medical Instrumentation,* 3rd ed. NYC, NY: Wiley, 1998.

[19] R. Chervin and M. Aldrich, "Effects of esophageal pressure monitoring on sleep architecture", AM J RESPIR CRIT CARE MED, vol. 156, pp. 881–885, 1997.

[20] A. BaHammam, "Comparison of nasal prong pressure and thermistor measurements for detecting respiratory events during sleep", Respiration vol. 71, pp. 385–390, 2004.

[21] N. Mandal, "Respirometers including spirometer, pneumotachograph and peak flow meter", Anaesthesia & intensive care medicine, vol. 7, pp. 1-5, 2006.

[22] T. Zhang, M. J. O'Brien, T.R. Mackie, and B.Paliwal, "Application of the spirometer in respiratory gated radiotherapy", American Association of Physicists in Medicine, vol. 30, pp. 3165-3171, 2003.

[23] K. Storck, M. Karlsson, D. Loyd, "Heat transfer evaluation of the nasal thermistor technique", IEEE Trans. Biomed. Eng., vol. 43, pp. 1187-1191, 1996.

[24] J. Siivola and A.H. Lang, "Non-invasive piezoelectric transducer for recording respiration at the level of diaphragm", Electroencephalography and clinical Neurophysiology, vol.106, pp. 552-553, 1998.

[25] R. Ishida., Y. Yonczawa, H. Maki, H. Ogawa, A.W. Hahn, and W.M. Caldwell, "A sleep apnea syndrome detection system", Biomed Sci. Instrum., vol. 40, pp. 458-462, 2004.

[26] M. Akiyama, Y. Morofuji, T. Kamohara, K. Nishikubo, M. Tsubai, O. Fukuda, and
N. Ueno, "Flexible piezoelectric pressure sensors using oriented aluminum nitride thin films prepared on polyethylene terephthalate films", J. Appl. Phys., vol. 100, pp. 114318-114318, 2006.

[27] J. Fraden, *Handbook of Modern Sensors: Physics, Designs, and Applications*, 2nd ed. Melville, NY: American Institute of Physics, 1996.

[28] S.O. Reza Moheimani and A.J. Fleming, *Piezoelectric transducers for vibration control and damping,* 1st ed. Verlag, London: Springer, 2006.

[29] C.H. Park, "On the circuit model of piezoceramics", Journal of intelligent material systems and structures, vol. 12, pp. 515-522, 2001.

[30] J. Aitsaria, S. Y. Choe, D. Shen, and D.J. Kim, "Modeling and analysis of a bimorph piezoelectric cantilever beam for voltage generation", Smart Materials and Structures, vol. 16, pp. 447-454, 2007.

[31] R. H. Bishop, *The Mechatronics Handbook*, 1st ed. Boca Raton, FL: CRC press, 1996.

[32] Q.M. Wang, X.H. Du, B. Xu, and L.E. Cross, "Electromechanical coupling and output efficiency of piezoelectric bending actuators", IEEE Trans. Ultrason., Ferroelect., Freq. Contr., vol. 46, pp. 638-645, 1999.

[33] M.R. Steel, F. Harrison, and P.G. Harper, "The piezoelectric bimorph: An experimental and theoretical study of its quasi static response", J. Phys. D: Appl. Phys, vol. 11, pp. 979-989, 1978.

[34] S. Gross, *Calculation and design of metal springs,* 1st ed. England: Chapman & Hall, 1966.

[35] Q. Wang, X. Du, B. Xu, and L. Cross, "Electromechanical coupling and output efficiency of piezoelectric bending actuators", IEEE Trans. Ultrason., Ferroelect., Freq. Contr., vol. 46, pp. 638-646, 1999.

[36] M.R. Steel, F. Harrison and P. G. Harper, "The piezoelectric bimorph: An experimental and theoretical study of its quasi static response", J. Phys. D: Appl. Phys., vol. 11, pp. 979-989, 1978.

[37] J. Smits and W. Choi, "The constituent equations of piezoelectric heterogeneous bimorphs", IEEE Trans. Ultrason., Ferroelect., Freq. Contr., vol.38, pp. 256-270, 1991.

[38] Q. M. Wang and L.E. Cross, "Performance analysis of piezoelectric cantilever bending Actuators", Ferroelectrics, vol. 215, pp 187-213, 1998.

[39] T.E. Faber, *Fluid Dynamics for Physicists*, 1st ed. NYC, NY: Cambridge University Press, 1995.

[40] R. Duggirala, S. Son, and A. Lal, "A pyroelectric-piezoelectric valve for integrated microfluidics", TRANSDUCERS, Solid-State Sensors, Actuators and Microsystems, vol. 2, pp. 1554-1557, 2003.

[41] U. Boutellier, U. Gomez, and G. Madder, "A piston pump for respiration simulation", J Appl. Physiol., vol. 50, pp. 663-664, 1981.

[42] R. Farré, M. Rotger, J.M. Montserrat, and D. Navajas, "A system to generate simultaneous forced oscillation and continuous positive airway pressure", Eur Respir J, vol.10, pp. 1349-1353, 1997

[43] W. Chen, X. Zhu, T. Nemoto, Y. Kanemitsu, K. Kitamura, and K. Yamakoshi, "Unconstrained detection of respiration rhythm and pulse rate with one under-pillow sensor during sleep", Med. Biol. Eng. Comput., vol. 43, pp. 306-312, 2005.

[44] H.F. Castro, S. Lanceros-Mendez, and J.G. Rocha, "Separation of the pyro- and piezoelectric response of electroactive polymers for sensor applications", Material Science Forum, vol. 514-516, pp. 202-206, 2006.

# Appendix A

## Electromechanical Coupling Coefficient

In Chapter 3, electromechanical coupling coefficient was calculated for the unimorph piezoelectric membrane sensor using various common substrates. The electromechanical coupling coefficient was used to determine the appropriate substrate to use from a number of substrates that are commonly used as well as to determine an appropriate thickness ratio of the substrate layer and the piezoelectric layer.

Table A-1 provides the values for the Young's modulus for various substrate materials used in equation A-1 and table A-2 provides the Young's modulus for the sol-gel PZT as well the calculated $k_{31}$ value.

Table A-1: Young's Modulus of common substrate materials.

| Substrate | Young's Modulus ($N/m^2$) |
|---|---|
| Aluminum | $6.5x10^{10}$ |
| Brass | $11x10^{10}$ |
| Stainless Steel | $2.069x10^{11}$ |
| Polyimide | $4.07x10^{9}$ |

Table A-2: Young's modulus for sol-gel PZT material

| Piezoelectric material | Young's Modulus ($N/m^2$) | $K_{31}$ |
|---|---|---|
| Sol-gel PZT | $1.5x10^{10}$ | -0.15 |

# Appendix B

## Experimental Results

In Chapter 5, Experimental Results were presented for pumping cycle of 30 cpm for varying airflow volume from 500ml to 100ml. Sensor output voltage and flow speed with respect to the measurement time were presented as well. In this appendix, data for 15, 45, 60, 75 and 90 cycles per min (cpm) are provided, including the sensor output voltage and flow speed. These data are presented in the raw format with the applied again ranging from 50dB to 70dB.

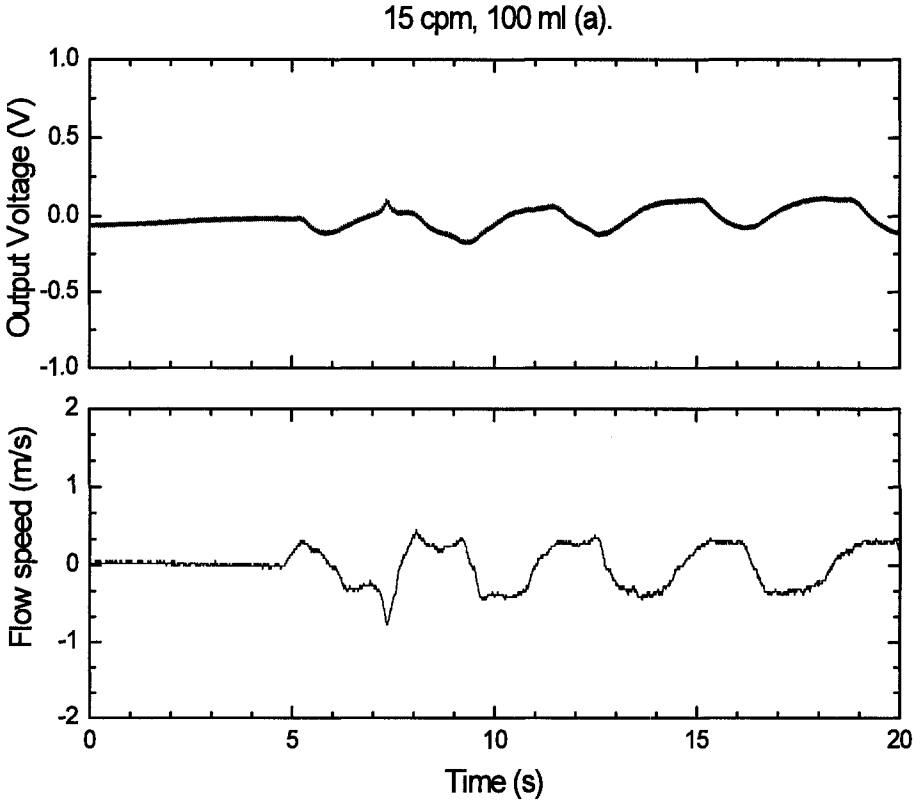


Figure B-1: Sensor output voltage for 15 cpm, airflow volume varying 100ml (a), 200 ml (b), 300 ml (c), 400 ml (d) and 500 ml (e). (Continued on next page).

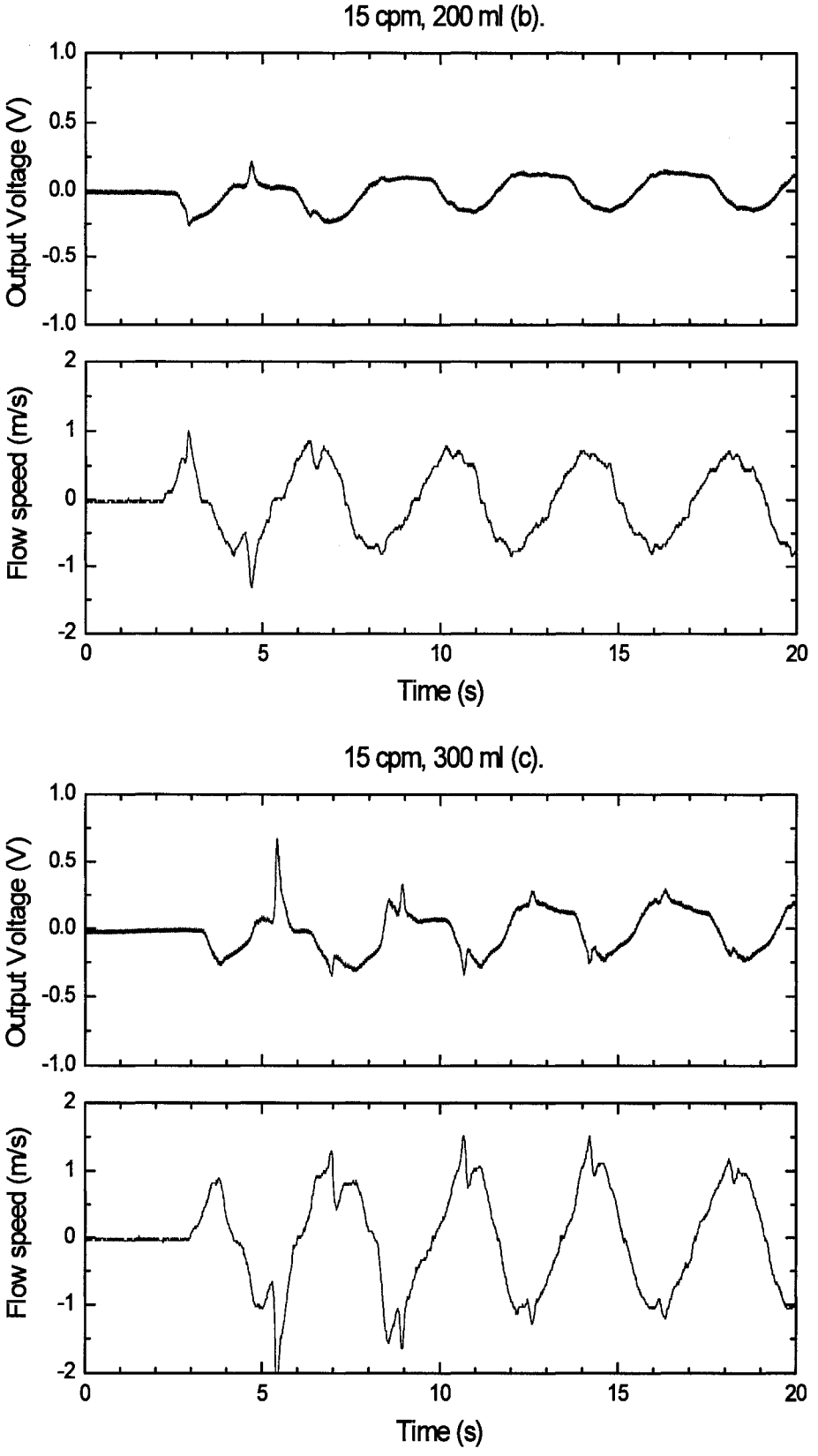


Figure B-1: Sensor output voltage for 15 cpm, airflow volume varying 100ml (a), 200 ml (b), 300 ml (c), 400 ml (d) and 500 ml (e). (Continued on next page).

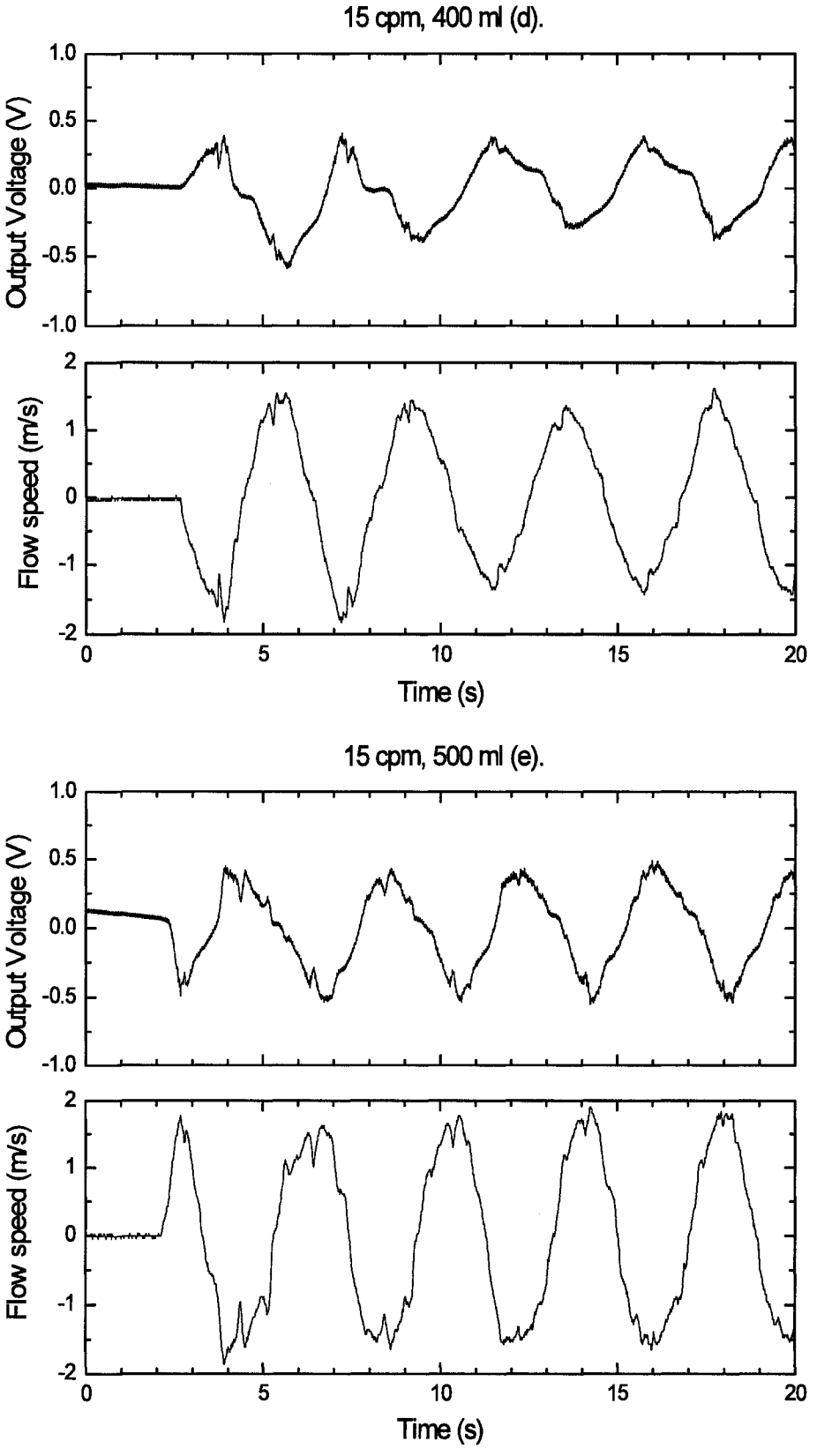


Figure B-1: Sensor output voltage for 15 cpm, airflow volume varying 100ml (a), 200 ml (b), 300 ml (c), 400 ml (d) and 500 ml (e).

Figure B-2 below provides sensor output voltage for 45 cpm, with airflow volume varying from 100 ml (a), 200 ml (b), 300 ml (c), 400 ml (d) and 500 ml (e).

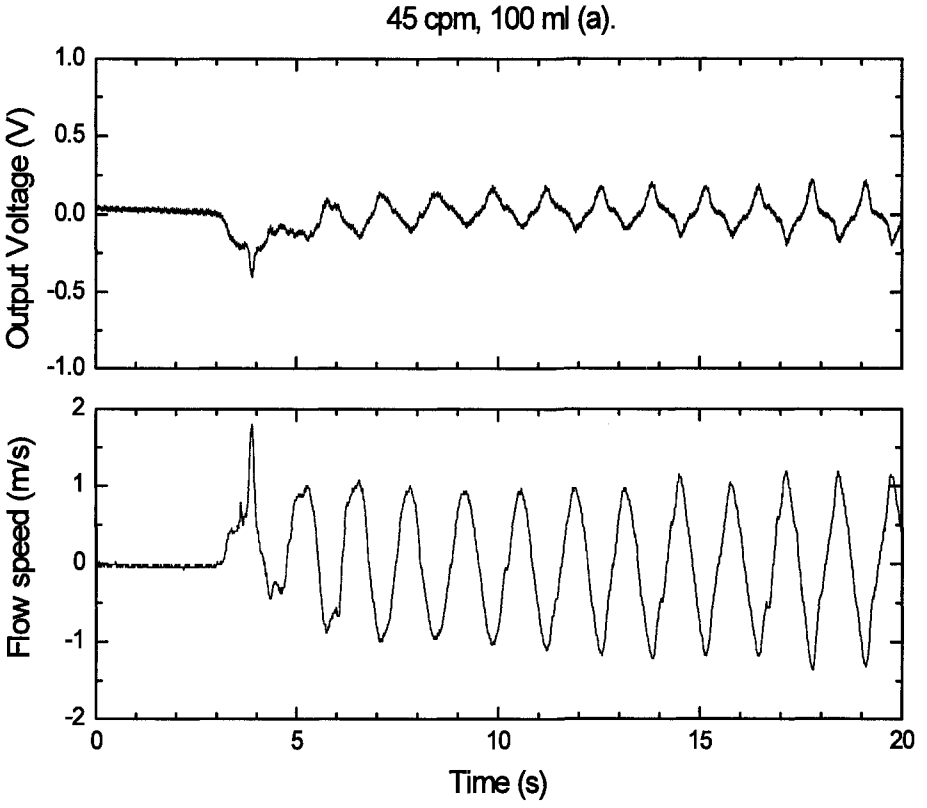


Figure B-2: Sensor output voltage for 45 cpm, airflow volume varying 100ml (a), 200 ml (b), 300 ml (c), 400 ml (d) and 500 ml (e). (Continued on next page)

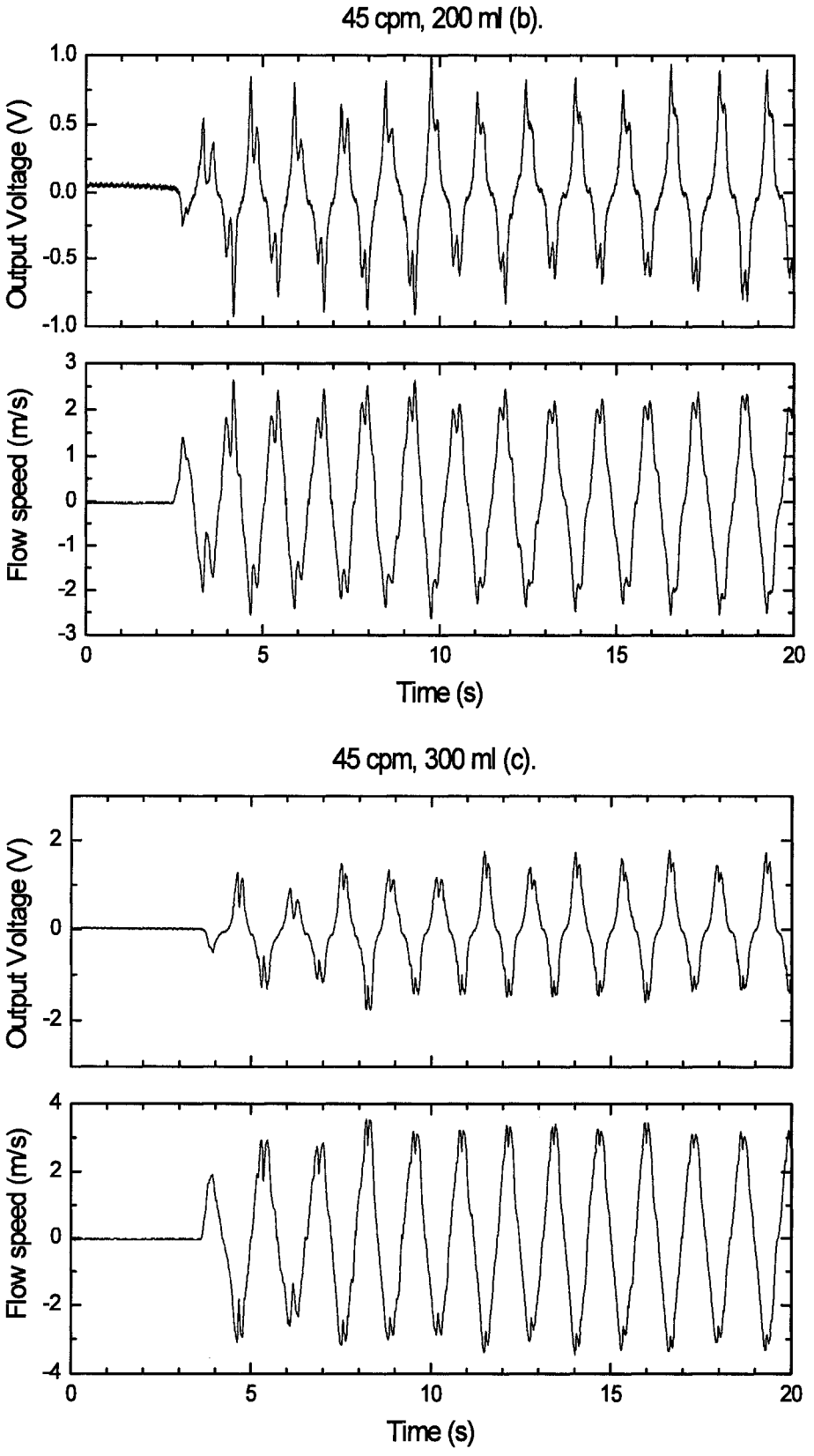


Figure B-2: Sensor output voltage for 45 cpm, airflow volume varying 100ml (a), 200 ml (b), 300 ml (c), 400 ml (d) and 500 ml (e). (Continued on next page)

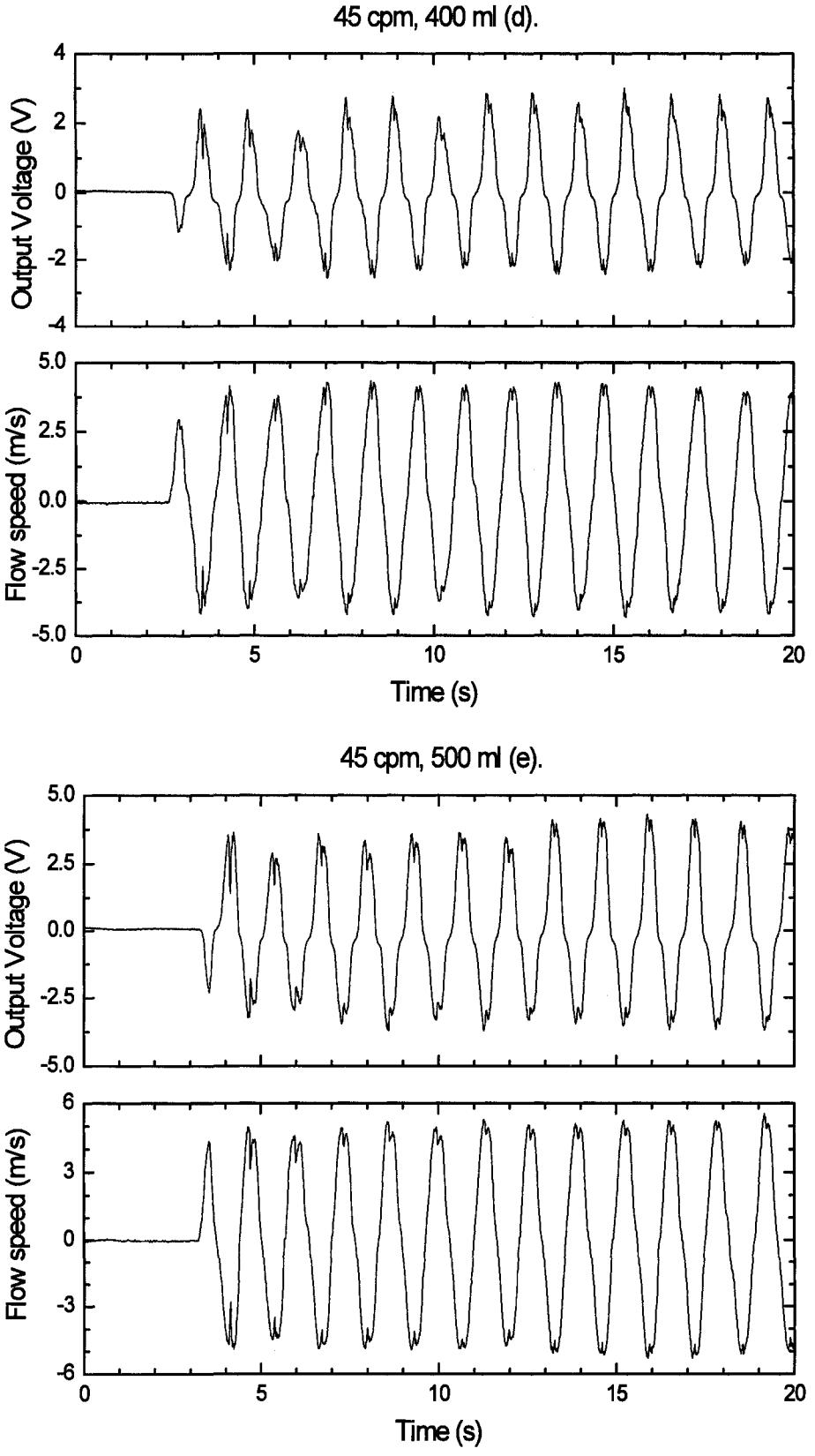


Figure B-2: Sensor output voltage for 45 cpm, airflow volume varying 100ml (a), 200 ml (b), 300 ml (c), 400 ml (d) and 500 ml (e).

Figure B-3 below provides sensor output voltage for 60 cpm, with airflow volume varying from 100 ml (a), 200 ml (b), 300 ml (c), 400 ml (d) and 500 ml (e).

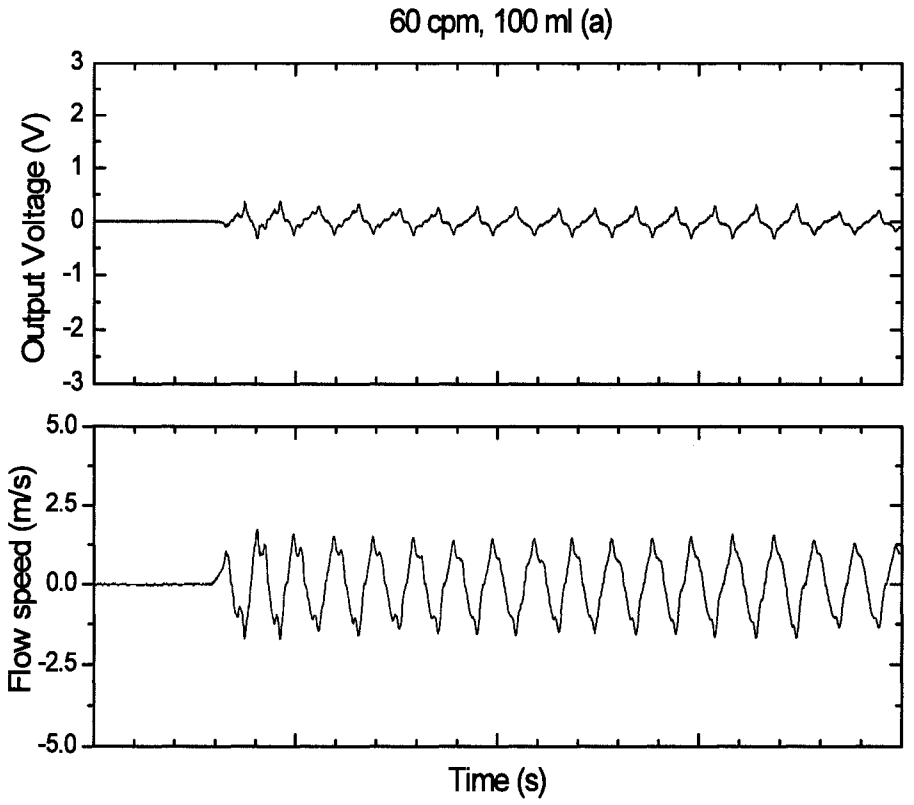


Figure B-3: Sensor output voltage for 60 cpm, airflow volume varying 100ml (a), 200 ml (b), 300 ml (c), 400 ml (d) and 500 ml (e). (Continued on next page)

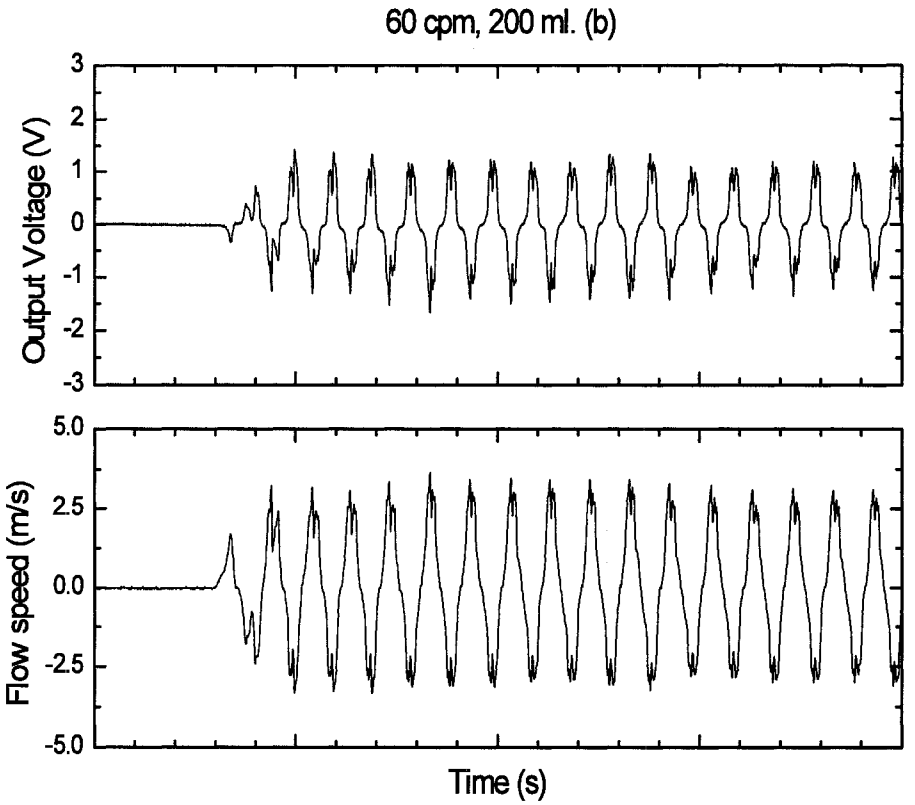


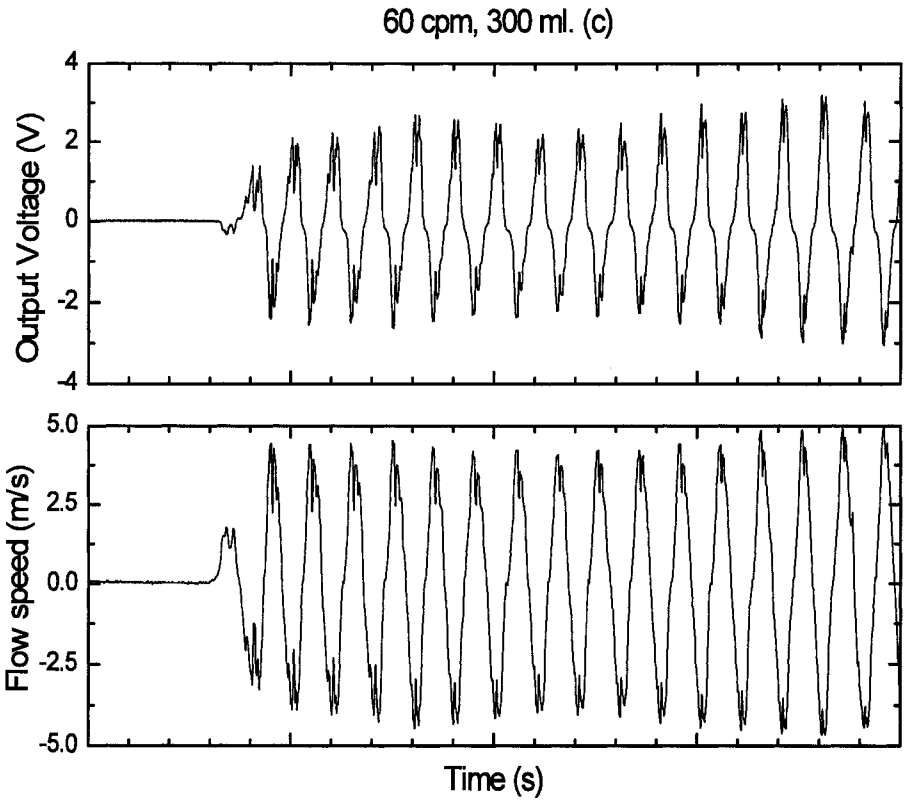


Figure B-3: Sensor output voltage for 60 cpm, airflow volume varying 100ml (a), 200 ml (b), 300 ml (c), 400 ml (d) and 500 ml (e). (Continued on next page)

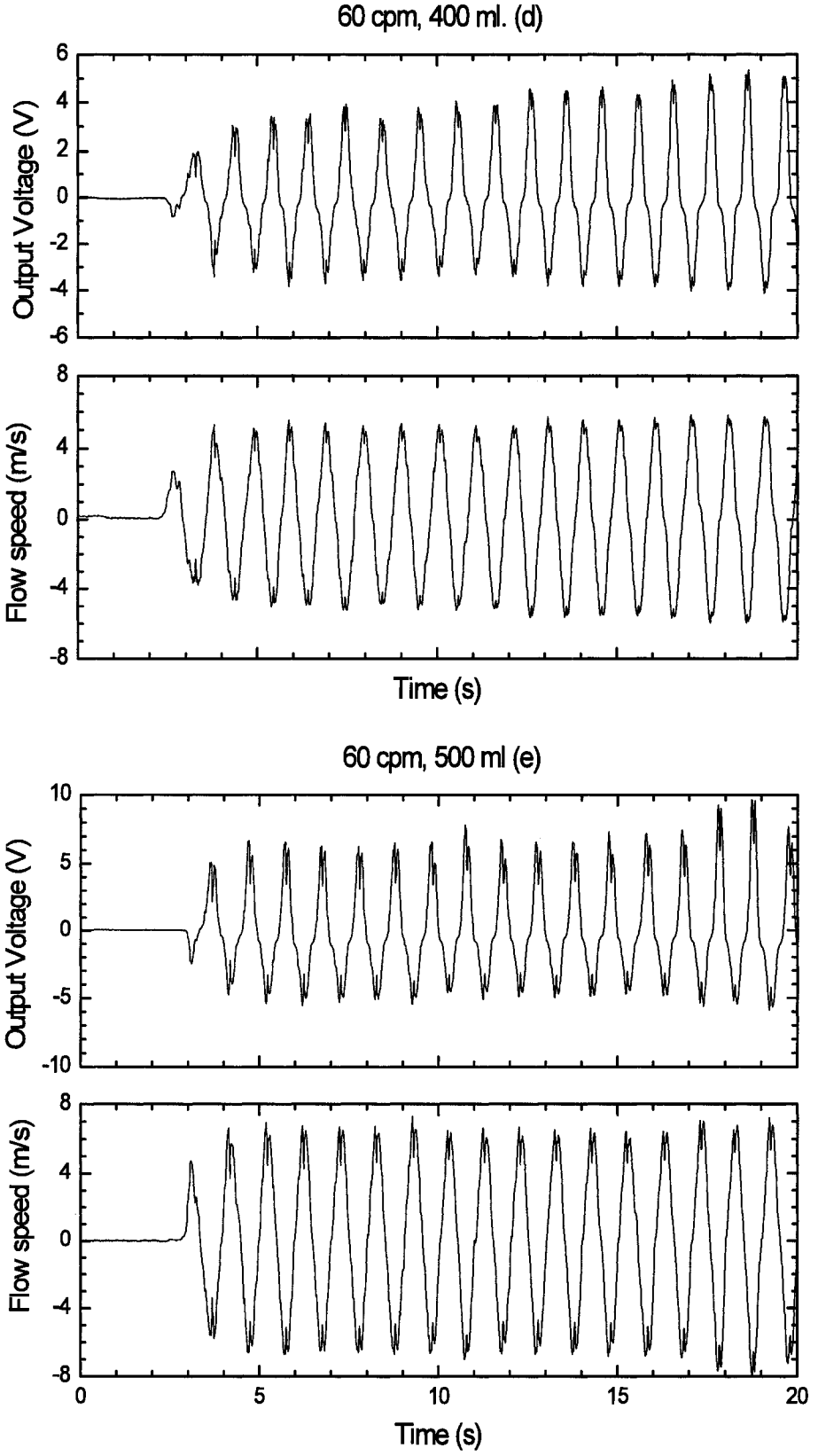


Figure B-3: Sensor output voltage for 60 cpm, airflow volume varying 100ml (a), 200 ml (b), 300 ml (c), 400 ml (d) and 500 ml (e).

Figure B-4 below provides sensor output voltage for 75 cpm, with airflow volume varying from 100 ml (a), 200 ml (b), 300 ml (c), 400 ml (d) and 500 ml (e).

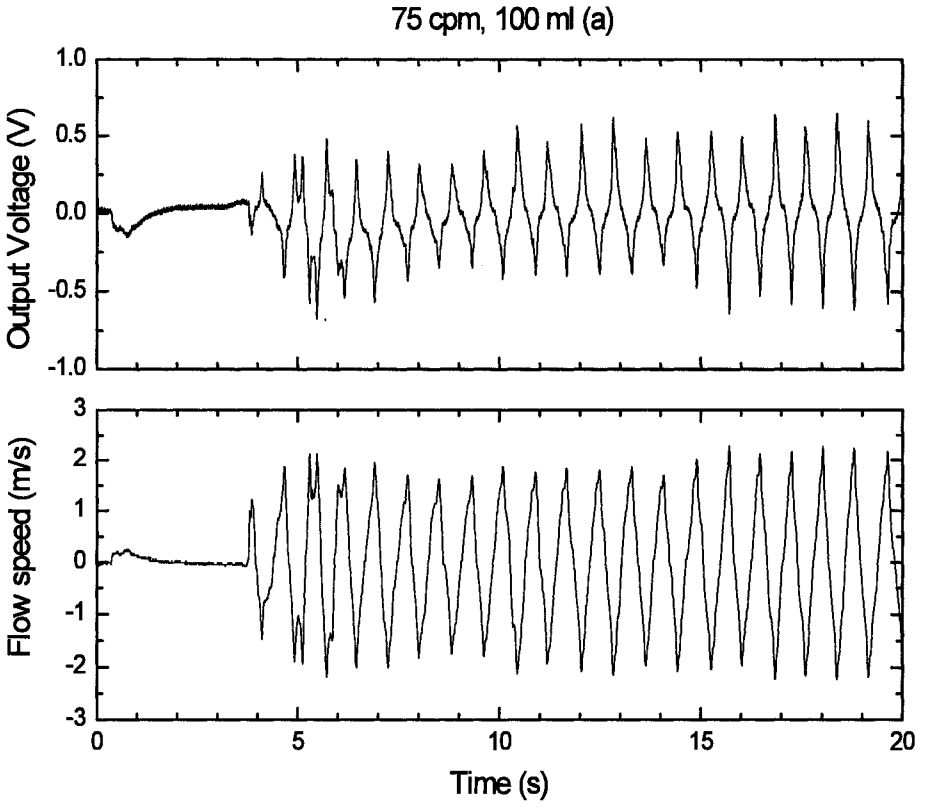


Figure B-4: Sensor output voltage for 75 cpm, airflow volume varying 100ml (a), 200 ml (b), 300 ml (c), 400 ml (d) and 500 ml (e). (Continued on next page)

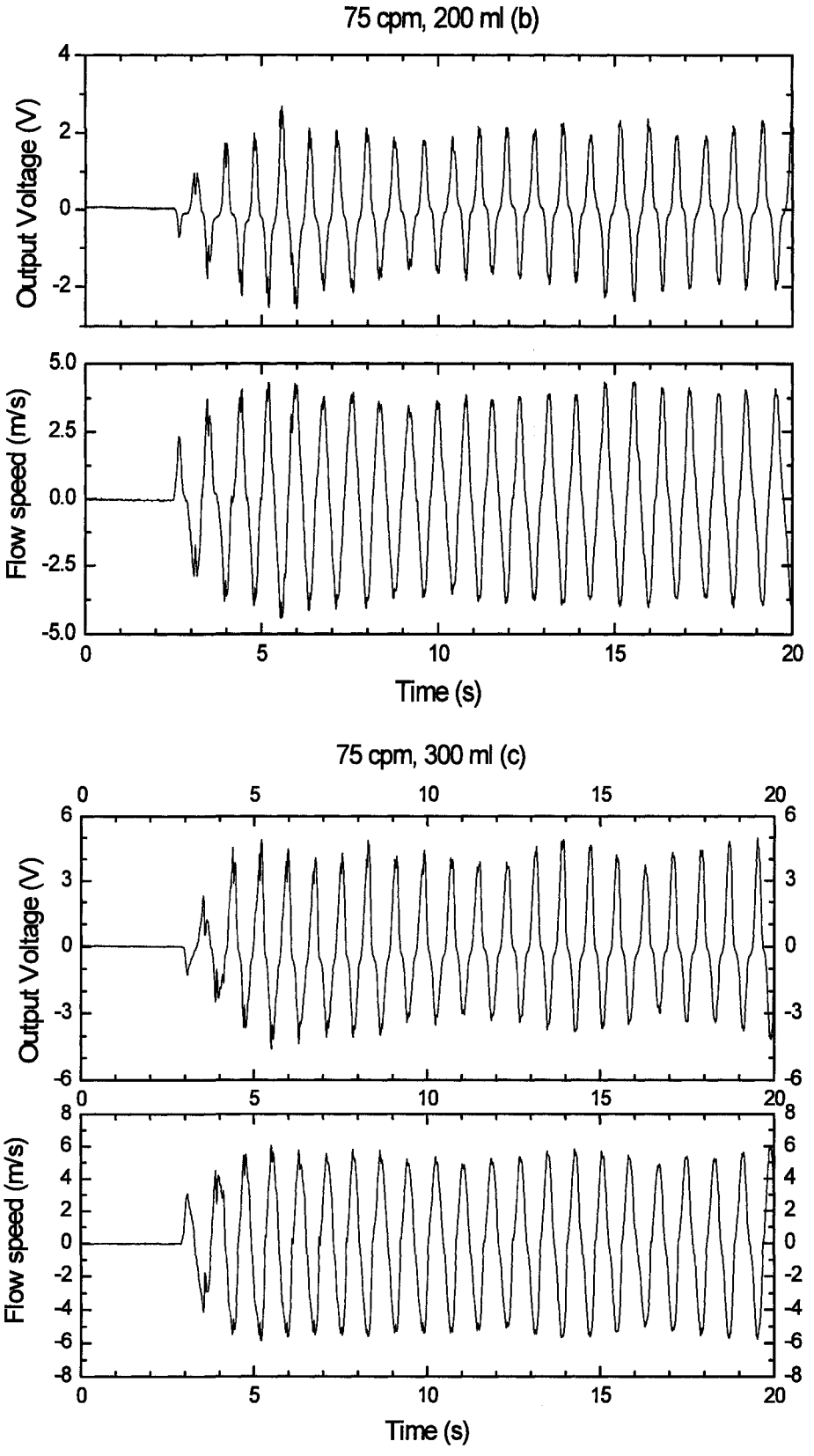


Figure B-4: Sensor output voltage for 75 cpm, airflow volume varying 100ml (a), 200 ml (b), 300 ml (c), 400 ml (d) and 500 ml (e). (Continued on next page)

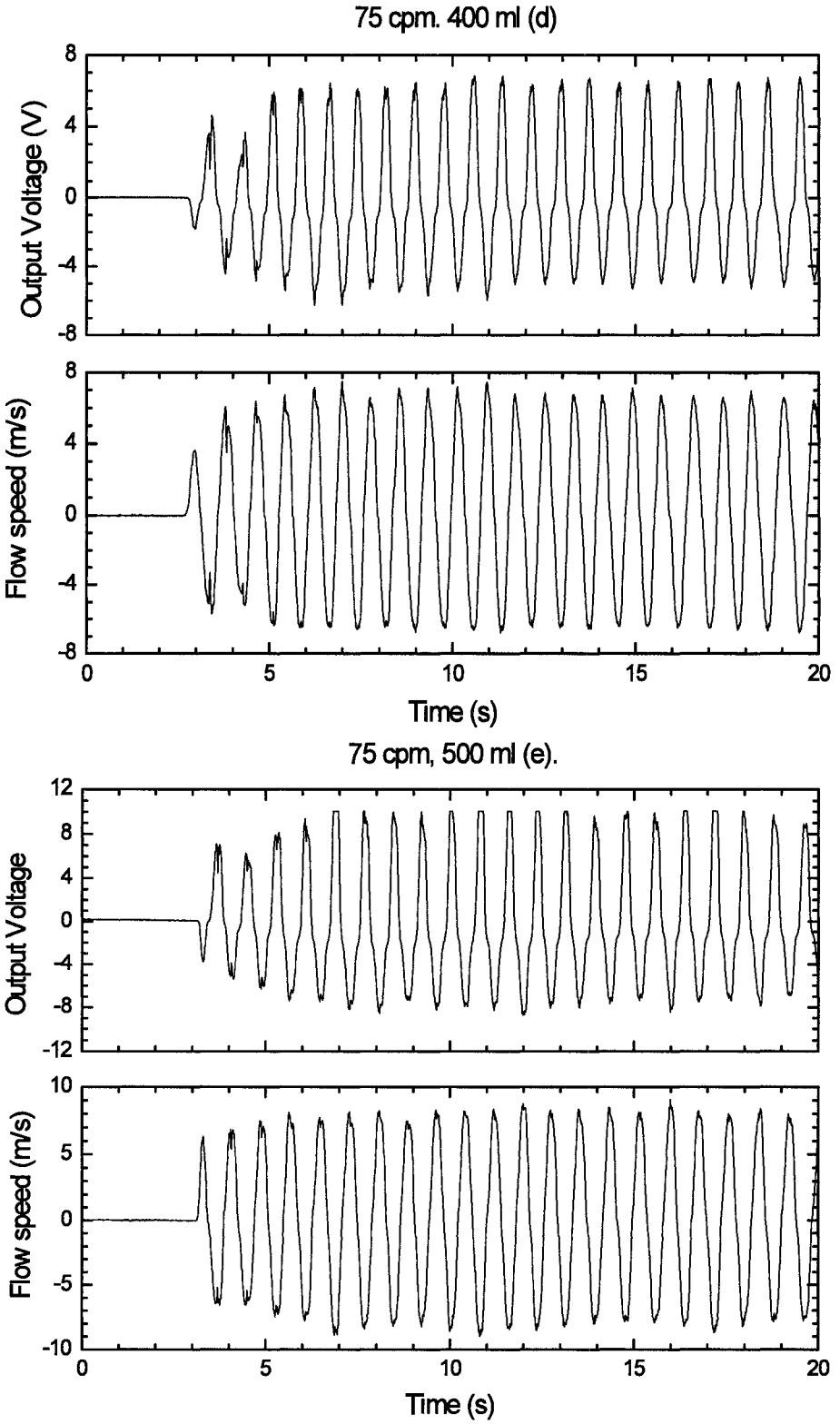


Figure B-4: Sensor output voltage for 75 cpm, airflow volume varying 100ml (a), 200 ml (b), 300 ml (c), 400 ml (d) and 500 ml (e).

Figure B-5 below provides sensor output voltage for 90 cpm, with airflow volume varying from 100 ml (a), 200 ml (b), and 300 ml (c). At this breathing cycle, the output sensor voltage for airflow volume 400ml and 500ml was getting saturated with clipping of the data.

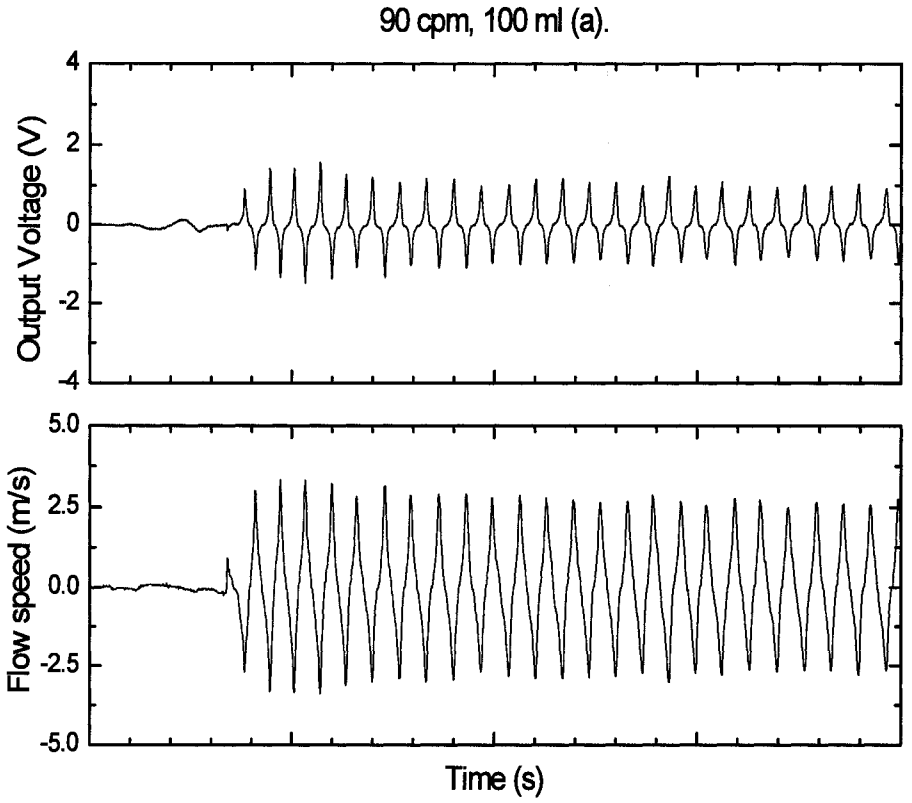


Figure B-5: Sensor output voltage for 90 cpm, airflow volume varying 100ml (a), 200 ml (b), and 300 ml (c). (Continued on the next page)

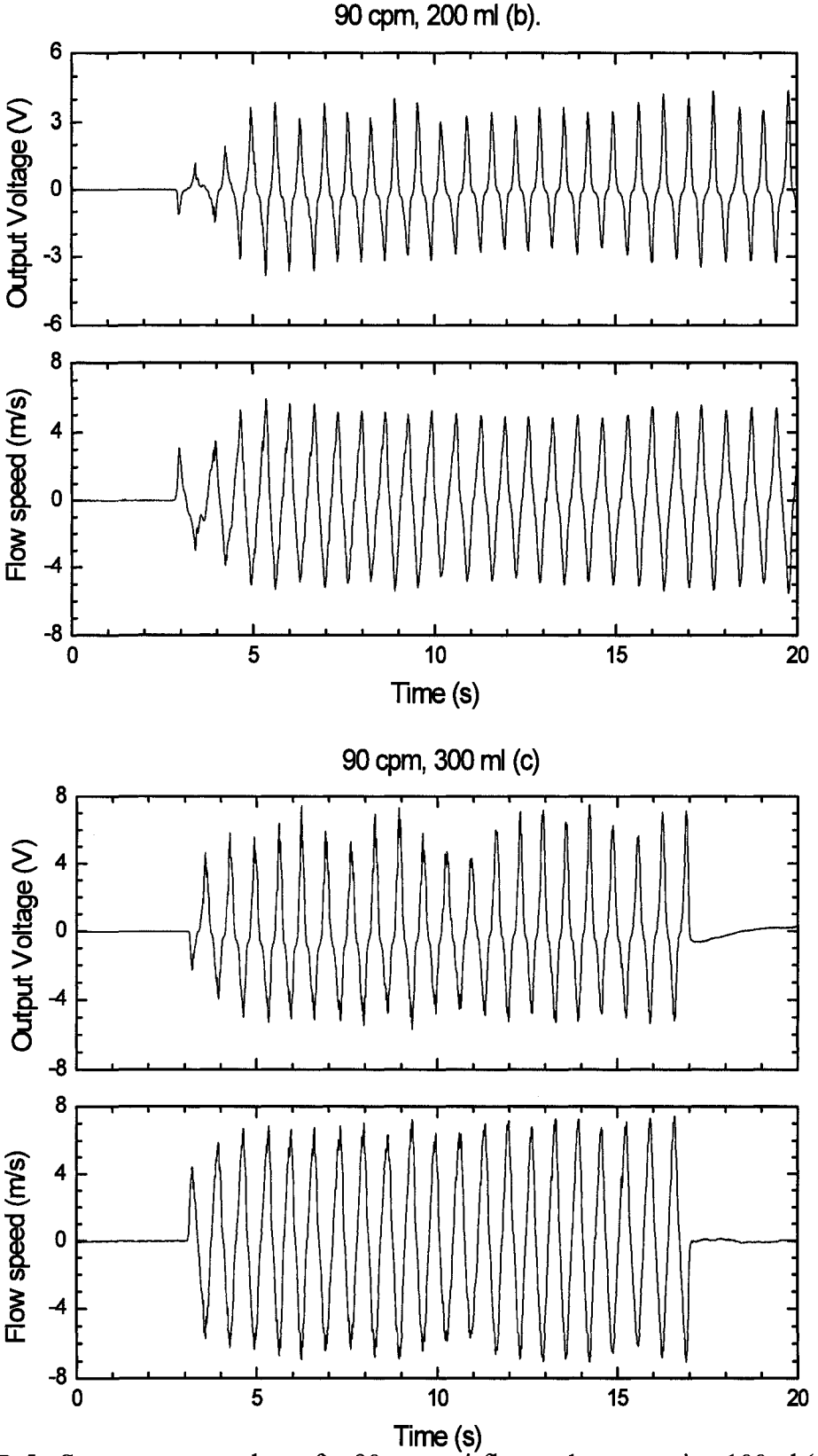


Figure B-5: Sensor output voltage for 90 cpm, airflow volume varying 100ml (a), 200 ml (b), and 300 ml (c).